Arabidopsis Mitogen-Activated Protein Kinase Kinase Kinase Family Members and Their Possible Role in Innate Immunity

By

Kristen Siegel

A thesis submitted to the Department of Biology

in conformity with the requirements for the

degree of Master of Science

Queen's University

Kingston, Ontario, Canada

(September 2019)

ABSTRACT

From an early developmental stage, plants are exposed to both beneficial and pathogenic microbes. Upon pathogen detection, receptor complexes on the cell surface can detect conserved microbial molecules, such as bacterial flagellin, to elicit an immune response. Several early immune outputs are triggered by receptor complex activation, such as the activation of MITOGEN-ACTIVATED PROTEIN KINASE (MAPK) cascades and the production of extracellular reactive oxygen species, which ultimately confer broad-spectrum immunity. While this response is necessary for survival, it is energetically costly and can result in developmental trade-offs. The CALCIUM-DEPENDENT PROTEIN KINASE (CPK28) negatively regulates immune output downstream of multiple receptor complexes by promoting turnover of a key positive regulator of immunity. To identify novel positive and regulators of the plant immune response, putative CPK28-associated proteins were previously identified through affinity purification of wild-type and kinase-dead CPK28 from stable *Arabidopsis thaliana* lines both before and after immune elicitation, followed by liquid chromatography and tandem mass spectrometry. A putative MAPK KINASE KINASE (MAPKKK), MLK/RAF-RELATED PROTEIN KINASE 1 (MRK1), and two protein phosphatase regulatory subunits, PROTEIN PHOSPHATASE 2A (PP2A)-Bα and PP2A-Bβ, were identified in this screen as potential CPK28-associated proteins. The primary objective of my thesis was to examine the role of MRK1, MRK1-related family members, and the PP2A-B subunits in the plant innate immune response. Through functional characterization of double null lines, I found that MRK1 and two closely related proteins, Raf26 and Raf39, may negatively regulate immune-induced oxidative burst in a partially redundant manner. I also observed that MRK1 localizes to the cytosol in Arabidopsis, and present preliminary findings which suggest that MRK1 may play a role in

normal rosette development. Taken together, this work suggests that MRK1 and related protein kinases may be acting as novel regulators of immunity, and primes future analysis on this previously unstudied family.

CO-AUTHORSHIP

All information presented in this thesis is co-authored by myself and Dr. Jacqueline Monaghan. Foundational knowledge and tools were generously provided by the following collaborators:

Dr. Frank Menke and Dr. Jacqueline Monaghan (The Sainsbury Laboratory, England, and Queen's University)

- Performed reverse genetic screen to identify CPK28-associated proteins (Figure 1)
- Provided essential background knowledge that formed the basis of this project

Dr. Jacqueline Monaghan (Queen's University)

- Performed most genetic crosses to generate double null lines (Appendix Table 4)

Danalyn Holmes (Queen's University)

- Generated CPK28, CAD1, and BIK1 clones for bimolecular fluorescence complementation (Appendix Table 1)

Dr. Cathrine Lillo (University of Stavanger, Norway)

- Provided homozygous *pp2a-bα* and *pp2a-bβ* lines (Appendix Table 4)

Dr. Geoffrey Wasteneys (University of British Columbia)

- Provided empty vector controls for bimolecular fluorescence complementation (Appendix Table 1)

ACKNOWLEDGEMENTS

I would like to thank my supervisor, Dr. Jacqueline Monaghan, for shaping my scientific and critical thinking over the course of my graduate studies, and for providing me with an interesting project that sparked my love of MAPKKKs. I would also like to extend my gratitude to the members of my committee, Dr. Bill Plaxton and Dr. Virginia Walker, who have inspired me in both undergraduate lectures and graduate work to nurture my scientific curiosity. In helping generate the foundational knowledge upon which my thesis work was built, I would like to thank Dr. Frank Menke and the Proteomics Group at the Sainsbury Laboratory in Norwich, UK for conducting the CPK28 IP-MS screen alongside Dr. Jacqueline Monaghan. I would also like to thank Dr. Cathrine Lillo and Dr. Geoffrey Wasteneys for providing seed lines and clones, respectively, which assisted in the functional characterization of the Raf-like MAPKKK Subgroup C7 members and PP2A-B subunits (Appendix Table 1 and 4). Finally, I am grateful to Jeffrey Rowbottom, Dale Kristensen, and Olivia Siemons for their work in maintaining greenhouse facilities and in plant care.

To both past and present lab mates, I am nearly certain that you are all superhuman. To be surrounded by such hard working, entertaining, and supportive individuals has been an exceptional experience, and I am so grateful to have met every one of you. Melissa, your scientific enthusiasm is contagious, and your continuous guidance both in and out of the lab has been instrumental to the completion of my thesis work. Irina, thank you for always lending an ear when the PCR didn’t work, and for indulging my constant (and horrible) puns. Lauren, thank you for engaging me in scientific discussions from my very first day in the lab, and for always reminding me to have fun - our mid-day Tim Horton’s runs and Big Band Fridays are deeply missed. To other lab members, Carmen Gonzales-Ferrer, Katy Dunning, Danielle Ciren, Kathy

Sihavong, Alysha Thomsen, Sydney Pascetta, Danalyn Holmes, Heather Galley, Alex Johnson Dingee, Jennifer Wesley, Ruxandra Bogdan, Mansuba Rana, Andrew Ji, Heather Hennessy, Cailun Tanney, Lindsay Marck, Chiara Gottheil, and Anushka Nair, thank you for building such an engaging and collaborative lab environment.

To my favourite BGSC Co-Chair and partner in crime, I am so grateful to have gotten to know you over the course of my graduate degree. Your support during this process made the bad days bearable and the best days better. Cale, thank you for always being there for me, and for putting up with my western blot stories for the twentieth time.

Finally, this thesis work would not have been possible without the support of my incredible family. Your kindness and understanding throughout my graduate work has meant the world to me. Dad, Laura, Bubby, Nana, Zaidy, and Grandad, thank you for checking in, for always having a bad joke at the ready, for listening to me explain what a "kinase" is (again), and for your unwavering support. I am so blessed to be surrounded by compassionate people like you.

This work was funded by an NSERC CGS-M and OGS award, as well as an NSERC Discovery and a CFI grant awarded to Dr. Jacqueline Monaghan.

TABLE OF CONTENTS

LIST OF TABLES

LIST OF FIGURES

LIST OF ABBREVIATIONS

ABRC	Arabidopsis Biological Resource Center
ANP	ARABIDOPSIS NUCLEUS AND PHRAGMOPLAST-LOCALIZED KINASE 1-RELATED KINASE
AtPep	ARABIDOPSIS PLANT ELICITOR PEPTIDES
BAK1	BRASSINOSTEROID INSENSITIVE 1-ASSOCIATED KINASE 1
BiFC	Bimolecular fluorescence complementation
BIK1	BOTRYTIS-INDUCED KINASE 1
BSK1	BRASSINOSTERIOD-SIGNALLING KINASE 1
CAD1	CONSTITUTIVELY ACTIVATED CELL DEATH 1
CaMV	Cauliflower mosaic virus
CBB	Coomassie Brilliant Blue
CBC	CONVERGENCE OF BLUE LIGHT AND CO_2
CDPK	CALCIUM-DEPENDENT PROTEIN KINASE
coIP	Co-immunoprecipitation
Col-0	Columbia ecotype
CPK28	CALCIUM-DEPENDENT PROTEIN KINASE 28
CrRLK1L	*Catharanthus roseus* RECEPTOR-LIKE KINASE 1-LIKE
CTR1	CONSTITUTIVE TRIPLE RESPONSE 1
DAMP	Damage-associated molecular pattern
dpi	Days post-infiltration
DTT	Dithiothreitol
EDR1	ENHANCED DISEASE RESISTANCE 1

EFR	ELONGATION FACTOR Tu RECEPTOR
elf18	Epitope of elongation factor Tu
ERK	EXTRACELLULAR SIGNAL-REGULATED KINASE
flg22	Epitope of bacterial flagellin
FLS2	FLAGELLIN SENSING 2
GFP	GREEN FLUORESCENT PROTEIN
GK	T-DNA insertion lines sourced from the GABI-Kat consortium
HRP	HORSERADISH PEROXIDASE
HT1	HIGH LEAF TEMPERATURE 1
IP	Immunoprecipitation
LB	Luria-Bertani
LC	Liquid chromatography
LRR	Leucine-rich repeat
MAPK	MITOGEN-ACTIVATED PROTEIN KINASE
MAPKK	MITOGEN-ACTIVATED PROTEIN KINASE KINASE
MAPKKK	MITOGEN-ACTIVATED PROTEIN KINASE KINASE KINASE
MEKK	MITOGEN-ACTIVATED PROTEIN KINASE/EXTRACELLULAR SIGNAL-REGULATED KINASE KINASE KINASE
MLK	MIXED-LINEAGE KINASE
MRK1	MIXED-LINEAGE KINASE/RAF-RELATED PROTEIN KINASE 1
MS	Mass spectrometry
MS-MS	Tandem mass spectrometry
MSO	Murashige and Skoog

NB-LRR	Nucleotide-binding leucine-rich repeat
OG	Oligogalacturonide
PAGE	Polyacrylamide gel electrophoresis
PAMP	Pathogen-associated molecular pattern
PBL	AVRPPHB SUSCEPTIBLE 1-LIKE
PCR	Polymerase chain reaction
PM-GFP	Plasma-membrane control LOW TEMPERATURE-INDUCED PROTEIN 6B GFP
PP2A	PROTEIN PHOSPHATASE 2A
PP2C	PROTEIN PHOSPHATASE 2C
PUB	PLANT U-BOX
PVDF	Polyvinylidene difluoride
qRT-PCR	Quantitative reverse transcription polymerase chain reaction
Raf	RAPIDLY ACCELERATED FIBROSARCOMA
RBOHD	RESPIRATORY BURST OXIDASE HOMOLOGUE D
RLCK	RECEPTOR-LIKE CYTOPLASMIC KINASE
RLK	RECEPTOR-LIKE KINASE
RLP	RECEPTOR-LIKE PROTEIN
ROS	Reactive oxygen species
RT	Reverse transcription
SAIL	T-DNA insertion lines sourced from the Syngenta Arabidopsis Insertion Library
SALK	T-DNA insertion lines sourced from the Salk Institute for Biological Studies
SDS	Sodium dodecyl sulfate

SLAC1	SLOW ANION CHANNEL ASSOCIATED 1
SUMM2	SUPPRESSOR OF MITOGEN-ACTIVATED PROTEIN KINASE KINASE 1 MITOGEN-ACTIVATED PROTEIN KINASE KINASE 2 2
TAIR	The Arabidopsis Information Resource
TBS	Tris-buffered saline
YFP	YELLOW FLUORESCENT PROTEIN
ZIK	ZINC RIBBON 1-INTERACTING KINASE

1. INTRODUCTION

1.1. Plant innate immunity

Since the first agricultural revolution in 8500 B.C. (Pringle, 1998), humans have been plagued by the spread of plant pathogens. While many examples have been cited, the most notable epidemic occurred in the mid-nineteenth century, when the oomycete *Phytophthera infestans* ravaged Irish crops and caused widespread potato blight (Yoshida et al., 2013). Now known as the Irish Potato Famine, this outbreak resulted in nearly one million deaths (Zadoks, 2008), and has been credited as a critical point in the development of plant pathology as a scientific discipline. More recently, the world's first widely cultivated banana cultivar, the Gros Michel, was completely decimated by the fungus *Fusarium oxysporum* in the late 1920s, forcing its replacement with the more resistant Cavendish cultivar (Ploetz, 1994). In the present day, African and Asian agricultural productivity is threatened by wheat stem and yellow stripe rust, which are respectively caused by the fungi *Puccinia graminis* and *Puccinia striiformis* (Singh et al., 2011). These diseases, and many others, contribute to the 15% of all global crop production that is currently lost to preharvest disease (Dangl et al., 2013). Despite the development of some chemical pesticides and disease-resistant crop varieties, the efficacy of these technologies must be improved to reduce food insecurity as our global population grows to 9.7 billion by 2050 (Béné et al., 2015).

Though they constantly interact with both beneficial and pathogenic microbes, the majority of plants appear healthy. The complex mechanisms used to achieve this disease resistance are not fully understood, but a framework for a multi-layered plant defense system has been established (Dangl et al., 2013). Upon infection, pathogens are first met with physical barriers to entry, such as cuticular waxes and the plant cell wall (L'Haridon et al., 2011;

Malinovsky et al., 2014). Should they achieve entry through stomatal pores or wound sites (Melotto et al., 2008), potential pathogens may be detected by immune receptors at the plasma membrane (Böhm et al., 2014; Couto and Zipfel, 2016). These receptors recognize highly conserved, microbe-derived molecules as well as damage-associated, modified-self molecules that are generated during infection (Schwessinger and Ronald, 2012; Couto and Zipfel, 2016). Upon activation, these immune receptors trigger intracellular signalling, including changes in ion flux, defense gene expression, and production of reactive oxygen species (ROS) (Couto and Zipfel, 2016). Together, these physiological changes confer broad-spectrum immunity to the plant cell, and are sufficient to defend against most pathogens. While necessary for survival, this defense response is energetically costly and can divert resources from developmental pathways. As a result, all plants are challenged to maintain homeostasis: they must defend against a vast spectrum of pathogens while maintaining normal growth and development.

Though critical to maintaining plant health, the diverse signalling cascades downstream of pathogen recognition have not been fully elucidated. To combat global agricultural disease, we must identify both positive and negative regulators of plant innate immunity that can confer disease resistance in crops while minimizing developmental defects.

1.1.1. Pattern recognition receptor (PRR)-mediated immunity

Lacking an acquired immune system, plants must rely on the ability of individual cells to initiate an innate immune response and defend against potential pathogens. Like animals, plants express high-affinity, cell-surface receptors that are capable of detecting highly conserved microbial molecules known as pathogen-associated molecular patterns (PAMPs) (Schwessinger and Ronald, 2012; Couto and Zipfel, 2016; Yu et al., 2017). PAMPs are often integral components of microbial lifestyles and cannot be lost or mutated without substantial fitness costs, making them ideal immune receptor ligands (Abramovitch et al., 2006; Ingle et al., 2006). For example, bacterial flagellin, a globular protein that functions in bacterial locomotion, can be detected by transmembrane receptors in both plants and animals (Felix et al., 1999; Hayashi et al., 2001). In addition, endogenous modified-self molecules, known as damage-associated molecular patterns (DAMPs), are released into the extracellular space upon wounding or by action of pathogen-secreted cell wall-degrading enzymes (Choi and Klessig, 2016; Davidsson et al., 2017). Small peptides generated by the plant cell, termed phytocytokines, can also be secreted into the extracellular space to mediate an immune response following infection (Luo, 2012; Segonzac and Monaghan, 2019). For example, the damage-associated oligogalacturonides (OGs) are fragments of the cell wall polypeptide homogalacturonan and are released by pathogen-derived polygalacturonases (Ferrari et al., 2013), while the phytocytokine plant elicitor peptides (AtPeps) are processed from 92 amino acid PROPEP precursors during wounding (Huffaker et al., 2006). In mammals, transmembrane Toll-like receptors, alongside cytosolic Nod proteins, are capable of recognizing P/DAMPs and initiating a response (Athman and Philpott, 2004; Philpott and Girardin, 2004). These P/DAMP-binding receptors are collectively known as PRRs (Couto and Zipfel, 2016). In plants, the transmembrane PRRs are composed of two main classes: receptor-like kinases (RLKs) and receptor-like proteins (RLPs) (Böhm et al., 2014; Couto and Zipfel, 2016). From a structural standpoint, RLKs contain a ligand-binding ectodomain, a transmembrane domain, and an intracellular protein kinase domain, allowing them to both detect P/DAMPs and transduce a signal (Zipfel, 2014; Couto and Zipfel, 2016). Conversely, RLPs contain only a ligand-binding ectodomain and a transmembrane domain, suggesting that they may rely on regulatory RLKs to relay their P/DAMP perception (Gust and Felix, 2014). The largest group of plant PRRs, the leucine-rich repeat (LRR)-containing RLKs, preferentially bind protein-based P/DAMPs (Shiu and Bleecker, 2001; Böhm et al., 2014), including the conserved 22-amino acid epitope on the N-terminus of bacterial flagellin (flg22) and the 18-amino acid epitope of elongation factor Tu (elf18) (Gómez-Gómez et al., 1999; Gómez-Gómez and Boller, 2000; Kunze et al., 2004; Zipfel et al., 2006). Both RLKs and RLPs form heteromeric complexes with regulatory co-receptors at the plasma membrane (Monaghan and Zipfel, 2012; Liebrand et al., 2014). The RLKs FLAGELLIN SENSING 2 (FLS2), EF-TU RECEPTOR (EFR), and PEP1 RECEPTOR 1 or 2 , which detect flg22, elf18, and AtPeps respectively, each associate with the co-receptor BRASSINOSTEROID-ASSOCIATED KINASE 1 (BAK1) upon P/DAMP perception (Gómez-Gómez and Boller, 2000; Yamaguchi et al., 2006; Zipfel et al., 2006; Yamaguchi et al., 2010; Monaghan and Zipfel, 2012). BAK1 also forms a trimeric complex with RLP23 and the LRR-RLK SUPPRESSOR OF BAK1-INTERACTING RECEPTOR-LIKE KINASE 1-1 to detect NECROSIS AND ETHYLENE-INDUCING PEPTIDE 1-LIKE PROTEINS (Albert et al., 2015), highlighting the essential role of BAK1-RLK and BAK1-RLP complexes in recognizing an array of microbial signatures. During microbial detection, the bacterial elicitor flg22 acts as a binding partner with both BAK1 and FLS2 ectodomains, which facilitates dynamic complex formation, a reciprocal transphosphorylation event between receptors, and ultimately, receptor complex activation (Chinchilla et al., 2007; Schulze et al., 2010; Sun et al., 2013).

Activated PRRs use intracellular receptor-like cytoplasmic kinases (RLCKs) as direct substrates to facilitate downstream signalling (Macho and Zipfel, 2014). While many of the 160 *Arabidopsis thaliana* (‘Arabidopsis’) RLCKs remain widely understudied, the RLCK BOTRYTIS-INDUCED KINASE 1 (BIK1) and closely related PBS1-LIKE (PBL1) play a critical role in the positive regulation of plant immunity, and act as convergent substrates of multiple PRRs (Lehti-Shiu et al., 2009; Lu et al., 2010; Zhang et al., 2010; Liu et al., 2013; Couto and Zipfel, 2016). Previously identified as a positive regulator of brassinosteroid signalling in plant development, the RLCK BRASSINOSTEROID-SIGNALING KINASE 1 (BSK1) also associates with FLS2 to mediate immune responses downstream of flg22 perception (Shi et al., 2013). Several RLCKs, including BIK1, PBL1, and BSK1, dissociate from receptor complexes following ligand detection to initiate intracellular signalling (Lu et al., 2010; Zhang et al., 2010; Shi et al., 2013). Ultimately, signal relay through plasma membrane-bound PRRs results in several early immune responses, including changes in ion-flux at the cell surface, increases in cytosolic Ca^{2+} levels, production of extracellular ROS, and the activation of cascades involving both MAPKs and CALCIUM-DEPENDENT PROTEIN KINASES (CDPKs) (Couto and Zipfel, 2016). In particular, the phosphorylation of four MAPKs through two parallel cascades, MPK3/6 and MPK4/11, promotes WRKY transcription factor activation and defense gene induction following pathogen perception (Petersen et al., 2000; Asai et al., 2002; Eschen-Lippold et al., 2012). Transcriptional, translational, and post-translational reprogramming resulting from these cascades is then used to prime the defense response through production of antimicrobial compounds, reducing guard cell turgidity to facilitate stomatal closure, and strengthening of extracellular barriers (Bigeard et al., 2015; Lee et al., 2015a). Collectively, this response is known as PRR-mediated immunity, and it is sufficient to provide broad-spectrum resistance against most non-adapted pathogens (Couto and Zipfel, 2016).

To counter this innate immune response, pathogens have evolved a suite of effector proteins that target key components of the plant immune system (Cui et al., 2015). In Gram-negative bacteria, a multimeric type III secretion pilus penetrates the plant plasma membrane to release effectors into the cytoplasm, while other pathogens can release effectors into the extracellular matrix (Büttner and He, 2009; Toruño et al., 2016). Perturbations caused by pathogen effectors can be detected by intracellular plant resistance proteins, which are predominantly members of the nucleotide-binding LRR (NB-LRR) receptor family (Wu et al., 2014). Through direct effector binding or indirect detection of effector-modified host proteins, activated NB-LRRs trigger sustained ROS production and MAPK activation, accumulation of salicylic acid , induction of pathogenesis-related genes, and a form of localized programmed cell death, known as the hypersensitive response (HR) (Cui et al., 2015). This stronger, prolonged immune output, termed NB-LRR-mediated immunity, limits nutrient availability to pathogens and halts proliferation at the site of infection (Cui et al., 2015).

1.1.2. Negative regulation of PRR-mediated immunity

Both in the presence and absence of pathogens, the plant immune response must be tightly controlled to prevent unnecessary activation. As misregulated responses can lead to host damage and autoimmunity (van Wersch et al., 2016), the negative regulation of immunity is achieved by several concurrent mechanisms, including but not limited to: (1) inhibiting receptor complex formation, (2) dephosphorylating key regulators of immunity, and (3) modifying the accumulation of key regulators of immunity (Couto and Zipfel, 2016). At the receptor level, the LRR-RLK BAK1-INTERACTING RECEPTOR-LIKE KINASE 2 associates with BAK1 under resting conditions to prevent FLS2-BAK1 complex formation (Halter et al., 2014). Following PAMP perception, BAK1-INTERACTING RECEPTOR-LIKE KINASE 2 dissociates from BAK1, allowing BAK1 to interact with relevant PRRs (Halter et al., 2014). Similarly, in the presence of flg22, the *Catharanthus roseus* RLK1-like (CrRLK1L) receptor ANXUR1 associates with BAK1 to inhibit FLS2-BAK1 complex formation and modulate the strength of the immune response (Mang et al., 2017). Interestingly, the CrRLK1L FERONIA positively regulates FLS2-

BAK1 and EFR-BAK1 complex formation by serving as a scaffold protein (Stegmann et al., 2017), and is the second closest homolog to ANXUR1.

Reversible phosphorylation or hyperphosphorylation of protein kinases is a common post-translational modification following pathogen recognition (Macho and Zipfel, 2014). Though these phosphorylation events do not always result in protein kinase activation (Li et al., 2016a), some protein kinases can be negatively regulated through dephosphorylation by serine/threonine (Ser/Thr) phosphatases, tyrosine phosphatases, or dual-specificity phosphatases (Suarez-Rodriguez et al., 2010; Macho and Zipfel, 2014). For example, the Ser/Thr phosphatase PROTEIN PHOSPHATASE 2C (PP2C) 38 negatively regulates elf18-induced hyperphosphorylation of the RLCK BIK1 and inhibits BIK1-mediated phosphorylation of downstream targets (Couto et al., 2016). Upon PAMP perception, PP2C38 is phosphorylated by BIK1, resulting in dissociation of PP2C38 from the FLS2/EFR-BAK1-BIK1 complex and activation of BIK1 (Couto et al., 2016). Using spaciotemporal separation, multiple protein phosphatases can also act on a single substrate at different time intervals in the innate immune response (Suarez-Rodriguez et al., 2010; Shubchynskyy et al., 2017). Roughly 15 minutes after bacterial invasion, the Ser/Thr phosphatase AP2C1 deactivates four MAPKs, MPK3/4/6/11, to prevent transcription factor activation and defense gene induction (Schweighofer et al., 2007), while the dual-specificity phosphatase MAP KINASE PHOSPHATASE 1 controls MPK3/6 deactivation at 30 minutes following immune elicitation (Bartels et al., 2009; Shubchynskyy et al., 2017). Conversely, dephosphorylation of the co-receptor BAK1 by a PP2A complex may affect its protein kinase activity both before and after immune induction (Segonzac et al., 2014). Unlike monomeric PP2Cs, PP2As are trimeric holoenzymes composed of a catalytic subunit (‘C’), a scaffold subunit (‘A’), and a regulatory subunit which facilitates localization and substrate specificity (‘B’) (Durian et al., 2016). A PP2A consisting of subunit C4, A1, and B’η or B’ζ constitutively associates with BAK1 to attenuate its activity in the presence or absence of pathogens (Segonzac et al., 2014), thus limiting unnecessary signal propagation. Essentially, dephosphorylation of key protein kinases appears to be a widespread mechanism for dampening innate immunity both intracellularly and at the plasma membrane.

Negative regulators of immunity may also alter accumulation of essential immune components, such as the RLCK BIK1. Under resting conditions, BIK1 associates with the FLS2-BAK1 complex at the plasma membrane (Lu et al., 2010). Perception of flg22 results in a reciprocal phosphorylation event between BIK1 and FLS2-BAK1 (Lu et al., 2010), causing BIK1 to dissociate from the receptor complex and subsequently activate the NADPH-oxidase RESPIRATORY BURST OXIDASE HOMOLOGUE D (RBOHD) to trigger an apoplastic ROS burst (Kadota et al., 2014; Li et al., 2014). Accumulation of BIK1 is monitored both before and after pathogen detection by a negative regulatory module comprised of CPK28 and two ubiquitin E3 ligases, PLANT U-BOX 25 and 26 (PUB25 and 26) (Monaghan et al., 2014; Wang et al., 2018b). Through CPK28-mediated phosphorylation of PUB25/26, active PUB25/26 can polyubiquitinate and target inactive BIK1 for degradation (Wang et al., 2018b). Upon flg22 detection, a pool of BIK1 is activated through phosphorylation at Ser-236 and Thr-237 in the kinase activation loop (Lu et al., 2010), and this subset of activated BIK1 is protected from PUB25/26-mediated degradation (Wang et al., 2018b). Through this interplay of phosphorylation and ubiquitination, a smaller inactive pool of BIK1 is available for turnover following immune elicitation, and BIK1 accumulation and signalling can be tightly regulated by CPK28 and PUB25/26. As BIK1 directly activates RBOHD (Kadota et al., 2014; Li et al., 2014), reduced BIK1 accumulation results in a smaller pool of activated RBOHD, impaired ROS production, and dampened immune signalling. Immune-induced activation of MAPK cascades can similarly be attenuated by modifying protein accumulation. A MAPKKK, ENHANCED DISEASE RESISTANCE 1 (EDR1), negatively regulates the accumulation of two mitogen-activated protein kinase kinases (MAPKKs), MKK4 and MKK5, to modulate defense responses (Zhao et al., 2014). Both MKK4/5 act upstream of MPK3/6 to positively regulate defense gene induction (Asai et al., 2002), and increasing levels of MKK4/5 can enhance immune output (Zhao et al., 2014). Though the mechanistic details of this regulatory module remain unclear, the pathogen-resistant phenotype of *edr1* plants can be suppressed by introducing a loss-of-function allele for an E3 ligase, KEEP ON GOING, suggesting it may be acting in the same pathway as EDR1 to facilitate protein polyubiquitination and proteolytic turnover (Wawrzynska et al., 2008). Ultimately, through the combined action of these diverse negative regulators, such as protein phosphatases and CPK28, plant innate immunity can be attenuated by several mechanisms including receptor complex inhibition, protein dephosphorylation, and protein turnover. In the absence of pathogens or by modifying the amplitude of the innate immune response, these regulatory modules can limit the harmful developmental trade-offs associated with unnecessary immune activation, such as dwarfism or constitutive defense gene expression (van Wersch et al., 2016).

1.2. MAPK cascades in Arabidopsis

Activation of MAPK cascades can facilitate intracellular signal transduction following ligand perception by RLKs and RLPs (MAPK Group, 2002). While MAPK activation plays a critical role in immune signalling downstream of PRRs (Meng and Zhang, 2013), these distinct cascades are also involved in wounding, osmotic stress tolerance, hormone signalling, salt stress tolerance, drought, cell division, and development, among other pathways (Suarez-Rodriguez et al., 2010;

Jagodzik et al., 2018). Classical MAPK cascades are composed of three protein kinases, a MAPKKK, a MAPKK, and a MAPK, which relay information through successive phosphorylation of their downstream kinase (MAPK Group, 2002). At the top of the cascade, a MAPKKK can be activated directly through receptor-mediated phosphorylation, or indirectly by MITOGEN-ACTIVATED PROTEIN KINASE KINASE KINASE KINASES or RLCKs (Bi et al., 2018; Jagodzik et al., 2018). Active MAPKKKs then facilitate the dual phosphorylation of their downstream MAPKK at two conserved Ser/Thr residues in an activation motif, S/T-X_5-S/T (Suarez-Rodriguez et al., 2010). Through sequential phosphorylation of a tyrosine and threonine residue in the MAPK consensus motif, T-X-Y, MAPKKs subsequently activate specific MAPKs to complete the cascade (Suarez-Rodriguez et al., 2010; Mithoe et al., 2016). While MAPKs are commonly phosphorylated by MAPKKs in the cytosol, active MAPKs often translocate to the nucleus to phosphorylate downstream targets, as nearly half of all identified MAPK substrates are transcription factors (Suarez-Rodriguez et al., 2010; Bigeard et al., 2015). For example, the YODA-MKK4/5-MPK3/6 cascade triggers phosphorylation of the basic helix-loop-helix transcription factor SPEECHLESS to regulate stomatal development (Lampard et al., 2008). Despite their role in multiple stress responses and developmental pathways, relatively few MAPK cascades with affiliate downstream targets have been fully elucidated.

In the Arabidopsis genome, there are 20 MAPKs, 10 MAPKKs, and 80 MAPKKKs that have been identified on the basis of sequence similarity (Colcombet and Hirt, 2008). For example, all Arabidopsis MAPKs possess a consensus motif (T(E/D)YVxTRWYRAPE(L/V)) in their catalytic domain, and can be further divided into four subgroups (A-D) (MAPK Group, 2002; Suarez-Rodriguez et al., 2010). Members of Group A-C have an activation motif similar to animal MAPKs (T-E-Y) and are generally well-studied (MAPK Group, 2002), such as the immune-activated MPK3/6 (Group A) and MPK4/11 (Group B), while members of Group D are relatively uncharacterized (Petersen et al., 2000; Asai et al., 2002; MAPK Group, 2002; Eschen-Lippold et al., 2012). Plant MAPKKs are similarly divided into four subgroups (A-D) (MAPK Group, 2002), with MKK1/2 (Group A) and MKK4/5 (Group C) playing an established role in immunity (Asai et al., 2002; Mészáros et al., 2006; Gao et al., 2008). In contrast to these families, Arabidopsis MAPKKKs have diverse domain structures, including members with LRR domains, a nuclear localization signal, or ankyrin repeats that promote protein-protein association (MAPK Group, 2002). They are classified into three subgroups based on the similarity of their catalytic domains to animal and yeast homologs: MITOGEN-ACTIVATED PROTEIN KINASE/EXTRACELLULAR SIGNAL-REGULATED KINASE KINASE KINASE (MEKK)-like MAPKKKs, RAPIDLY ACCELERATED FIBROSARCOMA (Raf)-like MAPKKKs, and ZINC RIBBON 1-INTERACTING KINASE (ZIK)-like MAPKKKs (Jonak et al., 2002). However, as MAPKKKs are first identified by sequence similarity and later confirmed by specific phosphorylation of a MAPKK, only members of the MEKK-like MAPKKK subgroup have been validated as canonical MAPKKKs (Suarez-Rodriguez et al., 2010). The MEKK-like MAPKKK family consists of 21 members in Arabidopsis and is characterized by the signature motif G(T/S)Px(W/Y/F)MAPEV (Jonak et al., 2002; Suarez-Rodriguez et al., 2010). Prominent members include MEKK1, MAPKKK3, and MAPKKK5, which serve distinct regulatory roles in two immune cascades (Suarez-Rodriguez et al., 2007; Gao et al., 2008; Sun et al., 2018), as well as ARABIDOPSIS NUCLEUS AND PHRAGMOPLAST-LOCALIZED KINASE 1-RELATED KINASE 1 (ANP1), ANP2, and ANP3, which function redundantly in a cascade to regulate cytokinesis (Krysan et al., 2002). The ZIK-like MAPKKKs, also known as WITH NO LYSINE

KINASES, comprise an 11-member family in Arabidopsis, and have been implicated in drought tolerance, regulating flowering time, and ABA responses (Jonak et al., 2002; Wang et al., 2008; Xie et al., 2014; Waadt et al., 2019). A 48-member family, the Raf-like MAPKKKs, is the most expansive group of MAPKKKs in Arabidopsis and is further divided into two classes, Subgroup B and C (MAPK Group, 2002). Though some Raf-like MAPKKK Subgroup B members have been widely studied, such as the negative immune regulator EDR1 (Frye and Innes, 1998) or the negative regulator of ethylene signalling CONSTITUTIVE TRIPLE RESPONSE 1 (CTR1) (Kieber et al., 1993), only select members of Subgroup C have been recently characterized. Further work will be required to assess the specific roles of ZIK-like and Raf-like MAPKKKs in either MAPKK-dependent or MAPKK-independent signalling pathways.

1.3. MAPK cascades in the innate immune response

Two MAPK cascades downstream of PAMP-mediated PRR activation have beenwell-studied, namely MEKK1-MKK1/2-MPK4 and MAPKKK3/5-MKK4/5-MPK3/6 (Gao et al., 2008; Sun et al., 2018). The MEKK1-MKK1/2-MPK4 cascade was originally identified as a negative regulatory module, as loss-of-function *mpk4*, *mkk1 mkk2*, and *mekk1* plants exhibit constitutive defense gene expression, ROS accumulation, salicylic acid accumulation, and dwarfism (Petersen et al., 2000; Suarez-Rodriguez et al., 2007; Qiu et al., 2008). MKK1/2 also interact with MEKK1 and MPK4 *in vivo* and phosphorylate MPK4 *in vitro* (Huang et al., 2000; Gao et al., 2008), confirming their role as canonical MAPKKs in this cascade. However, the constitutive defense activation of *mkk1 mkk2* and *mekk1* can be suppressed by a loss-of-function allele for the NB-LRR SUPPRESSOR OF MITOGEN-ACTIVATED PROTEIN KINASE KINASE 1 MITOGEN-ACTIVATED PROTEIN KINASE KINASE 2 2 (SUMM2) (Zhang et al., 2012), suggesting that the integrity of this cascade may be monitored to enable NB-LRR-mediated immunity. As SUMM2 associates with the MPK4 target CALMODULIN-BINDING RECEPTOR-LIKE CYTOPLASMIC KINASE 3 (Zhang et al., 2017), SUMM2 may be detecting MEKK1-MKK1/2-MPK4 activity by monitoring the phosphorylation status of this cytoplasmic kinase. Accordingly, a conserved effector from the bacterial pathogen *Pseudomonas syringae*, HopAI1, inhibits flg22-mediated MPK4 activation (Zhang et al., 2012). In the absence of SUMM2, loss-of-function *mekk1 summ2* and *mkk1 mkk2 summ2* lines support increased growth of the strain *P. syringae* pv. *tomato* DC3000 relative to *summ2* (Zhang et al., 2012), suggesting that MEKK1 and MKK1/2 play a positive role in regulating basal immunity. A second NB-LRR, RESISTANCE TO PSEUDOMONAS SYRINGAE 6, also monitors the disruption of MEKK1-MKK1/2-MPK4 activity mediated by the *P. syringae* pv. *syringae* strain 61 effector HopA1 (Takagi et al., 2019), though the exact mechanism of this host-pathogen interaction is unknown. Interestingly, the constitutive defense phenotype of *mekk1* plants can be complemented by a kinase-dead variant of MEKK1 (MEKK1^{K361M}) (Suarez-Rodriguez et al., 2007), suggesting that this cascade may function atypically and independently of MEKK1-mediated phosphorylation of MKK1/2.

The second cascade, MAPKKK3/5-MKK4/5-MPK3/6, is involved in stomatal defense, synthesis of the antimicrobial compound camalexin, and ethylene production in the presence of necrotrophic pathogens (Thulasi Devendrakumar et al., 2018). Though this cascade functions downstream of multiple PRRs (Bi et al., 2018), the mechanism for MAPKKK3/5 activation following receptor complex formation has been debated. Several members of the RLCK VII subfamily, which contains 46 RLCKs in 9 subclades (Rao et al., 2018), associate with MAPKKK5 *in vivo* (Bi et al., 2018). While BIK1 and PBL1 belong to RLCK VII subclade 8 (hereafter referred to as RLCK VII-8), they do not associate with MAPKKK5 in yeast 2-hybrid assays and loss-of-function mutants have normal immune-induced MAPK activation (Feng et al., 2012; Yamada et al., 2016). Members of RLCK VII-4 can phosphorylate MAPKKK5 *in vitro* at Ser-599 to promote MPK3/6 activation (Bi et al., 2018). A member of RLCK VII-1, PBL27, also phosphorylates MAPKKK5 at six different residues to promote MPK3/6 activation (Yamada et al., 2016), though this could not be reproduced genetically, even in septuple loss-of-function mutants for the entire RLCK VII-1 clade (Bi et al., 2018). Interestingly, the rice ortholog of PBL27, OsRLCK185, also phosphorylates the MAPKKK5 ortholog OsMAPKKK18 *in vitro* (Yamada et al., 2017), highlighting that RLCK VII-mediated MAPKKK5 activation may require validation in both model systems. A third regulator downstream of PRR activation, the RLCK XII subfamily member BSK1, phosphorylates MAPKKK5 at Ser-289 and this may be necessary for MAPKKK5-mediated resistance to *P. syringae* pv. *tomato* DC3000 (Yan et al., 2018). In essence, activation of MAPKKK5 could be facilitated by multiple RLCKs downstream of PRR complex formation, though additional work may be needed to confirm existing data. The immune-induced MAPK activation phenotype of *mapkkk5* lines is also a point of debate, as plants can exhibit either wild-type (Bi et al., 2018; Sun et al., 2018) or reduced MPK3/6 activation (Yamada et al., 2016) following PAMP treatment. However, *mapkkk5 mapkkk3* mutants consistently have reduced MAPK activation after elicitation (Bi et al., 2018; Sun et al., 2018), suggesting that MAPKKK3/5 function redundantly in this cascade. Typical of a canonical MAPK cascade, MAPKKK3/5 associate with MKK4/5 *in vivo*, and MAPKKK5 can phosphorylate the activation motif of MKK4/5 *in vitro* (Yamada et al., 2016; Sun et al., 2018). MKK4/5 then redundantly activate MPK3/6 to complete the cascade (Asai et al., 2002), and MPK6 may further activate MAPKKK5 through phosphorylation at Ser-682 and Ser-692 in a positive feedback loop (Bi et al., 2018). MPK3/6 also act on multiple downstream targets, such as ACC SYNTHASE 2 and 6 which catalyze the rate-limiting step in ethylene biosynthesis, and WRKY33 which facilitates the transcription of camalexin biosynthetic genes (Liu and Zhang, 2004; Li et al., 2012).

Few other MEKK-like MAPKKK members have been implicated in plant innate immunity aside from these fully resolved cascades. While the MAPKKK7 negatively regulates flg22-mediated basal immunity in association with FLS2 (Mithoe et al., 2016), no downstream targets have been identified to assess its role in signal transduction. As many Raf-like and ZIK-like MAPKKKs remain uncharacterized, these protein kinase families may contain novel signalling nodes in the positive and negative regulation of basal defense.

1.4. Raf-like MAPKKKs function in development and stress tolerance

Plant Raf-like MAPKKKs share sequence similarity with both animal mixed-lineage kinases (MLKs) and Raf-like kinases, and are classified based on the conserved consensus motif GTxx(W/Y)MAPE in their catalytic domain (Suarez-Rodriguez et al., 2010). As several animal MLKs phosphorylate non-MAPKK substrates (Suarez-Rodriguez et al., 2010), the role of plant Raf-like MAPKKKs as *bona fide* MAPKKKs has been questioned. Though direct phosphorylation of a MAPKK by a Raf-like MAPKKK has not been reported in Arabidopsis, several members of this family function upstream of MAPKKs in signalling pathways (Yoo et al., 2008; Zhao et al., 2014). Identifying targets of Raf-like MAPKKK family members could play a fundamental role in classifying this divergent group of plant protein kinases.

Both Raf-like MAPKKK Subgroup B and C family members have been implicated in plant responses to abiotic stress, pathogen infection, hormone biosynthesis, and developmental cues (Meng and Zhang, 2013; Jagodzik et al., 2018). In Subgroup B, EDR1 negatively regulates innate immunity by modulating the accumulation of MKK4/5 (Zhao et al., 2014). Accordingly, loss-of-function *edr1* lines display enhanced resistance to both *P. syringae* pv. *tomato* DC3000 and have increased defense gene induction following pathogen infection (Zhao et al., 2014). Another Subgroup B member, CTR1, negatively regulates ethylene signalling downstream of two receptors, ETHYLENE RECEPTOR 1 and ETHYLENE RESPONSE SENSOR (Clark et al., 1998). Though the exact biochemical mechanism is unknown, CTR1 inhibits MKK9-mediated phosphorylation of MPK3/6 in the absence of ethylene (Yoo et al., 2008). Upon ethylene perception, CTR1 is inactivated to promote MPK3/6 activation and subsequent phosphorylation of the ethylene-responsive transcription factor ETHYLENE INSENSITIVE 3 (Tanimoto et al., 1995; Yoo et al., 2008). While the remaining 20 members of Subgroup B are mostly unstudied, the CTR1- and EDR1-related SUGAR INSENSITIVE 8 negatively regulates salt tolerance (Gao and Xiang, 2008) and two other members, Raf10 and Raf11, play a redundant role in the positive regulation of seed dormancy (Lee et al., 2015b).

The Raf-like MAPKKK Subgroup C contains 26 members and can be further divided into seven subclades (C1-C7) (MAPK Group, 2002). At the plasma membrane, the Subgroup C1 INTEGRIN-LINKED KINASE 1 promotes accumulation of the K^+ transporter HIGH AFFINITY K^+ TRANSPORTER 5 to mediate ion flux upon flg22 perception (Brauer et al., 2016). Other Subgroup C1 members include VH1-INTERACTING KINASE which functions in vacuolar monosaccharide accumulation (Wingenter et al., 2011), and BLUE LIGHT-DEPENDENT H^+-ATPASE PHOSPHORYLATION which facilitates stomatal opening under high levels of blue light (Hayashi et al., 2017), thus enabling gas exchange during photosynthetically favourable conditions. All three Subgroup C2 members phosphorylate chloroplast precursor proteins and act redundantly to regulate chloroplast development (Martin et al., 2006; Lamberti et al., 2011), while no members of Subgroup C3 or C4 have been functionally characterized. Two members of Subgroup C5, Raf43 and HIGH LEAF TEMPERATURE 1 (HT1), play a role in multiple abiotic stress responses and CO_2-induced stomatal closure, respectively (Hashimoto et al., 2006; Virk et al., 2015). In particular, HT1 negatively regulates anion efflux in guard cells under low levels of intracellular CO_2, and is repressed under high CO_2 to promote anion channel activation and facilitate stomatal closure (Tian et al., 2015). As both water vapour and CO_2 are exchanged through the stomatal pore, this prevents water loss when carbon uptake is not required. Both members of Subgroup C6, Raf22 and Raf28, function redundantly to regulate embryo development (Wang et al., 2018a), though Raf22 also promotes seed oil accumulation independently of Raf28 (Ramachandiran et al., 2018). Finally, Raf-like MAPKKK Subgroup C7 members were not functionally characterized until recently, when two members were identified in a phosphoproteomic screen for regulators of blue light signalling (Hiyama et al., 2017). Both Raf38 and Raf33, also known as CONVERGENCE OF BLUE LIGHT AND CO_2 1 and 2 (CBC1/2) respectively, function redundantly to positively regulate blue light- and CO_2-induced stomatal opening (Hiyama et al., 2017). In the presence of blue light, activated PHOTOTROPIN 1 and 2 receptors facilitate H^+-ATPase-mediated plasma membrane hyperpolarization, which results in stomatal opening and increased gas exchange at the stomatal pore (Kinoshita et al., 2001). Anion channels such as SLOW ANION CHANNEL ASSOCIATED 1 (SLAC1) are also deactivated following blue light perception to inhibit membrane depolarization (Marten et al., 2007). In the presence of high intracellular CO_2, the protein kinase OPEN STOMATA 1 activates SLAC1 to trigger an anion efflux and ultimately cause stomatal closure (Xue et al., 2011). To increase carbon uptake under low CO_2, HT1 inhibits OPEN STOMATA 1 activation and facilitates SLAC1 inactivation (Tian et al., 2015), which in turn enhances water uptake in guard cells and results in stomatal opening. Both Raf33 and Raf38 function in the same pathway as SLAC1 and may be acting upstream of this anion channel based on epistatic analysis (Hiyama et al., 2017). Raf33 and Raf38 are also phosphorylated by HT1 and only Raf38 is phosphorylated by PHOTOTROPIN 1 *in vitro* (Hiyama et al., 2017), suggesting that these Subgroup C7 members may integrate signals from both pathways to regulate stomatal opening. The remaining three members of the Raf-like MAPKKK Subgroup C7 are Raf26, Raf39, and MRK1, and little is currently known about their function. The protein kinase AVRPTO PROXIMAL KINASE 2 from *Nicotiana benthamiana* shares 72% amino acid identity with AtRaf39 and was identified as a proximal protein to the *P. syringae* pv. *tomato* effector AvrPto in biotin labelling assays (Conlan et al., 2018). Though MRK1 homologs have not been studied, expression of *MRK1* increases by 10-fold in Arabidopsis after a two-hour treatment with damage-associated OGs (Moscatiello et al., 2006). Importantly, MRK1 protein abundance is reduced by 50% in plasma membrane fractions following flg22 treatment (Benschop et al., 2007), suggesting that it may be translocated or degraded upon elicitor detection. Taken together, Arabidopsis Raf-like MAPKKKs appear to play diverse and complex roles in multiple signalling cascades downstream of receptor complex activation. Based on evidence from large-scale datasets and other model species, the functional characterization of unstudied Raf-like MAPKKK members may assist in identifying novel signalling nodes in plant innate immunity or in other stress response pathways.

1.5. Research objectives

As CPK28 mediates BIK1 turnover downstream of multiple PRRs (Monaghan et al., 2014; Wang et al., 2018b), it could serve as a bait protein to identify novel positive and negative regulators of immunity in several pathways. In collaboration with Frank Menke (Sainsbury Lab, UK), our lab previously conducted an investigation of *in vivo* CPK28-associated proteins through affinity purification of CPK28 and its putative interacting partners from *cpk28-1/CPK28-YFP* or kinase-dead *cpk28-1/CPK28^{D188A}-YFP* stable lines both before and after elf18 treatment, alongside plasma-membrane GFP controls (Bender et al., 2017). This was followed by protein digestion and peptide sequencing via liquid chromatography (LC) and tandem mass spectrometry (MS-MS), generating a large dataset of putative interactors that associated specifically with CPK28 or CPK28^{D188A} but not with plasma-membrane controls. From this list, we identified two protein families of interest that were relatively uncharacterized and had some support for their involvement in plant immunity: the Raf-like MAPKKK Subgroup C7 family (containing MRK1, Raf26, Raf39, Raf33, and Raf38) and the PP2A-B subunits (containing PP2A-Bα and PP2A-Bβ) . Within these families, both PP2A-B subunits and MRK1 were identified as putative CPK28-associated proteins in the LC-MS/MS screen. While MRK1 function has not been established, both PP2A-B subunits play a role in regulating flowering time and nitrogen assimilation in Arabidopsis (Heidari et al., 2011; Heidari et al., 2013). The primary aim of this thesis work was to examine the role of MRK1 and related Raf-like MAPKKK Subgroup C7 members in regulating Arabidopsis innate immunity. I hypothesized that MRK1 may function redundantly with Subgroup C7 members to regulate immune responses downstream of PRR activation, and that MRK1 may associate with CPK28. A secondary aim of this work was to assess the role of PP2A-B subunits in the Arabidopsis innate immune response. These protein families were analyzedthrough the following specific objectives: (1) characterize loss-of-function Raf-like MAPKKK Subgroup C7 and PP2A-B mutants to analyze their role in immunity, (2) confirm association of MRK1 and CPK28 *in vivo*, and (3) determine the subcellular localization of MRK1. This work will provide foundational knowledge and a toolkit for the assessment of these previously understudied protein families. By identifying novel signalling nodes in plant innate immunity, we may be able to engineer pathogen-resistant crop strains to combat the global threat of agricultural disease.

2. MATERIALS AND METHODS

2.1. Molecular cloning

2.1.1. Gibson assembly

Several *MRK1* (AT3G63260) constructs were obtained from the Arabidopsis Biological Resource Center (ABRC) for use in Gateway cloning (Invitrogen) and *in planta* expression (Appendix Table 1). Gibson assembly (Gibson et al., 2009) was performed to generate other Gateway-compatible MRK1 entry clones to develop additional *in planta* expression vectors. As some destination vectors contained an existing promoter, entry clones containing either no promoter or the native *MRK1* promoter were generated. For a *pENTR-MRK1* clone with no promoter, the *MRK1* coding sequence was PCR-amplified from an existing ABRC construct using Q5 DNA polymerase (New England Biolabs) with Gibson-compatible primers (Appendix Table 2). An insert fragment containing genomic *MRK1* and a predicted promoter sequence (1000 bp upstream of the start codon) was similarly amplified from Arabidopsis ecotype Columbia (Col-0) gDNA. The pENTR backbone (Invitrogen) was PCR-amplified and digested with *DpnI* at 37°C for 3 h to remove any *E.coli*-derived template. All insert and backbone fragments were either desalted or gel extracted using a GenepHlow™ Gel/PCR kit (Geneaid), and concentration was quantified using a NanoDrop™ One spectrophotometer (ThermoFisher Scientific). Gibson assembly was performed at 50°C for 30 min using Gibson Assembly® Master Mix (New England Biolabs) with 0.02 pmol of backbone fragment and 0.06 pmol of insert fragment. Chemically competent TOP10 *E. coli* (Invitrogen) were transformed with the Gibson product by heat-shock, and successful colonies were screened by restriction digest and verified by Sanger sequencing (The Centre for Applied Genomics, Toronto) with gene- and backbone-specific primers (Appendix Table 2).

2.1.2. Gateway cloning

The Gateway cloning system (Invitrogen) was used to generate GFP-tagged plant expression vectors for MRK1, as well as nYFP- or cYFP-tagged clones for use in bimolecular fluorescence complementation (BiFC) (Appendix Table 1). *pUBC-pUBQ10:nYFP* and *pUBC-pUBQ10:cYFP* destination vectors were kindly provided by Geoff Wasteneys (University of British Columbia) and have been previously described (Grefen et al., 2010). Gateway reactions were performed using 150 ng of the entry vector, 75 ng of the destination vector, Tris-EDTA buffer (pH 8), and 0.5 µL of LR Clonase II™ Enzyme mix (Invitrogen), in a total reaction volume of 2.5 µL. Following incubation at 25°C overnight, reactions were terminated through incubation with 0.5 µL of Proteinase K (Invitrogen) at 37°C for 30 min. Chemically competent TOP10 *E. coli* (Invitrogen) were transformed with the entire reaction product by heat-shock, and successful colonies were identified by colony PCR and verified by Sanger sequencing (The Centre for Applied Genomics, Toronto) with gene- and backbone-specific primers (Appendix Table 2).

2.2. Plant materials and growth conditions

2.2.1. Plant growth conditions

Arabidopsis was grown in an Econair AC-60 growth chamber under 10-h-light/14-h-dark cycle at 22°C, with 30% relative humidity and a light intensity of 150 µE m^2 s^{-1}. Unless otherwise specified, Arabidopsis seeds were suspended in a 0.1% (w/v) agar solution and cold-stratified at 4°C for 24-72h. Seeds were sown in circular 6.5 cm pots containing Sunshine Mix #1 (Sun Gro Horticulture), and transplanted to either circular 6.5 cm pots for photographing developmental stages, square 10 cm pots for *Agrobacterium*-mediated floral dips, or 72-well trays for bioassays. Plants were fertilized biweekly using a 1g/L solution of 20:20:20 N:P:K and bioassays were performed at 5-6 weeks post-germination.

For Arabidopsis seedlings grown in sterile conditions, seeds were washed in 70% (v/v) ethanol for 1 min and incubated in 40% (v/v) bleach for 17 min on a rotating mixer. Seeds were rinsed four times in sterile ddH_2O, vortexed between each wash, centrifuged at 650 x *g* for 30 sec after the final wash, and resuspended in sterile 0.1% (w/v) agar (Bioshop Canada). The seeds were plated on Murashige and Skoog (MSO) agar medium (0.5X MSO with vitamins (Cedarlane Labs), 0.8% agar) containing an appropriate selection marker (Appendix Table 3) and cold-stratified at 4°C for 48-72h. Plates were incubated at room temperature with a light intensity of approximately 50 $\mu E\ m^2\ s^{-1}$. For plants grown in liquid culture, seedlings were transplanted to sterile 6-well culture plates (Corning Incorporated Costar) containing liquid MSO medium (0.5X MSO with vitamins (Cedarlane Labs), 1% (w/v) sucrose) after 4 d of growth and returned to the cart for 7-10 d prior to collection.

N. benthamiana was grown in an Adaptis A1000 growth chamber (Conviron) under a 16-h-light/8-h-dark cycle at 22˚C, with 30% relative humidity and a light intensity of 150 $\mu E\ m^2\ s^{-1}$, or at room temperature (22-25°C) with a light intensity of approximately 50 $\mu E\ m^2\ s^{-1}$. Plants were fertilized once a week using a solution of 1g/L 20:20:20 of N:P:K and 0.3g/L iron. *N. benthamiana* were grown for 4-5 weeks prior to *Agrobacterium*-mediated transient transformation, and were maintained by Danalyn Holmes, Jeffrey Rowbottom, and Irina Sementchoukova. Both *N. benthamiana* and Arabidopsis soil plants were grown in the Queen's Phytotron, which was maintained by Dale Kristensen.

2.2.2. Identifying homozygous T-DNA insertion lines

Segregating T-DNA insertion lines were obtained from the ABRC for each MAPKKK Subgroup C7 family member, and homozygous T-DNA insertion lines were kindly provided by Cathrine Lillo (University of Stavanger) for both PP2A-B subunits (Appendix Table 4). To identify or confirm homozygous T-DNA insertion lines, leaf tissue was pressed into Whatman® FTA® cards (GE Healthcare) and stored at room temperature for 1 h. A 1.5 mm biopsy punch (Integra Miltex) was used to remove one leaf disc from each FTA® leaf press, and leaf discs were incubated in 200 µL of 1X FTA buffer (10 mM Tris-HCl (pH 8), 2 mM EDTA, 0.1% Tween-20) for 30 min in an unskirted 96-well PCR plate (Diamed). Leaf discs were then washed twice in TE-1 buffer (10 mM Tris-HCl (pH 8), 0.1 mM EDTA) for 10 min each. A PCR master mix was applied containing 2.5 µL PCR buffer (0.5 M KCl, 15 mM $MgCl_2$, 100 mM Tris-HCl (pH 8)), 0.5 µL of 10 mM dNTPs, 0.5 µL of 10 µM forward and reverse primer, and 0.2 µL of GeneDireX *Taq* polymerase (Froggabio). PCR amplification was performed using the following thermocycler program: initial denaturation for 5 min at 94°C, followed by denaturation (per cycle) for 30 sec at 94°C, annealing (per cycle) for 45 sec at 55°C, extension (per cycle) for 2 min at 72°C, and a final extension for 10 min at 72°C, with 40 cycles total. An aliquot of 15 µL of each PCR product was visualized on a 1% (w/v) agarose gel containing ethidium bromide, using a MultiImage™ Light Cabinet transilluminator (Alpha Innotech). Homozygous plants were identified using both gene-specific primer sets (to establish homozygosity for the desired allele) and T-DNA-specific primer sets (to confirm presence of the insertion) (Appendix Table 5).

2.2.3. Genetic crosses

Crosses were performed to generate homozygous double null lines for MAPKKK Subgroup C7 family members, using closely related protein pairs to mitigate against functional redundancy (Appendix Table 4). For female donors, unopened buds were demasculated to expose the carpel, and cross-pollination was performed using a developed flower from the male donor. Elongated siliques were allowed to dry and were harvested, and the presence of T-DNA insertions for both alleles was confirmed in the F_1 generation through PCR-based genotyping (see Section 2.3.2). In the F_2 generation, plants segregating at both alleles were sown and transplanted to soil, and homozygous double null lines were identified through gene-specific and T-DNA-specific PCR-based genotyping (see Section 2.3.2). Several crosses were kindly performed by Jacqueline Monaghan (Appendix Table 4).

2.2.4. *Agrobacterium*-mediated floral dip

To generate *MRK1* overexpression lines in a Col-0 background and complementation lines in a *mrk1-1* null background, *Agrobacterium*-mediated floral dip was performed. Electrocompetent *Agrobacterium tumefaciens* GV3101 cells were transformed with either *pK7FWG2-35S:cMRK1-GFP* or *pGWB4-pMRK1:gMRK1-GFP* through electroporation, and grown on Luria-Bertani (LB) plates containing the appropriate antibiotics at 28°C for 48 h. A single colony was used to inoculate a 5 mL liquid LB culture containing antibiotics and was grown at 28°C for 12-16 h. A larger 200 mL liquid LB culture containing antibiotics was inoculated using 2-4 mL of the 5 mL culture, and grown at 28°C for 16-24 h until an OD_{600} of 0.8 was reached. Cells were harvested through centrifugation at 4424 x *g* for 20 min in an Avanti® J-E high-speed centrifuge (Beckman Coulter) with a JA-10 rotor (Beckman Coulter) at room temperature. The pellet was resuspended in 50 mL of a 5% sucrose solution and diluted to a final OD_{6oo} of 0.8. Prior to floral dip, 0.05% Xiameter OFX-8803 was added to each culture. Col-0 and *mrk1-1* plants were grown in long-day conditions (14-h-light/10-h-dark cycle, 22°C, 150 μE m^2 s^{-1} light intensity) for 4-5 weeks, and bolts were trimmed to induce branching and bud formation at 6-7 d before transformation. For each genetic background, 20 plants were inverted in either *pGWB4-pMRK1:gMRK1-GFP* or *pK7FWG2-35S:cMRK1-GFP* suspensions for 30 sec, and placed on their side in a dark, humid environment overnight to facilitate transformation (Clough and Bent, 1998). Seed was harvested at 4 weeks post-transformation, and T_1 transgenics were selected on MSO plates containing appropriate antibiotics (Appendix Table 3) as described in Section 2.3.1. T_1 plants were transplanted to soil after 10 d of selection, grown in short-day conditions (see Section 2.3.1), verified for genetic background in *mrk1-1* plants through PCR-based genotyping with T-DNA specific primers (Appendix Table 5), verified for *MRK1-GFP* expression through immunoblotting, and allowed to self-fertilize. T_2 plants were similarly selected on MSO medium containing antibiotics to identify lines with a single, dominant T-DNA insertion, as these lines would segregate to produce a 3:1 ratio of alive:dead seedlings. Finally, T_2 plants were allowed to self-fertilize, and homozygous T_3 lines were identified through segregation analysis as those with a 100% survival rate upon antibiotic selection. Transgenic material generated through *Agrobacterium*-mediated floral dip is listed in Appendix Table 3.

2.3. *Agrobacterium*-mediated transient transformation of *Nicotiana benthamiana*

Electrocompetent *Agrobacterium* GV3101 cells were electroporated with the desired plant expression vector and transformants were grown on LB plates containing appropriate antibiotics at 28˚C for 48 h. A single colony was transferred to liquid LB media with antibiotics, and grown for 12-16 h at 28˚C. Cells were pelleted gently at 600 x *g* for 15 min, resuspended in an induction buffer (10 mM $MgCl_2$, 10 mM MES (pH 6.3)), incubated for 2-3 h at room temperature, and normalized to OD600 = 0.2 – 0.3 using a multi-mode microplate reader with the absorption module (SpectraMax Paradigm). Fully expanded, upper leaves were selected from 4-5 week-old *N. benthamiana* plants for transformation. All constructs were transformed alongside viral suppressor P19 (Lakatos et al., 2004), and leaves were infiltrated on the abaxial side using a 1 mL needleless syringe. Tissue for co-immunoprecipitation (coIP), BiFC, and subcellular localization was harvested at three days post-infiltration (dpi).

2.4. Co-immunoprecipitation

Four-week-old *N. benthamiana* plants were infiltrated with *A. tumefaciens* containing *MRK1* and *CPK28* plant expression vectors (Appendix Table 1), and whole leaves were harvested at 3 dpi. Leaves were halved, each half was vacuum-infiltrated with ddH_2O or 100 nM flg22 (EZ Biolab), and all tissue was flash-frozen in liquid N_2 approximately 10 min post-infiltration. Frozen tissue was ground in liquid N_2 in a cooled mortar and pestle, and protein was extracted at 4˚C using an extraction buffer (5 mM dithiothreitol (DTT), 1% (v/v) protease inhibitor P9599 (Sigma Aldrich), 1% (v/v) Igepal, 2 mM Na_2MoO_4, 2.5 mM NaF, 1.5 mM activated Na_3VO_4, 50 mM Tris-HCl pH 7.5, 150 mM NaCl, 1 mM phenylmethylsulfonyl fluoride). Tissue was then pelleted by centrifugation at 11500 x *g* for 30 min at 4˚C, and the supernatant was filtered once through miracloth. Protein concentrations were determined using a Coomassie G-250 Protein Assay Kit (ThermoFisher Scientific) using bovine serum albumin as a protein standard. A 50 μL aliquot of each sample was set aside for later use as an input fraction, and the remaining protein extracts were incubated with 15 μL of α-GFP μMACs microbeads (Miltenyi Biotec) for 3 h with shaking at 4˚C. μMACs magnetic columns were equilibrated using wash buffer (20 mM Tris-HCl, 150 mM NaCl, 1% (v/v) protease inhibitor P9599 (Sigma Aldrich), 1 mM DTT, 1% (v/v) Igepal), and total protein samples were applied. Columns were washed three times using wash buffer, and bound proteins were eluted with 30 μL of the supplied μMACs elution buffer (50 mM Tris-HCl (pH 6.8), 50 mM DTT, 1% (w/v) SDS, 0.005% (w/v) bromophenol blue, 10% (v/v) glyercol), which was pre-heated to 80˚C. Eluted proteins were then separated by SDS-PAGE and analyzed by immunoblotting.

2.5. Sodium dodecyl sulfate (SDS)-polyacrylamide gel electrophoresis (PAGE) and immunoblotting

Apart from coIP samples eluted in μMACs elution buffer, all protein samples were denatured at 80˚C for 5 min in 50 μL of Laemmli sample buffer with DTT (44% glycerol, 1% SDS, 0.28 M Tris (pH 6.8), 0.6 mM bromophenol blue, 50 mM DTT) and centrifuged for 1 min at 6700 x *g*. A 12-15μL aliquot of each sample was loaded on a 10% SDS polyacrylamide mini-gel using a Bio-Rad PROTEAN III system and separated at 75 V for 40 min followed by 150 V for 50 min in 1x SDS running buffer (25 mM Tris-HCl (pH 6.8), 190 mM glycine, 0.1% (w/v) SDS). Proteins were then transferred to an EtOH-activated polyvinylidene difluoride (PVDF) membrane at 100 V for 1 h at 4˚C in a wet transfer buffer (25 mM Tris-HCl (pH 6.8), 190 mM glycine, 20% EtOH). For MAPK activation assays, proteins were transferred to an EtOH-activated PVDF membrane using a semi-dry Trans-Blot Turbo transfer system (Bio-Rad) at 25 V for 10 min in Towbin buffer (25 mM Tris-HCl (pH 6.8), 190 mM glycine, 20% MeOH). Membranes were blocked in a 5% milk/Tris-buffered saline (TBS)-Tween (20 mM Tris-HCl (pH 6.8), 150 mM NaCl, 0.1% Tween-20 (Bioshop Canada)) solution for 1 h at room temperature, and incubated in the appropriate primary antibody for 12-16 h at 4˚C. All antibodies and titers that were used are listed in (Appendix Table 6). Should the primary antibody not have been conjugated to horseradish peroxidase (HRP), the membrane was washed in TBS-Tween three times for 10 min each, and incubated in an α-mouse-HRP (Sigma Aldrich, 1:10000) or an α-rabbit-HRP (Sigma Aldrich, 1:10000) secondary antibody for 1 h at 4˚C. All membranes were washed twice in TBS-Tween and once in TBS (20 mM Tris-HCl pH 6.8, 150 mM NaCl) for 10 min prior to enhanced chemiluminescence (ECL) detection. Membranes were treated with Clarity™ or Clarity Max™ ECL reagent (Bio-Rad) and visualized on a ChemiDoc™ Touch Imaging System (Bio-Rad).

2.6. Confocal microscopy

For BiFC and MRK1 subcellular localization in *N. benthamiana*, four-week-old plants were transiently transformed with nYFP- and cYFP-tagged constructs or *MRK1-GFP* constructs, respectively (see Section 2.4). Leaf discs were sampled at 3 dpi using a 4 mm biopsy punch (Integra Miltex), and were wet mounted with the abaxial surface facing upwards prior to confocal imaging. Imaging was performed using a Zeiss LSM 710 confocal microscope with excitation at 488 nM for GFP/YFP and a range of 510-540 nM for measuring emission. To detect chlorophyll autofluorescence or mCherry fluorescence, an excitation wavelength of 543 nM and a range of 680-760 nM for detecting emission was used. Following imaging, leaf discs from MRK1 subcellular localization were flash-frozen in liquid N_2 and assayed for *MRK1-GFP* expression through SDS-PAGE and α-GFP immunoblotting (see Section 2.6). As nYFP- and cYFP-specific antibodies were unavailable, similar assays could not be performed on leaf discs from BiFC.

2.7. RNA extraction, cDNA synthesis, and qRT-PCR

RNA extraction was performed using an Aurum™ Total RNA Mini Kit (Bio-Rad). Briefly, either seedlings from sterile 6-well culture plates or whole leaves from 4-5 week-old soil plants were flash-frozen in liquid N_2 and ground finely using a mortar and pestle. Tissue was disrupted in Aurum™ lysis buffer supplemented with 2% polyvinylpyrrolidone-40 through vortexing, and the supernatant was combined with 70% ethanol before passing through an RNA binding column. The column was washed once using Aurum™ low stringency wash solution, and incubated with RNase-free DNase I for 15 min. The column was then washed once with Aurum™ high stringency wash solution and once with Aurum™ low stringency wash solution, prior to eluting total RNA in 40 μL of diethyl pyrocarbonate-treated water. RNA quality was confirmed through visualization of 18S and 28S rRNA banding on a 1% agarose gel and RNA concentration was determined using a NanoDrop™ One spectrophotometer (ThermoFisher Scientific).

Reverse transcription (RT) was carried out using 2 μg of total RNA, 1 μL of oligo(dT)20, 0.5 mM dNTPs (FroggaBio), 1X First-Strand Buffer (Invitrogen), 1 μL of RNaseOUT™ Recombinant RNase Inhibitor (Invitrogen), 5 mM DTT, and 1 μL of SuperScript™III Reverse Transcriptase (Invitrogen). This was incubated at 50˚C for 1 h, followed by inactivation at 70˚C for 15 min. All samples were diluted using 60 μL ddH_2O.

RT-PCR was performed using 0.2 μL of 10 μM forward and reverse primer, 1 μL of diluted cDNA, and 5 μL of SsoAdvanced™ Universal SYBR® Green Supermix, in a total reaction volume of 10 μL. Reactions were prepared in skirted, white Hard-Shell® 96-Well PCR plates (Bio-Rad), sealed with Microseal® 'B' seals (Bio-Rad) and placed in a CFX96 Touch™ Real-Time PCR Detection System (Bio-Rad) with the following program: Initial denaturation for 2 min at 95°C, followed by denaturation (per cycle) for 5 sec at 95°C, and annealing (per cycle) for 15 sec at 60°C, with 45 cycles total. Fluorescence was recorded during the annealing step, and each primer set (Appendix Table 5) was subjected to melting curve analysis to ensure that it produced a single amplicon.

2.8. Immune-induced oxidative burst assay

For each genotype, six leaf discs were sampled from 5-6 week-old plants using a 4 mm biopsy punch (Integra Miltex), and placed in 100 μL of ddH_2O in a white, skirted 96-well plate (Caplugs Evergreen) overnight. Following overnight recovery, ddH_2O was removed using a multi-channel pipette and replaced with 100 μL of reaction solution (100 μM luminol (Sigma-Aldrich), 10 μg/mL HRP (Sigma-Aldrich), and either 100 nM of synthesized flg22 or elf18 peptide (EZ

Biolabs) or 500 nM of synthesized AtPep1 peptide (EZ Biolabs)). Luminescence was immediately measured using a SpectraMax Paradigm Multi Mode Microplate Reader with a LUM Module over a 40 min period with a 2 min interval and a 1 sec integration time.

2.9. MAPK activation assay

To test immune-induced MAPK activation in null lines for MAPKKK Subgroup C7 family members, seeds were surface-sterilized, cold stratified at 4°C for 72 h, and transplanted to sterile 6-well culture plates after 4 d of growth (see Section 2.3.1). After 7 d in liquid culture, seedlings were treated with either ddH_2O ("mock") or 200 nM elf18 (EZ Biolabs), and immune-treated samples were flash-frozen after 5, 10, and 30 min. Tissue was ground in liquid N_2 with a mortar and pestle, total protein was extracted, and protein concentration was normalized using a Coomassie G-250 Protein Assay Kit (ThermoFisher Scientific) (see Section 2.5). Samples were separated by SDS-PAGE and transferred to an EtOH-activated PVDF membrane through semi-dry transfer (see Section 2.6). Membranes were blocked in a 5% milk/TBS-Tween solution overnight, and immunoblotting was performed using a phosphosite-specific -p44/42 MAPK (EXTRACELLULAR SIGNAL-REGULATED KINASE 1/2) (Thr202/204) antibody (Cell Signaling Technology) (see Appendix Table 6). Immune-induced phosphorylation of MPK 3/4/6/11 (Petersen et al., 2000; Asai et al., 2002; Eschen-Lippold et al., 2012) was visualized using Clarity Max^{TM} ECL reagent (Bio-Rad).

2.10. Immune-induced stomatal aperture assay

For each genotype, twelve whole leaves were submerged in stomatal opening buffer (50 mM KCl, 10 mM MES-KOH (pH 6.15), 10 μM $CaCl_2$, and 0.01% Tween 20), placing six leaves each in two beakers containing 50 mL of buffer. Leaves were placed in an Econair AC-60 growth chamber (see Section 2.3.1) for 2 h, then 5 μM flg22 (EZ Biolabs) was added to one beaker for 1

h. Leaves were removed from the buffer and dried, and the abaxial surface of each leaf was coated with a fine layer of Sally Hansen® Hard As Nails® Xtreme Wear® Nail Color Invisible as described (Wu and Zhao, 2017). After 10 min of setting, epidermal peels were taken and stomatal aperture was imaged at 400x magnification using an Axio Imager M2 microscope (Zeiss). Stomatal width and length were measured using ImageJ 1.52a, and the stomatal aperture index was calculated using the following formula: (Stomatal Aperture Width in μM)/(Stomatal Aperture Length in μM).

2.11. Immune-induced phosphorylation assay

Twelve whole leaves from 5-week-old *mrk1-1/35S:cMRK1-GFP 1* plants were vacuum-infiltrated with either ddH_2O or 200 nM elf18 for 20 min and flash-frozen in liquid N_2. Total protein was extracted and normalized using a Coomassie Protein Assay Kit (ThermoFisher Scientific) (see Section 2.5). Immunoprecipitation (IP) of *MRK1-GFP* was performed using 15 μL of α-GFP μMACs microbeads (Miltenyi Biotec), washing the μMACs magnetic columns six times with wash buffer, and eluting in 50 μL of preheated μMACs elution buffer (see Section 2.6). Eluted proteins were separated by SDS-PAGE and analyzed by α-GFP immunoblot to detect MRK1-GFP accumulation (see Section 2.6) or by pIMAGO™-biotin Phosphoprotein Detection Kit (Tymora Analytical Operations) for total phosphorylated protein. For pIMAGO™, proteins were transferred to an EtOH-activated PVDF membrane by wet transfer (see Section 2.6) and incubated in 1X pIMAGO™ blocking buffer at 4°C overnight. Membranes were then incubated in pIMAGO™ reagent (1:1000) in 1X pIMAGO™ buffer for 1h at room temperature, and washed three times with the provided 1X wash buffer and once with TBS-Tween. The avidin-HRP antibody (1:1000) in 1X pIMAGO™ blocking buffer was applied for 1 h at room temperature, and the membrane was washed three times with TBS-Tween and once with TBS prior to imaging with Clarity™ ECL reagent and Chemidoc Imaging System (Bio-Rad).

3. RESULTS

3.1. Identification of MRK1 as a putative CPK28-associated protein in an immunoprecipitation (IP)-mass spectrometry (MS) screen

A list of putative CPK28 interactors was previously generated through treatment of *cpk28-1/CPK28-YFP* or kinase-dead *cpk28-1/CPK28^{D188A}-YFP* lines with or without elf18, followed by affinity purification of CPK28 and LC/MS-MS to identify associated proteins, as described (Bender et al., 2017). Tryptic peptides corresponding to the putative MAPKKK, MRK1, were found in both CPK28-YFP and CPK28^{D188A}-YFP immunoprecipitates, as well as before and after PAMP treatment (Figure 1A). Importantly, MRK1 was not identified in immunoprecipitates from the plasma membrane LOW TEMPERATURE-INDUCED PROTEIN 6B-GFP control ('PM-GFP') (Cutler et al., 2000), suggesting that association with CPK28 was specific (Figure 1A). MRK1 was previously classified as an Arabidopsis Raf-like MAPKKK based on a conserved consensus motif in the catalytic domain, GTxx(W/Y)MAPE (MAPK Group, 2002; Suarez-Rodriguez et al., 2010). MRK1 also has three predicted domains based on protein sequence analysis: (1) A short N-terminal domain, (2) a kinase domain containing the consensus motif, and (3) a short C-terminal domain (Figure 1B). Belonging to the Arabidopsis Raf-like MAPKKK Subgroup C7, MRK1 has four closely-related family members: Raf26, Raf39, Raf33, and Raf38 (Figure 1C) (MAPK Group, 2002). While no established function has been discerned for MRK1, Raf26 or Raf39, both Raf33 and Raf38 have been shown to facilitate stomatal opening under photosynthetically favourable conditions such as high levels of blue light (Hiyama et al., 2017). To determine the level of protein sequence similarity shared between Raf-like MAPKKK Subgroup C7 members, I performed a multiple sequence alignment using Clustal Omega. MRK1 was found to have high sequence similarity to all four family members (RAF39 -

93%, RAF26 - 91%, RAF33 - 86%, and RAF38 - 81%), suggesting that they may be able to perform similar molecular roles within the cell (Figure 1C). Here, I examined the potential role of Raf-like MAPKKK Subgroup C7 members in the innate immune response.

3.2. Confirmatory protein-protein association assays between MRK1 and CPK28 are inconclusive

To validate the initial IP-MS screen, association between MRK1 and CPK28 was tested using two complementary *in vivo* approaches. First, MRK1-His and CPK28-YFP were transiently co-expressed in *N. benthamiana* and association was examined by coIP. MRK1-His was also expressed alone to serve as a negative control. Following affinity purification of CPK28-YFP, the presence of MRK1-His in CPK28 immunoprecipitates was analyzed by immunoblotting to detect association. While MRK1 co-immunoprecipitated with CPK28-YFP, it was also identified in the negative control, suggesting that MRK1 may be binding non-specifically (Figure 2A). As a result, the association of MRK1 and CPK28 could not be validated using the coIP technique.

I then tested association between MRK1 and CPK28 through BiFC. I transiently co-expressed CPK28-nYFP and MRK1-cYFP in *N. benthamiana* and tested for reconstitution of YFP using confocal microscopy. Association between MRK1 and BIK1 was also tested, as BIK1 is an established CPK28 interactor (Monaghan et al., 2014). Co-expression of MRK1 with CONSTITUTIVELY ACTIVATED CELL DEATH 1 (CAD1), an unrelated regulator of immunity (Morita-Yamamuro et al., 2005), served as a negative protein control, and co-expression of MRK1 with the empty nYFP vector was used as an additional negative control. Strong reconstitution of YFP was observed in both MRK1-CPK28 and MRK1-BIK1 samples (Figure 2B). However, a similar strength of signal was seen when MRK1 was co-expressed with either the negative protein control, CAD1, or the empty vector (Figure 2B). Assays performed in the reverse orientation using MRK1-nYFP had similar results (data not shown). This suggests that MRK1 may be promiscuously associating under constitutive expression for BiFC, and the association of CPK28 and MRK1 remained inconclusive.

3.3. Generating null mutant lines for Raf-like MAPKKK Subgroup C7 members

While association with CPK28 could not be validated, I sought to determine whether MRK1 or other Raf-like MAPKKK Subgroup C7 members could be playing a role in Arabidopsis immunity or development. First, expression profiles at different developmental stages were obtained for all Raf-like MAPKKK Subgroup C7 members using the eNorthern tool from the Bio-Analytic Resource for Plant Biology (BAR Version 15.08, http://bar.utoronto.ca/). *RAF26* and *RAF39* are highly expressed in mature pollen and weakly expressed at other stages (Figure 3A). *MRK1*, *RAF33*, and *RAF38* had mostly uniform expression across all developmental stages (Figure 3A). However, when examining expression profiles from specific cell types, *RAF33* and *RAF38* were strongly expressed in guard cells (Figure 3B), which corroborates their established role in blue light-induced stomatal opening (Hiyama et al., 2017).

Expression profiles following pathogen or elicitor treatment were also extracted for Raf-like MAPKKK Subgroup C7 members using the eNorthern tool (Toufighi et al., 2005). Expression of *RAF26* increased approximately 7-fold after treatment with the virulent biotrophic bacterial pathogen *P. syringae* pv. *maculicola* ES4326 or the avirulent strain ES4326 avrRpt2 (Figure 3C), which contains a copy of the AvrRpt2 effector from *P. syringae* pv. *tomato* and induces HR (Hendrickson et al., 2000). *RAF26* was also induced 12-fold following infection by the hemibiotrophic oomycete *Hyaloperonospora arabidopsidis* (Figure 3C). A portion of these assays were done in the *rpp4* background, as Arabidopsis plants containing a functional copy of the RPP4 immune receptor will induce an HR following *H. arabidopsidis* infection (van der

Biezen et al., 2002). *RAF26* expression additionally increased following infection with the necotrophic fungus *Botrytis cinerea* and the biotrophic fungus *Erysiphe orontii*, a pathogen that causes pea powdery mildew (Micali et al., 2008) (Figure 3C). While MRK1 and other Raf-like MAPKKK Subgroup C7 members had no striking changes in expression following immune induction (Figure 3C), these data may suggest an important role for Raf26 (and possibly related Raf-like MAPKKKs) in immune signalling.

To functionally characterize the Raf-like MAPKKK Subgroup C7 members, I obtained T-DNA insertion lines for each member through the ABRC (Figure 4A and Appendix Table 4). Where possible, multiple lines were obtained for each gene, as T-DNA insertion does not always disrupt gene function (O'Malley et al., 2015). All Raf-like MAPKKK Subgroup C7 members contain multiple introns and exons, and insertion lines within exons were obtained when available to increase the likelihood of interfering with coding regions (Figure 4A). T-DNA insertion lines were PCR-genotyped to homozygosity using gene-specific and insertion-specific primer sets (Appendix Table 5). As *RAF33* and *RAF38* evolved from a gene duplication event and exhibit functional redundancy in blue-light induced stomatal opening (Hiyama et al., 2017), I generated double null lines between all closely related Subgroup C7 members to ensure that any immune phenotypes were not masked by redundancy. From phylogenetic analyses, I also categorized the Raf-like MAPKKK Subgroup C7 into two subclades, Subgroup C7-1 and C7-2, which contain MRK1/Raf26/Raf39 and Raf33/Raf38, respectively (Figure 4A). Crosses were performed between homozygous insertion lines for the following related pairs within each subclade: (1) *RAF26* and *RAF39*, (2) *RAF33* and *RAF38*, (3) *RAF39* and *MRK1*, and (4) *RAF26* and *MRK1* (Figure 4A). To confirm that T-DNA insertion resulted in null alleles, RT-qPCR was performed using cDNA from the double mutant lines. In most lines, expression of the Raf-like

MAPKKK Subgroup C7 member was reduced in T-DNA insertion mutants relative to Col-0 (Figure 4B). However, expression of *MRK1* was increased in *mrk1-1* compared to wild-type, suggesting that this allele may not disrupt gene function. To assess the translated product of the *mrk1-1* insertion, the region surrounding the annotated insertion was PCR-amplified using T-DNA specific primers (Appendix Table 5) and Sanger sequenced. I found that the *mrk1-1* insertion results in a premature stop codon in the *MRK1* transcript and that the insertion site is slightly downstream from the annotated position (Figure 4C), indicating that this allele may still disrupt *MRK1* function. To assess the role of Raf-like MAPKKK Subgroup C7 members in growth and development at multiple stages, photos of rosettes for all double null lines were taken at 4 weeks (Figure 5A) and 6.5 weeks (Figure 5B) post-germination, though no developmental differences from Col-0 could be distinguished in vegetative rosettes. As *RAF26* and *RAF39* are highly expressed in pollen (Figure 3A), I assessed stem elongation and flowering phenotypes in all double lines following reproductive transition. Similar to earlier developmental stages, no phenotypic differences could be discerned in Raf-like MAPKKK Subgroup C7 double null lines relative to wild-type (Figure 5C).

3.4. MRK1, RAF26, and RAF39 may function redundantly to regulate early pattern-triggered immune responses

As MRK1 was identified as a putative CPK28-associated protein in the CPK28 IP-MS screen and its protein abundance is reduced by 50% in plasma membrane fractions following flg22 treatment (Benschop et al., 2007), coupled with the upregulation of *RAF26* following immune treatment (Figure 3C), I tested if the Subgroup C7-1 members may play a role in innate immunity. Upon pathogen perception, an apoplastic ROS burst is produced by RBOHD/F to serve as a signalling molecule and an antimicrobial agent (O'Brien et al., 2012). Quantification of this extracellular burst is commonly used as a marker for innate immune output in Arabidopsis (Bredow et al., 2019). Using a luminol-based method, I examined the ROS burst in single and double null lines for *MRK1*, *RAF26*, and *RAF39* following application of the bacterial elicitor elf18. In single mutants, ROS burst did not differ significantly from Col-0 upon immune elicitation (Figure 6A). However, *mrk1 raf39* and *mrk1 raf26* null lines displayed a significantly higher ROS burst than Col-0 following elf18 treatment in 8 of 12 technical replicates (Figure 6B), suggesting that these genes may be functioning redundantly to negatively regulate the immune-induced oxidative burst. Data from individual replicates are summarized in Appendix Table 7. Interestingly, no difference in ROS burst was observed in *raf26 raf39* mutants (Figure 6B), suggesting that the presence of MRK1 may be sufficient to elicit a wild-type oxidative burst. Similar results were obtained using the bacterial elicitor flg22 (Appendix Figure 1A) and the damage-associated elicitor AtPep1 (Appendix Figure 1B).

In parallel with ROS production, MAPK cascades are activated following pathogen perception to initiate downstream signalling and activate transcription factors (Thulasi Devendrakumar et al., 2018). As Raf-like MAPKKK Subgroup C7 members could function as upstream protein kinases in a MAPK cascade, I examined whether Subgroup C7-1 members play a role in immune-induced MAPK activation. Double *mrk1 raf39* and *mrk1 raf26* seedlings were treated with the bacterial elicitor elf18 and sampled at multiple time points over 30 min. Protein extracts were analyzed by immunoblot to detect activated MAPKs using a phosphosite-specific antibody for a conserved activation motif (pT-X-pY) (Taj et al., 2010), which can detect activated MPK3/4/6/11 following immune elicitation (Xu et al., 2014). As expected, activation of MPK3/4/6/11 was observed in Col-0 samples following immune induction, with peak MAPK activation occurring at 10 min following PAMP perception (Petersen et al., 2000; Asai et al., 2002; Eschen-Lippold et al., 2012) (Figure 6C). However, immune-induced MAPK activation was not substantially different in *mrk1 raf39* and *mrk1 raf26* lines, suggesting that the Subgroup C7-1 members negatively regulate RBOHD-mediated immunity but not the parallel MAPK pathway.

In addition to controlling water and CO_2 flux for photosynthesis, specialized guard cells on the leaf epidermis can limit pathogen entry by regulating stomatal aperture (Melotto et al., 2006). Upon pathogen recognition, apoplastic ROS is internalized through aquaporins, a family of water transport channels, causing cytosolic ROS accumulation (Rodrigues et al., 2017). While the ROS detection mechanism and downstream signalling remain unknown, this ultimately leads to stomatal closure (Rodrigues et al., 2017) and can serve as a physical barrier to infection. As *mrk1 raf39* and *mrk1 raf26* double null lines had increased PAMP-induced ROS production relative to Col-0 (Figure 6B), I examined whether these lines would also display aberrant stomatal closure following immune elicitation. I subjected *raf26 raf39*, *mrk1 raf39*, and *mrk1 raf26* lines to treatment with or without the bacterial elicitor flg22, and examined stomatal aperture using epidermal peels. I also assessed the *raf33 raf38* double null line for immune-induced stomatal aperture, as Raf33 and Raf38 play a redundant role in regulating blue light-induced stomatal opening (Hiyama et al., 2017) and may also regulate stomatal aperture upon pathogen detection. In all genotypes tested, significant differences in stomatal aperture were observed between “mock” and flg22-treated samples (Figure 6D), suggesting that immune-induced stomatal closure was not affected in the MAPKKK Subgroup C7 mutants. However, as it may be difficult to discern stomata with significantly smaller aperture relative to wild-type following immune induction, as would be expected for lines with increased apoplastic ROS production (ex. *mrk1 raf39* and *mrk1 raf26*), a more sensitive assay may be required to detect this phenotype (ex. assessing stomatal conductance through gas exchange). In agreement with published data (Hiyama et al., 2017), smaller stomatal aperture was observed for *raf33 raf38* mutants relative to Col-0 under "mock" conditions (Figure 6D).

To determine if Subgroup C7-2 members may also be regulating early immune outputs, I examined immune-induced ROS burst in null lines. Following elicitation with elf18, no differences were observed compared to wild-type for either single (Figure 7A) or double (Figure 7B) null lines, suggesting that Raf33 and Raf38 do not regulate the immune-induced oxidative burst. Similar results were obtained using the bacterial elicitor flg22 (Appendix Figure 2A) and the damage-associated elicitor AtPep1 (Appendix Figure 2B). Therefore, it is likely that Subgroup C7-1 and C7-2 clades play distinct roles in innate immunity and stomatal responses to blue light and CO_2, despite high sequence similarity between all Subgroup C7 members (Figure 1C).

3.5. Overexpression of *MRK1* may result in abnormal rosette development

In some cases, overexpression of a gene can result in abnormal phenotypes (Prelich, 2012). To further unravel the regulation of early immune outputs by MRK1 and assess its role in development, I generated *MRK1-OE* lines through *Agrobacterium*-mediated floral dip. Stable transformation of Col-0 plants was performed using cauliflower mosaic virus (CaMV) 35S promoter-driven and native promoter-driven *MRK1-GFP* constructs. Two independent lines were selected for each construct and homozygous lines were identified in the T_3 generation through antibiotic selection. Rosette photos were taken of *Col-0/35S:cMRK1-GFP* and *Col-0/pMRK1:gMRK1-GFP* lines at 4 weeks post-germination. While both *Col-0/pMRK1:gMRK1-GFP* lines and *Col-0/35S:cMRK1-GFP 4-9* appeared developmentally indistinguishable from wild-type, *Col-0/35S:cMRK1-GFP 10-12* plants had abnormal leaf shape and white, spiked leaves at the center of the rosette (Figure 8A). However, as this may be attributed to positional effects of the *MRK1-GFP* insertion in the Arabidopsis genome, isolation of additional *Col-0/35S:cMRK1-GFP* lines will be necessary to confirm this phenotype. Overexpression of *MRK1* in *MRK1-OE* lines was also confirmed through qRT-PCR. In all lines, *MRK1* transcript accumulation was higher in *MRK1-OE* relative to Col-0, with the highest levels observed in *Col-0/35S:cMRK1-GFP 10-12* (Figure 8B). To assess early immune outputs in *MRK1-OE* lines, immune-induced oxidative burst was examined. Following elicitation with the bacterial elicitor elf18, no differences in ROS burst were observed relative to Col-0 in any of the *MRK1-OE* lines (Figure 8C). Similar results were observed using the bacterial elicitor flg22 (Appendix Figure 3A) and the damage-associated elicitor AtPep1 (Appendix Figure 3B). Thus, although highest levels of MRK1 transcript may confer a developmental phenotype, it does not result in lower immune-induced oxidative burst, as might be expected based on *mrk1 raf39* and *mrk1 raf26* phenotypes.

3.6. MRK1 localizes to the cytosol in *N. benthamiana* and Arabidopsis

Subcellular localization can serve as a predictive tool when assessing the function or possible interaction partners of a protein. To examine the localization of MRK1 in a heterologous system, *N. benthamiana* was transiently transformed with *35S:cMRK1-GFP* or *pMRK1:gMRK1-GFP* and excitation of fluorescent proteins was observed through confocal imaging. Under the CaMV 35S promoter, MRK1-GFP localized to the cytosol in *N. benthamiana*, as evidenced by fluorescent signal at cell boundaries and by cytoplasmic streaming (Figure 9A). No signal was detected for MRK1-GFP under the Arabidopsis *MRK1* promoter, suggesting that low MRK1-GFP expression may be beyond the equipment detection range (Figure 9A). Accumulation of MRK1-GFP in both samples was confirmed by immunoblot (Figure 9B). To verify cytosolic localization in *N. benthamiana*, *35S:cMRK1-GFP* was co-expressed with the cytosolicmarker free mCherry (Nelson et al., 2007), and co-localization was observed (Figure 9A). Localization of MRK1-GFP was also assessed in the native system using stable Arabidopsis *Col-0/35S:cMRK1-GFP* and *Col-0/pMRK1:gMRK1-GFP* lines. Confocal imaging was performed using 5-week-old homozygous T_3 *Col-0/35S:cMRK1-GFP 10-12* and *Col-0/pMRK1:gMRK1-GFP 11-10* plants. As in *N. benthamiana*, cytosolicsignal was observed in MRK1-GFP under CaMV 35S promoter, but no signal could be detected under the native promoter (Figure 9C). Autofluorescence of lignified stomatal pores was also observed in *Col-0/pMRK1:gMRK1-GFP 11-10* lines (Shtein et al., 2017). Accumulation of MRK1-GFP in Arabidopsis tissue was confirmed by immunoblotting (Figure 9D).

3.7. MRK1 may be less phosphorylated following immune induction

When expressed in a cell-free system and treated with a luminescent phosphoprotein detection kit, MRK1 autophosphorylation was observed in a stringent screen for Arabidopsis protein kinase activity (Nemoto et al., 2011), suggesting that it is a true kinase. Several phosphorylated residues have also been identified on MRK1 and other Subgroup C7 members in large-scale phosphoproteomic datasets (Figure 1C). Two residues on MRK1, pT41 and pT121, were reported to be less phosphorylated following treatment with the bacterial elicitor flg22 or the fungal elicitor xylanase, respectively (Benschop et al., 2007; Nühse et al., 2007). A conserved phosphorylation site has not been identified for Subgroup C7-1 or C7-2 members (Figure 1C), suggesting that they may be differentially regulated by post-translational modifications or have not been analyzed with sufficient coverage. As MRK1 may play a regulatory role in early immune outputs, I tested whether the phosphorylation status of MRK1 differed following immune elicitation due to auto- or transphosphorylation. Null *mrk1-1* lines were stably transformed with *35S:cMRK1-GFP* through *Agrobacterium*-mediated floral dip, and antibiotic-selected T_2 plants were treated with or without the bacterial elicitor elf18. Immunoprecipitated MRK1-GFP was analyzed by immunoblot or using a phosphoprotein detection system. In one preliminary experiment, MRK1-GFP was less phosphorylated following elf18 treatment (Appendix Figure 4). However, as this assay was only performed once and may be confounded by excessive or uneven protein loading, further replicates are required to confirm this initial result.

3.8. PP2A-B subunits were identified as putative CPK28-associated proteins and do not play a role in immune-induced oxidative burst

Two additional proteins of interest, PP2A-Bα and PP2A-Bβ, were identified as putative CPK28 interactors in the initial IP-MS screen (Bender et al., 2017). They function as the regulatory component of multimeric PP2As, coupled with a scaffolding and a catalytic subunit. Both PP2A-Bα and PP2A-Bβ are the sole members of their distinct PP2A-B regulatory subfamily and have been implicated in the regulation of flowering time and nitrogen assimilation (Heidari et al., 2011; Heidari et al., 2013). PP2A-Bα and PP2A-Bβ were identified in CPK28-YFP and $CPK28^{D188A}$-YFP immunoprecipitates, both before and after PAMP treatment (Appendix Figure 5A). Both subunits had low or no peptide counts associated with the PM-GFP control, suggesting specificity of the putative CPK28 interaction (Appendix Figure 5A). While PP2A-B subunits have no established role in immunity, members of a separate PP2A regulatory subfamily, PP2A-B', act alongside PP2A-A and PP2A-C subunits to negatively regulate the co-receptor BAK1 (Segonzac et al., 2014). As both members of the PP2A-B subfamily were identified in the CPK28 IP-MS screen alongside other scaffolding and catalytic subunits (data not shown), I sought to determine whether these PP2A-B subunits could similarly be acting as regulators of immunity in Arabidopsis.

To assess their potential role in immunity, expression profiles following pathogen or elicitor treatment were extracted for *PP2A-Bα* and *PP2A-Bβ* using the eNorthern tool (Toufighi et al., 2005). While *PP2A-Bβ* was strongly expressed following treatment with the fungal pathogen *Golovinomyces orontii*, no stark changes in *PP2A-Bα* expression were observed upon immune elicitation (Appendix Figure 5B). I also examined *PP2A-Bα* and *PP2A-Bβ* expression profiles at different developmental stages. While *PP2A-Bβ* had somewhat high expression in mature pollen, both subunits had mostly uniform expression across developmental time (Appendix Figure 5B). I then acquired T-DNA insertion lines for *PP2A-Bα* (SALK_032080) and *PP2A-Bβ* (SALK_062514) from Dr. Cathrine Lillo (University of Stavanger, Norway) and confirmed that the lines were homozygous using PCR-genotyping. *PP2A-Bα* and *PP2A-Bβ* both contain multiple exons and introns, and T-DNA insertions for *pp2a-bα-1* and *pp2a-bβ-1* are situated in introns (Appendix Figure 6A). In agreement with published results, I anecdotally observed an early flowering phenotype in *pp2a-bα-1* and *pp2a-bβ-1* (Heidari et al., 2013). To determine whether PP2A-Bα and PP2A-Bβ may regulate early immune responses, I examined immune-induced oxidative burst following treatment with the bacterial elicitor elf18. Null lines for both PP2A-B subunits exhibited a ROS burst similar to wild-type, suggesting that they do not regulate immune-induced oxidative burst (Appendix Figure 6B). As the double null *pp2a-bα pp2a-bβ* mutant is embryo lethal (Heidari et al., 2011), I was unable to confirm whether the PP2A-B subunits could be acting redundantly to regulate early immune outputs in Arabidopsis. Further work will be required to determine if the PP2A-B subunits are associating with CPK28 *in vivo* or if they may be acting alongside CPK28 in developmental pathways.

A

ACCESSION ID	IDENTIFIED PROTEIN	MOLECULAR WEIGHT (kDa)	PEPTIDE COUNTS				
			cpk28-1/ CPK28-YFP (-elf18)	*cpk28-1/ CPK28-YFP (+elf18)*	*cpk28-1/ CPK28^{D188A}-YFP (-elf18)*	*cpk28-1/ CPK28^{D188A}-YFP (+elf18)*	*PM-GFP (control)*
AT3G63260.1	AtMRK1 (mixed-lineage kinase/Raf-related protein kinase 1)	42.5	25	19	4	2	0

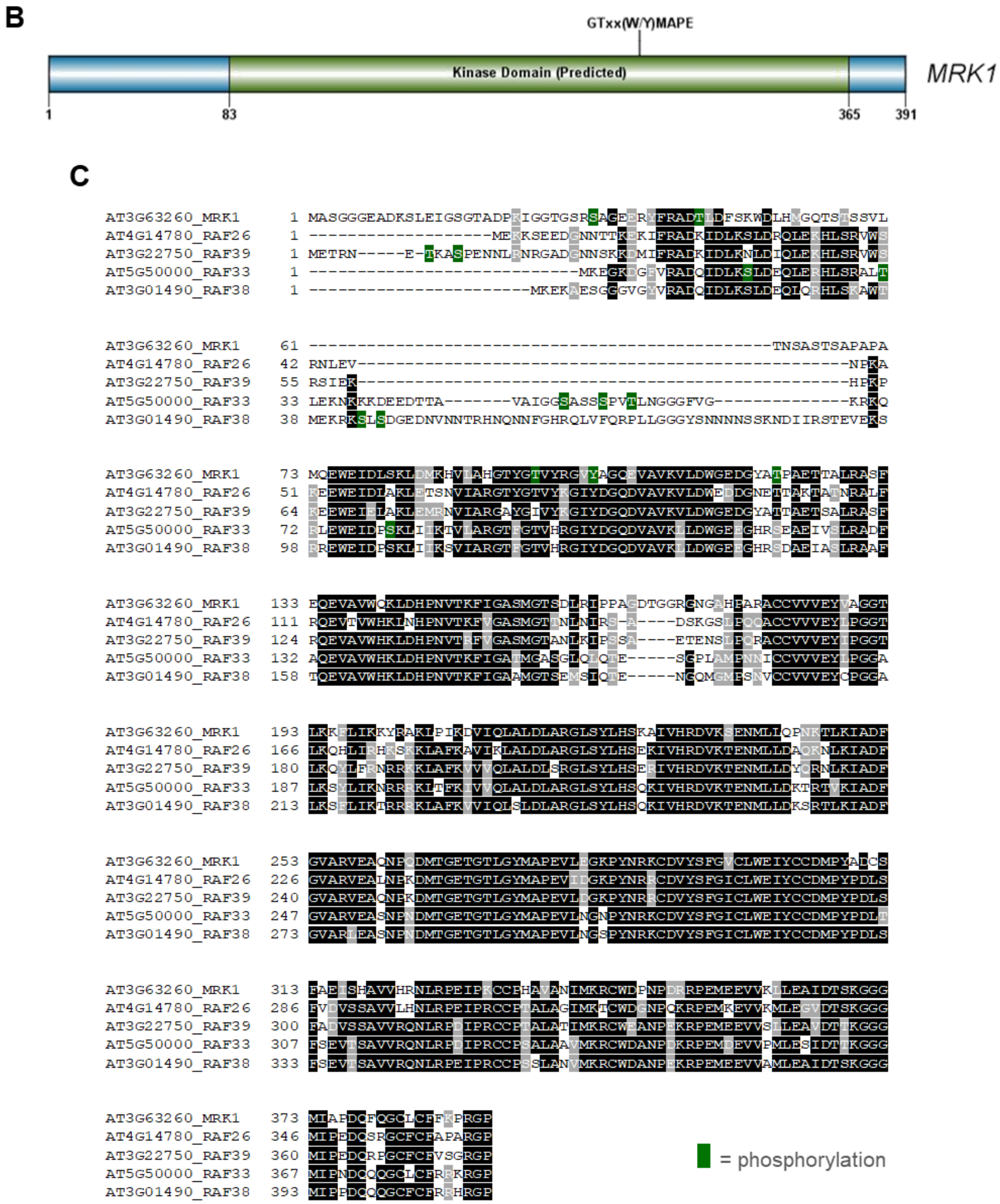

Figure 1. MRK1 was identified as a putative CPK28-associated protein in a reverse genetics screen. (A) Peptide counts for MIXED-LINEAGE KINASE/RAF-RELATED PROTEIN KINASE 1 (MRK1; AT3G63260) identified in CALCIUM-DEPENDENT PROTEIN KINASE 28 (CPK28)-YFP or plasma-membrane control LOW TEMPERATURE-INDUCED PROTEIN 6B-GFP ('PM-GFP') immunoprecipitates through liquid chromatography and tandem mass spectrometry (LC/MS-MS). Loss-of-function *cpk28-1* lines were stably transformed with wild-type or kinase-dead (CPK28^{D188A}) variants of CPK28-YFP (Matschi et al., 2013), treated with or without 200 nM elf18, and subjected to affinity purification and LC-MS/MS as previously described (Bender et al., 2017) alongside a *Col-0/PM-GFP* control. (B) Predicted protein domain structure of MRK1. The amino acid sequence for MRK1 was obtained using the Arabidopsis Information Resource (TAIR) and analyzed with Interpro 74.0 (https://www.ebi.ac.uk/interpro/). The consensus Raf-like MAPKKK motif (GTxx(W/Y)MAPE) (Suarez-Rodriguez et al., 2010) is annotated, and the graphic was built using the IBS: Illustrator for Biological Sequences version 1.0.3. (C) Multiple sequence alignment for MAPKKK Subgroup C7 members in Arabidopsis. Amino acid sequences for MRK1 (AT3G63260), Raf26 (AT4G14780), Raf39 (AT3G22750), Raf33 (AT5G50000), and Raf38 (AT3G01490) were extracted from TAIR and aligned using Clustal Omega. Residues that were somewhat or highly conserved were shaded in grey and black, respectively, using BoxShade version 3.2. Phosphorylated residues that have been identified in existing phosphoproteomic screens were curated using The Arabidopsis Protein Phosphorylation Site Database version 4.0, and are highlighted in green.

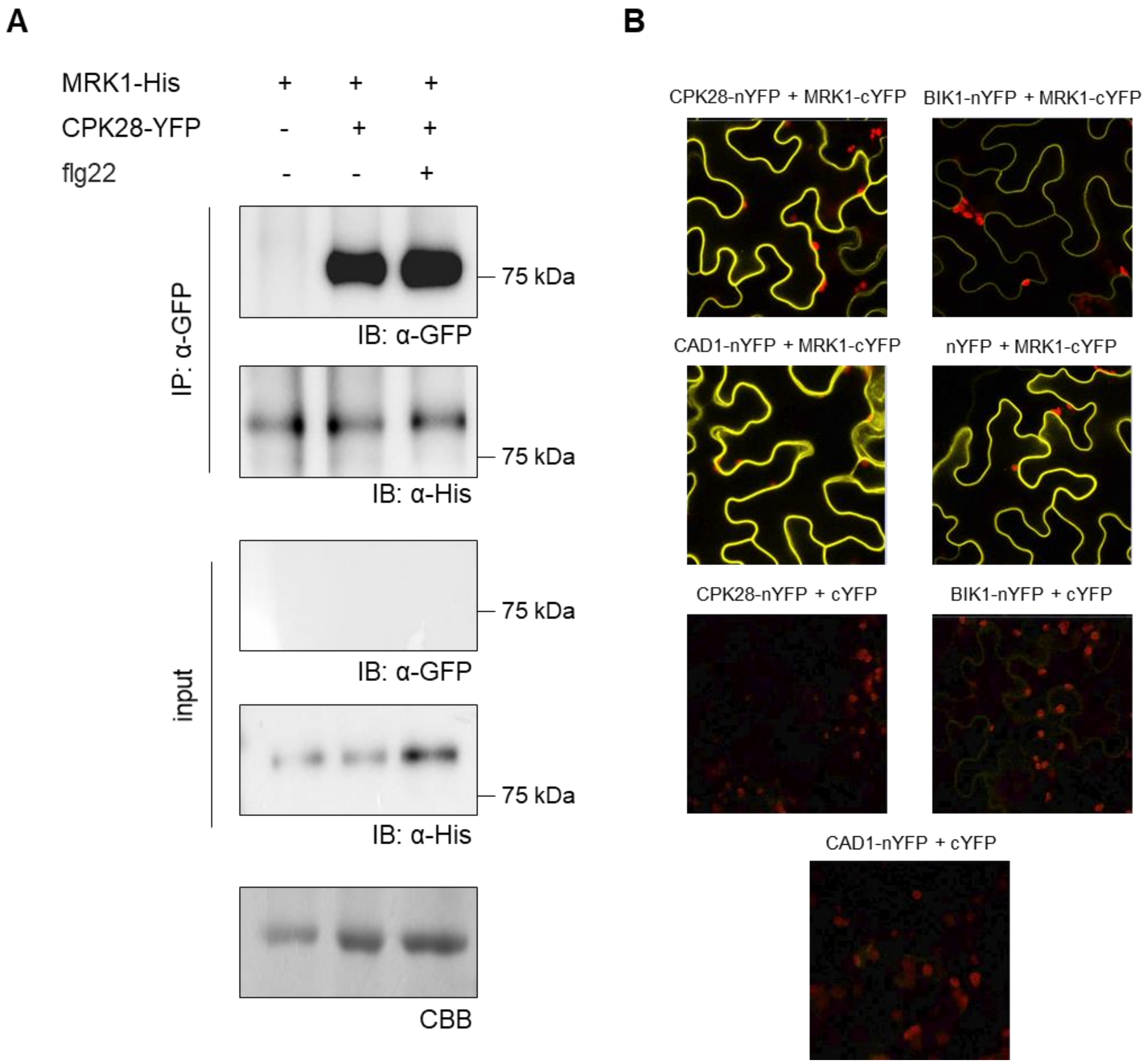

Figure 2. MRK1 associates with the negative control in protein-protein association assays. (A) 35S:cMRK1-His and 35S:cCPK28-YFP were transiently expressed in four-week-old *Nicotiana benthamiana* plants, and tissue was treated with or without 100 nM flg22 at 3 days post infiltration (dpi). Tissue expressing only 35S:cMRK1-His was included to serve as a negative control. Protein was extracted and equivalent protein titers were immunoprecipitated using μMACs α-GFP beads. Presence of MRK1-His and CPK28-YFP were detected via immunoblot using 4 μg of protein for each lane in input fractions, and Coomassie Brilliant Blue (CBB) staining was included as a protein loading control. As MRK1-His was identified in the

negative control following immunoprecipitation, the association of MRK1 and CPK28 is inconclusive. Similar results were observed in three replicates. (B) nYFP- and cYFP-tagged constructs were co-infiltrated in four-week-old *N. benthamiana* leaves three days prior to confocal microscopy. Reconstitution of YFP was detected alongside chlorophyll autofluorescence, and strong signal was observed following co-infiltration of MRK1-cYFP with CPK28-nYFP, BOTRYTIS-INDUCED KINASE 1 (BIK1)-nYFP, the empty vector control, or the negative protein control CAD1-nYFP. Similar results were observed in three replicates.

A

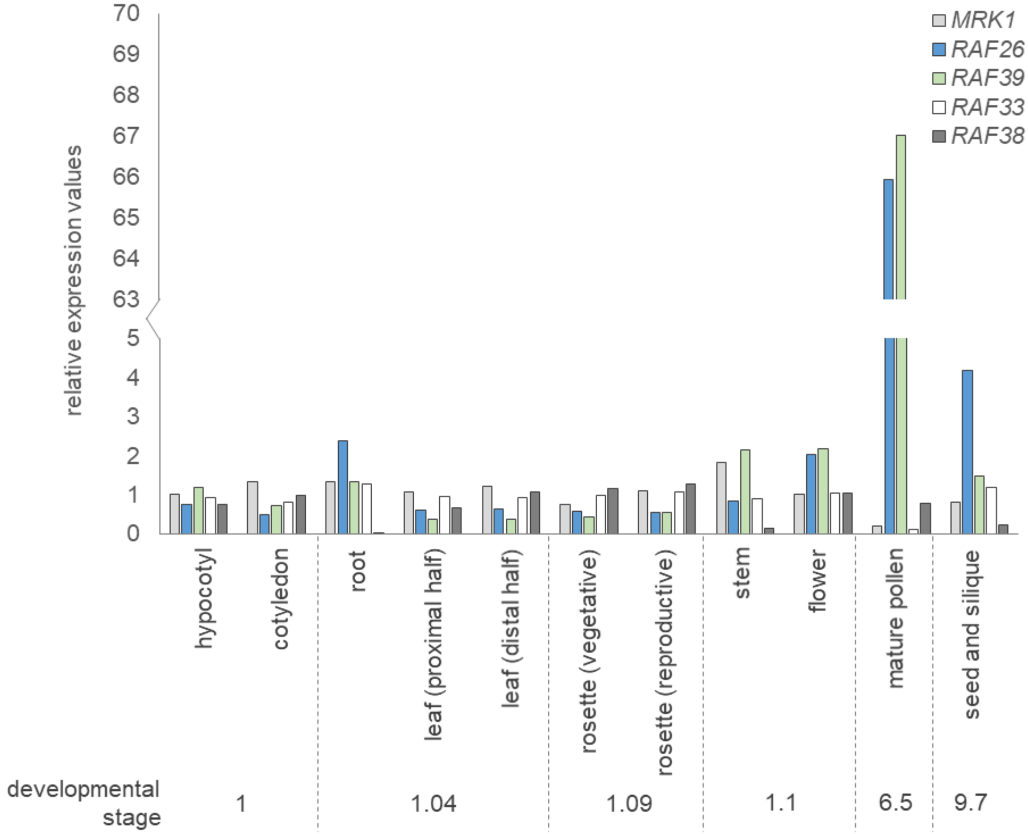
70
69
68
67
66
65
64
63
5
4
3
2
1
0
relative expression values
MRK1
RAF26
RAF39
RAF33
RAF38
hypocotyl
cotyledon
root
leaf (proximal half)
leaf (distal half)
rosette (vegetative)
rosette (reproductive)
stem
flower
mature pollen
seed and silique
developmental stage
1
1.04
1.09
1.1
6.5
9.7

B

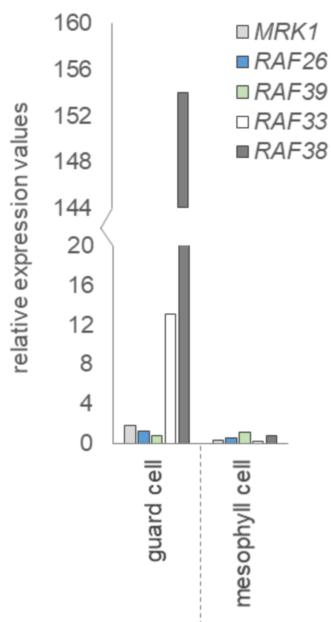
160
156
152
148
144
20
16
12
8
4
0
relative expression values
MRK1
RAF26
RAF39
RAF33
RAF38
guard cell
mesophyll cell

C

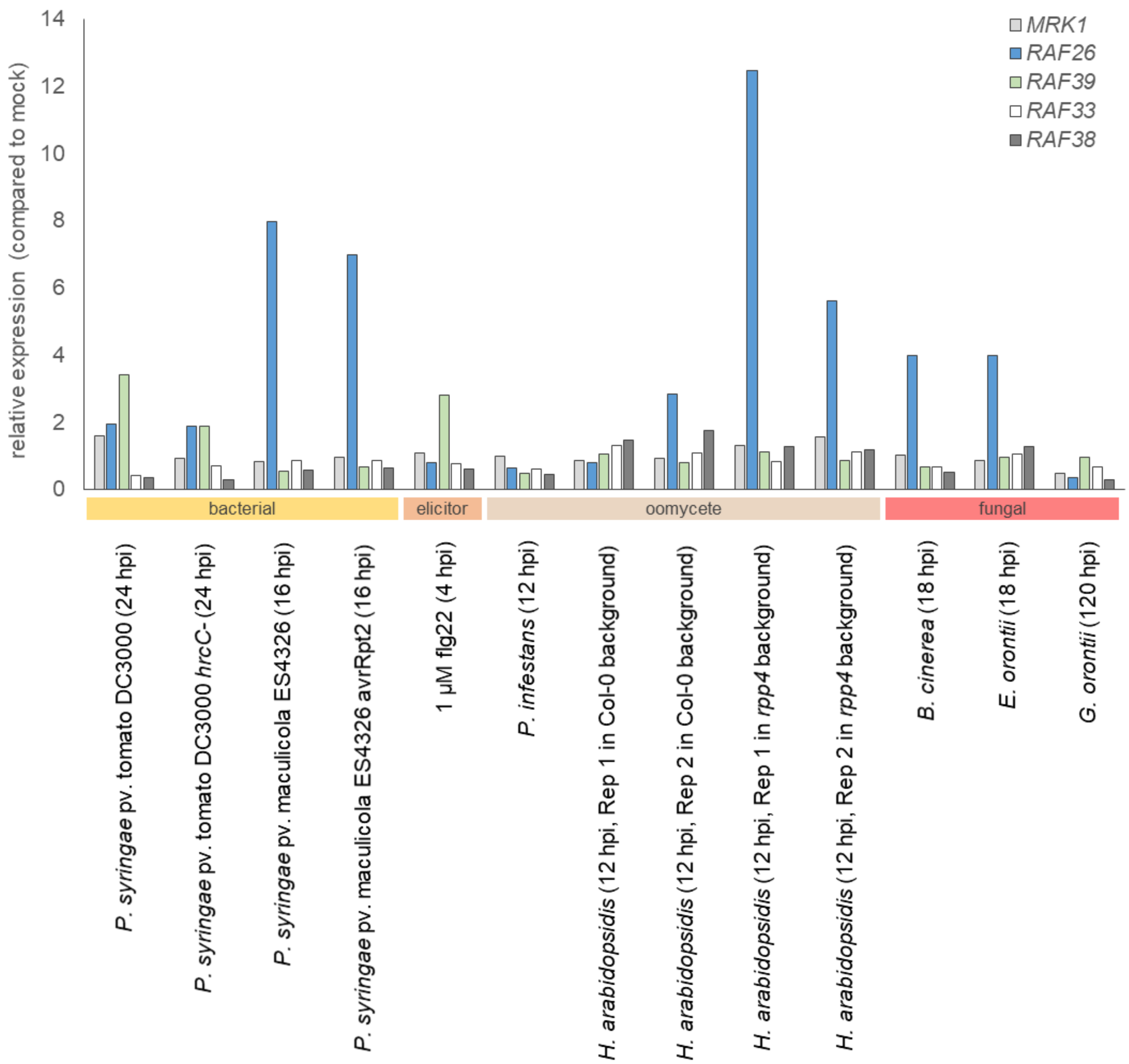

Figure 3. Expression profiles of Raf-like MAPKKK Subgroup C7 members in development and following immune treatment. (A, B) Gene expression of Raf-like MAPKKK Subgroup C7 members from Arabidopsis at various developmental stages and in specific tissue types. Relative expression values were obtained using the Extended Tissue Series under the eNorthern Expression Browser tool from the Bio-Analytic Resource for Plant Biology (Toufighi et al., 2005). *RAF26* and *RAF39* were highly expressed in mature pollen, while *RAF33* and *RAF38* were highly expressed in guard cells. (C) Gene expression of Raf-like MAPKKK Subgroup C7

members from Arabidopsis following pathogen or elicitor treatment. Expression values relative to a “mock” control were extracted using the Pathogen Series under the eNorthern Expression Browser tool from the Bio-Analytic Resource for Plant Biology (Toufighi et al., 2005). *RAF26* was upregulated following treatment with the virulent strain of *Pseudomonas syringae* pv. *maculicola* ES4326, the avirulent *P. syringae* pv. *maculicola* ES4326 avrRpt2, the oomycete pathogen *Hyaloperonospora arabidopsidis*, and the fungal pathogens *Botrytis cinerea* and *Erysiphe orontii*.

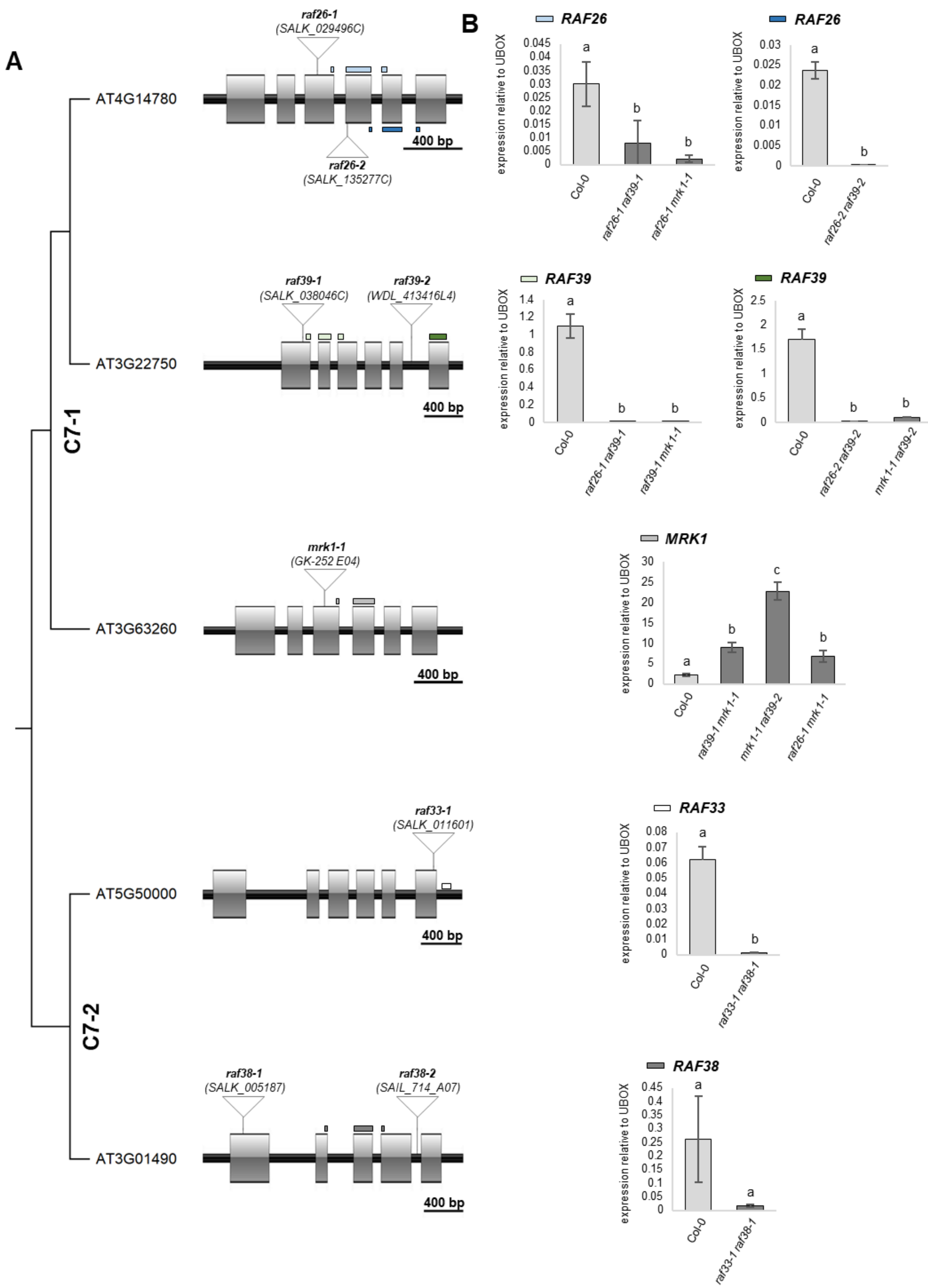

A
B
C7-1
C7-2
AT4G14780
AT3G22750
AT3G63260
AT5G50000
AT3G01490
raf26-1
(SALK_029496C)
raf26-2
(SALK_135277C)
raf39-1
(SALK_038046C)
raf39-2
(WDL_413416L4)
mrk1-1
(GK-252 E04)
raf33-1
(SALK_011601)
raf38-1
(SALK_005187)
raf38-2
(SAIL_714_A07)
400 bp
RAF26
RAF39
MRK1
RAF33
RAF38
expression relative to UBOX
Col-0
raf26-1 raf39-1
raf26-1 mrk1-1
raf26-2 raf39-2
raf39-1 mrk1-1
mrk1-1 raf39-2
raf33-1 raf38-1

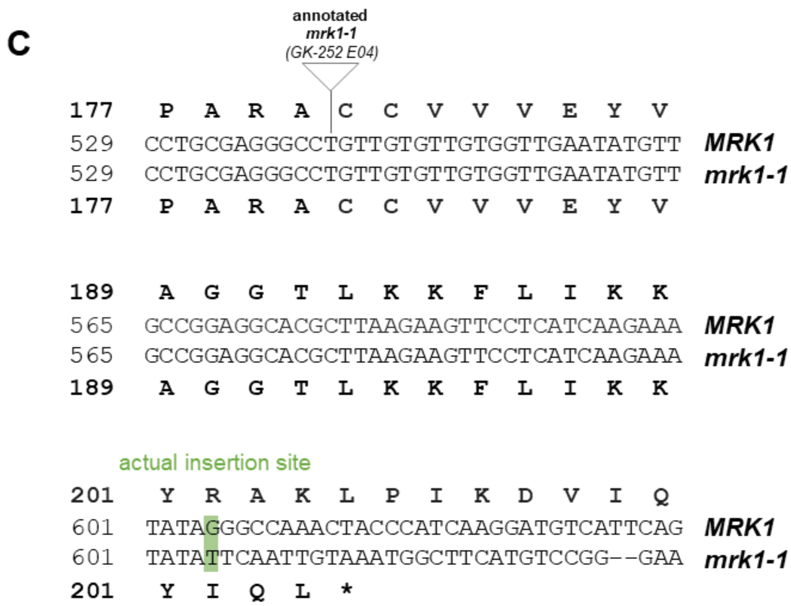

Figure 4. Characterization of null alleles for Raf-like MAPKKK Subgroup C7 members. (A) Phylogeny and gene structure of Raf-like MAPKKK Subgroup C7 members in Arabidopsis. Multiple sequence alignment was performed with Clustal Omega, and a rooted phylogenetic tree was created with MEGA-X 10.0.5 using a Neighbour-Joining method and tested by bootstrapping with 1000 replicates. The gene structure of *MRK1* (AT3G63260), *RAF26* (AT4G14780), *RAF39* (AT3G22750), *RAF33* (AT5G50000), and *RAF38* (AT3G01490) was visualized using the IBS: Illustrator for Biological Sequences version 1.0.3, and T-DNA insertions were annotated using information curated from The Arabidopsis Information Resource (TAIR). Introns and untranslated regions are represented by a black line, and exons are annotated using light gray boxes. (B) Gene expression analysis of Raf-like MAPKKK Subgroup C7 members relative to *UBOX* in double null lines. Regions amplified for qRT-PCR are annotated in gene structure diagrams from (A) using coloured bars. Error bars represent standard deviation, and similar results were observed in two independent replicates. (C) Position and translated product of the *mrk1-1* insertion. The sequence upstream and downstream of the annotated *mrk1-1* insertion was analyzed by Sanger sequencing. Multiple sequence alignment of wild-type

MRK1 and sequenced *mrk1-1* was performed using Clustal Omega. While the annotated insertion is at position 541 (indicated by the black triangle), the actual *mrk1-1* insertion was found at position 605 (indicated by the green box) and resulted in a premature stop codon.

A

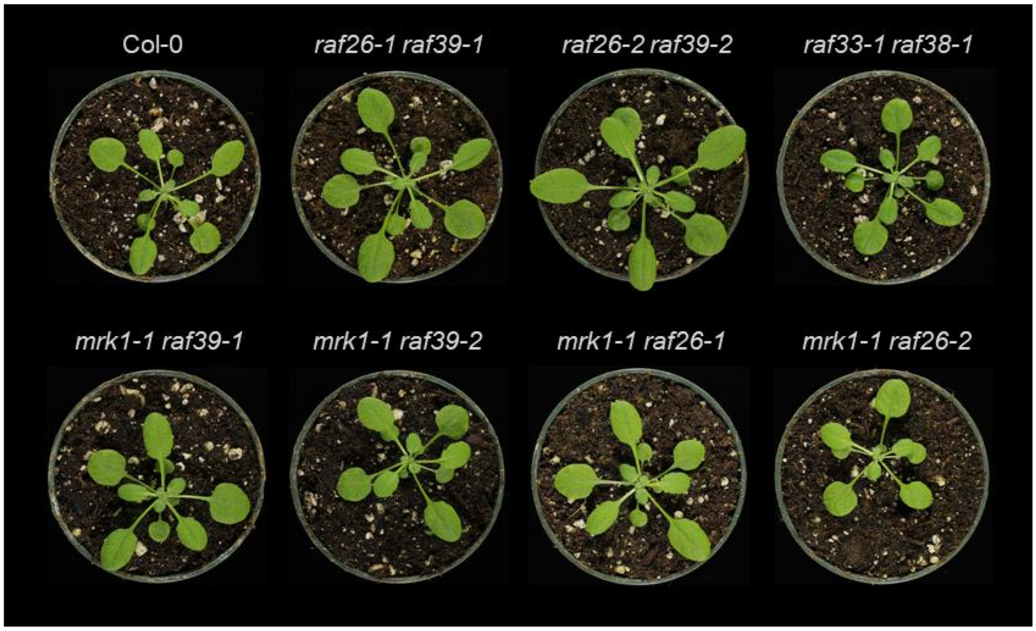
Col-0
raf26-1 raf39-1
raf26-2 raf39-2
raf33-1 raf38-1
mrk1-1 raf39-1
mrk1-1 raf39-2
mrk1-1 raf26-1
mrk1-1 raf26-2

B

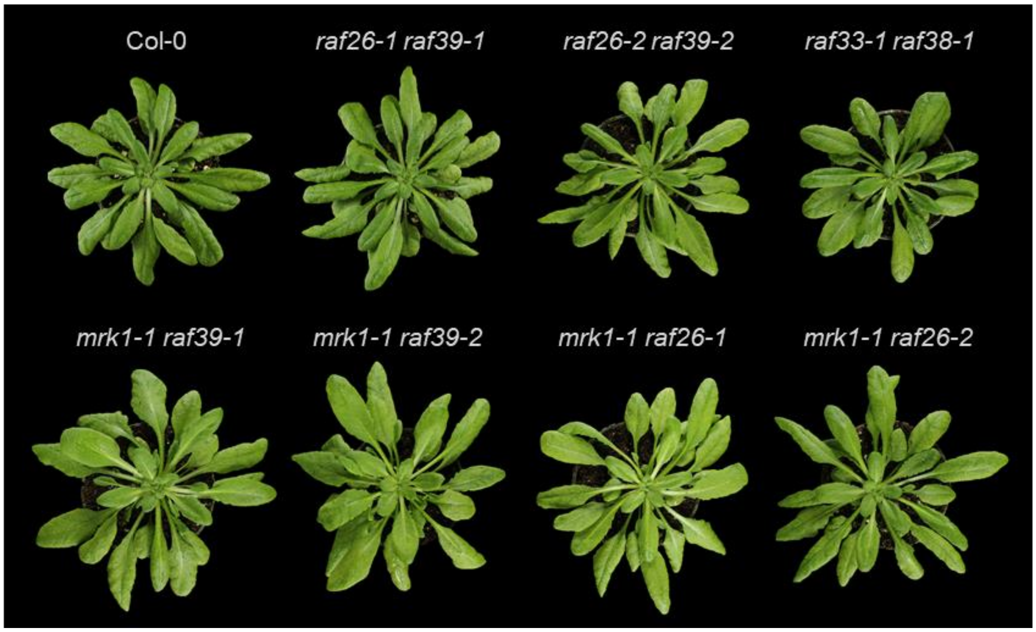
Col-0
raf26-1 raf39-1
raf26-2 raf39-2
raf33-1 raf38-1
mrk1-1 raf39-1
mrk1-1 raf39-2
mrk1-1 raf26-1
mrk1-1 raf26-2

C

Figure 5. Raf-like MAPKKK Subgroup C7 members display a wild-type rosette phenotype. Rosette photos of double null lines for Raf-like MAPKKK Subgroup C7 members relative to Col-0 either (A) at 4 weeks post-germination, (B) at 6.5 weeks post-germination, or (C) following reproductive transition (at roughly 8 weeks post-germination).

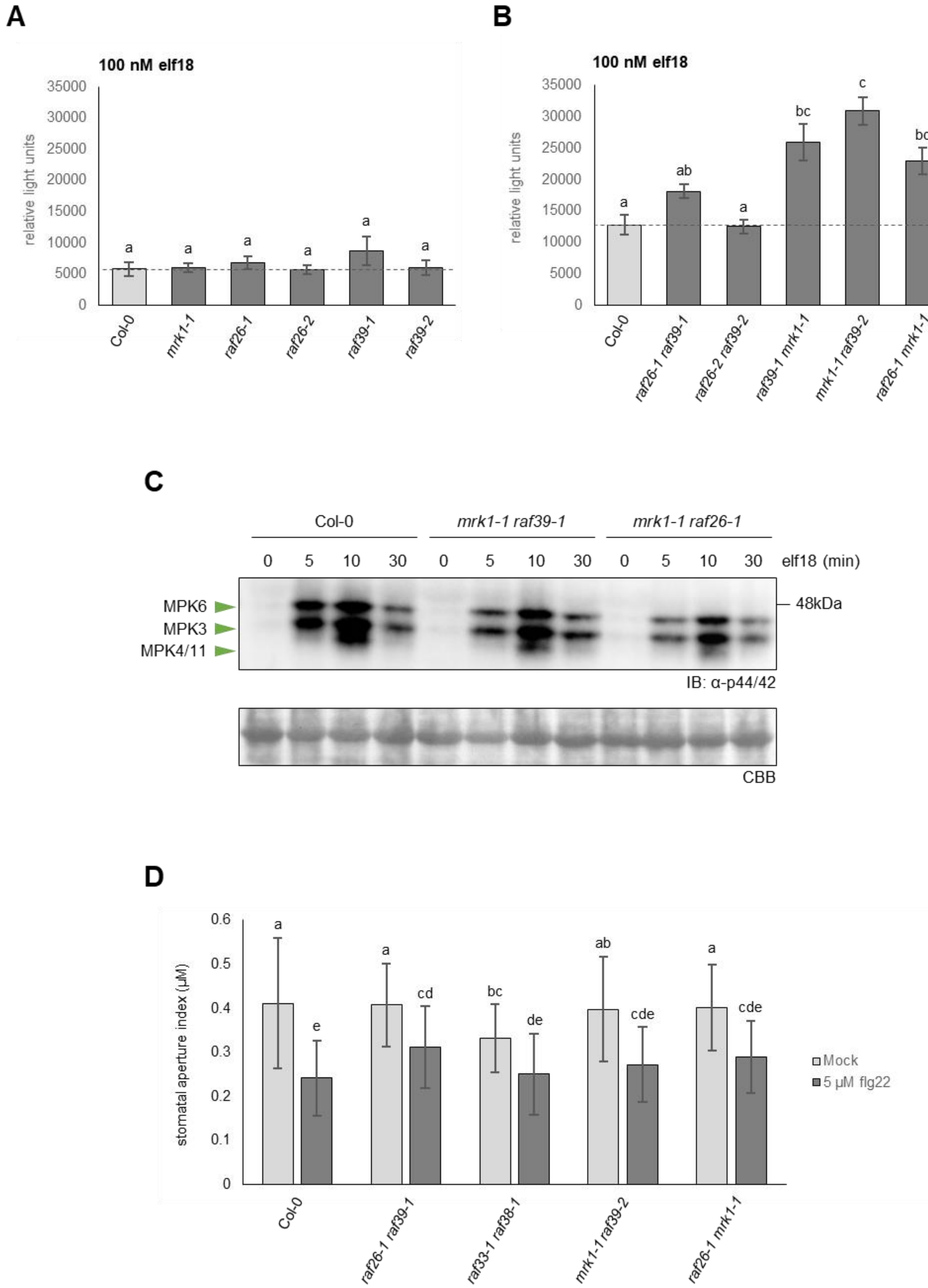
A
100 nM elf18
relative light units
Col-0
mrk1-1
raf26-1
raf26-2
raf39-1
raf39-2
B
100 nM elf18
relative light units
Col-0
raf26-1 raf39-1
raf26-2 raf39-2
raf39-1 mrk1-1
mrk1-1 raf39-2
raf26-1 mrk1-1
raf26-2 mrk1-1
C
Col-0
mrk1-1 raf39-1
mrk1-1 raf26-1
0 5 10 30 0 5 10 30 0 5 10 30 elf18 (min)
MPK6
MPK3
MPK4/11
48kDa
IB: α-p44/42
CBB
D
stomatal aperture index (μM)
Col-0
raf26-1 raf39-1
raf33-1 raf38-1
mrk1-1 raf39-2
raf26-1 mrk1-1
Mock
5 μM flg22

Figure 6. Raf-like MAPKKK Subgroup C7-1 members may function redundantly to regulate immune-induced oxidative burst. (A, B) Oxidative burst was analyzed in single and double null lines for *MRK1*, *RAF39*, and *RAF26* at 5 weeks post-germination following elicitation with 100 nM elf18. Average total photon counts over 40 minutes are shown in relative light units, and error bars represent standard error of the mean (n = 6 leaf discs from independent plants). Statistical differences were calculated by one-way ANOVA followed by a post-hoc Tukey's Honest Significant Difference test ($p<0.05$) and groupings are represented by lower-case letters. The dashed line indicates the average total photon count for the wild-type control (Col-0). Similar results were observed in 8 of 12 technical replicates from three independent biological replicates. (C) MAPK activation of 14-day-old *mrk1-1 raf39-1* and *mrk1-1 raf26-1* seedlings relative to Col-0 at 0, 5, 10, or 30 min following elicitation with 200 nM elf18. Samples were analyzed by immunoblot with anti-p44/42 MAPK (ERK1/2) (Thr202/204) using 8 µg of protein per lane and CBB staining was included as a protein loading control. Similar results were observed in two of three replicates. (D) Stomatal aperture of 5-week-old Raf-like MAPKKK Subgroup C7 double null lines after treatment with or without 5 µM flg22 for 2 h. Stomatal aperture index is shown (n = 40-50 stomata) and was calculated by dividing stomatal width (in µM) by stomatal length (in µM). Error bars represent standard deviation, and lower-case letters represent statistically significant groups as calculated by one-way ANOVA followed by a post-hoc Tukey's Honest Significant Difference test ($p<0.05$). Similar results were observed in two independent experiments.

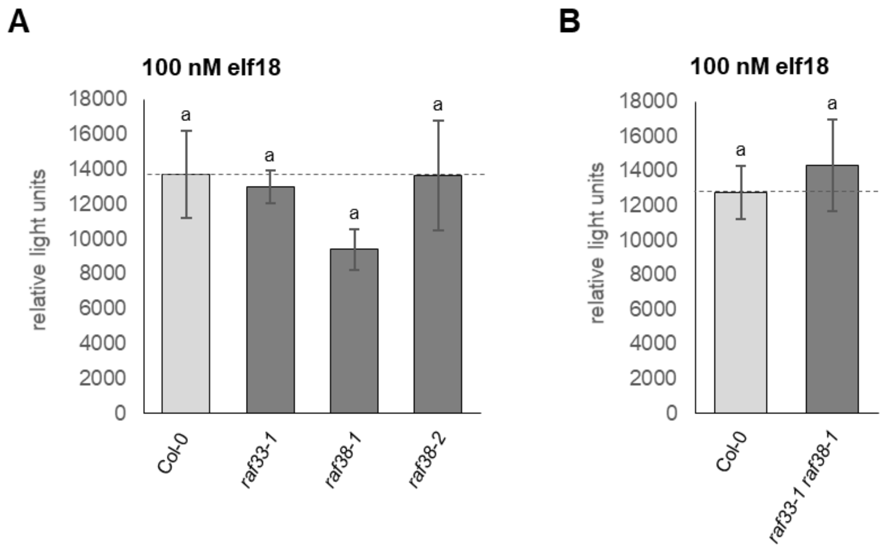

Figure 7. Raf-like MAPKKK Subgroup C7-2 members do not play a role in immune-induced oxidative burst. Oxidative burst was analyzed in single (A) and double (B) null lines for *RAF33* and *RAF38* at 5 weeks post-germination following elicitation with 100 nM elf18. Average total photon counts over 40 minutes are shown in relative light units, and error bars represent standard error of the mean (n = 6 leaf discs from independent plants). Statistical differences were calculated by one-way ANOVA followed by a post-hoc Tukey's Honest Significant Difference test ($p<0.05$) and groupings are represented by lower-case letters. The dashed line indicates the average total photon count for the wild-type control (Col-0). Similar results were observed in three independent replicates.

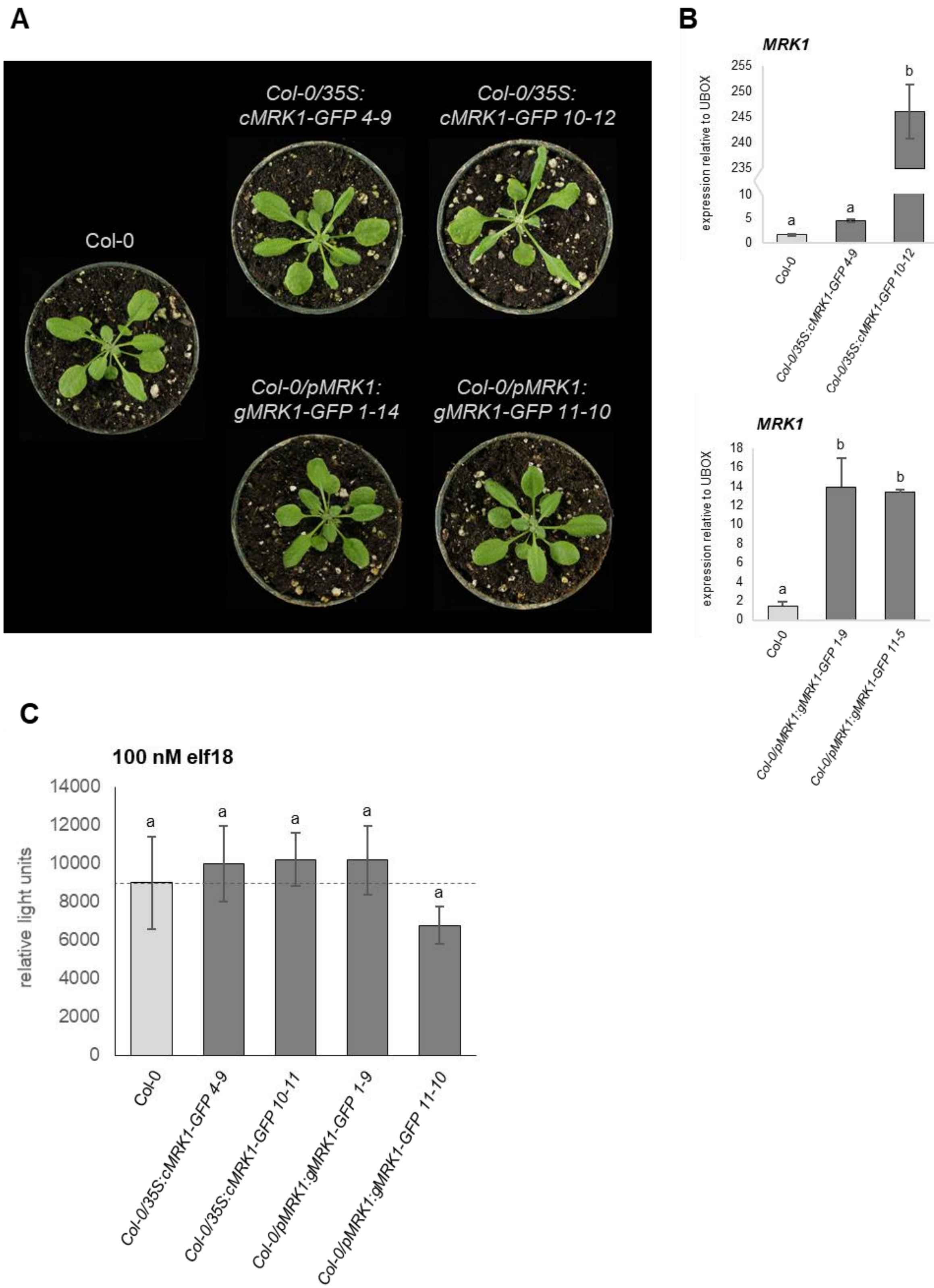
A
Col-0
Col-0/35S:
cMRK1-GFP 4-9
Col-0/35S:
cMRK1-GFP 10-12
Col-0/pMRK1:
gMRK1-GFP 1-14
Col-0/pMRK1:
gMRK1-GFP 11-10
B
MRK1
expression relative to UBOX
255
250
245
240
235
10
5
0
a
a
b
Col-0
Col-0/35S:cMRK1-GFP 4-9
Col-0/35S:cMRK1-GFP 10-12
MRK1
expression relative to UBOX
18
16
14
12
10
8
6
4
2
0
a
b
b
Col-0
Col-0/pMRK1:gMRK1-GFP 1-9
Col-0/pMRK1:gMRK1-GFP 11-5
C
100 nM elf18
relative light units
14000
12000
10000
8000
6000
4000
2000
0
a
a
a
a
a
Col-0
Col-0/35S:cMRK1-GFP 4-9
Col-0/35S:cMRK1-GFP 10-11
Col-0/pMRK1:gMRK1-GFP 1-9
Col-0/pMRK1:gMRK1-GFP 11-10

Figure 8. *MRK1-OE* lines display an abnormal rosette phenotype and a wild-type oxidative burst. (A) Rosette photos of *MRK1-OE* lines relative to Col-0 at 4 weeks post-germination in the T_3 generation. (B) Gene expression analysis of *MRK1* relative to *UBOX* in CaMV 35S-driven and native promoter-driven *MRK1-OE* lines. Error bars represent standard deviation, and similar results were observed in two independent replicates. (C) Oxidative burst was analyzed in homozygous or antibiotic-selected T_3 *MRK1-OE* lines at 5 weeks post-germination following elicitation with 100 nM elf18. Average total photon counts over 40 minutes are shown in relative light units, and error bars represent standard error of the mean (n = 6 leaf discs from independent plants). Similar results were observed in three independent replicates. Statistical differences for both gene expression and oxidative burst were calculated by one-way ANOVA followed by a post-hoc Tukey's Honest Significant Difference test ($p<0.05$) and groupings are represented by lower-case letters. The dashed line indicates the average total photon count for the wild-type control (Col-0). Siblings from each independent line are annotated using dashed numbers (ex. 10-11 and 10-12 are siblings from the same line).

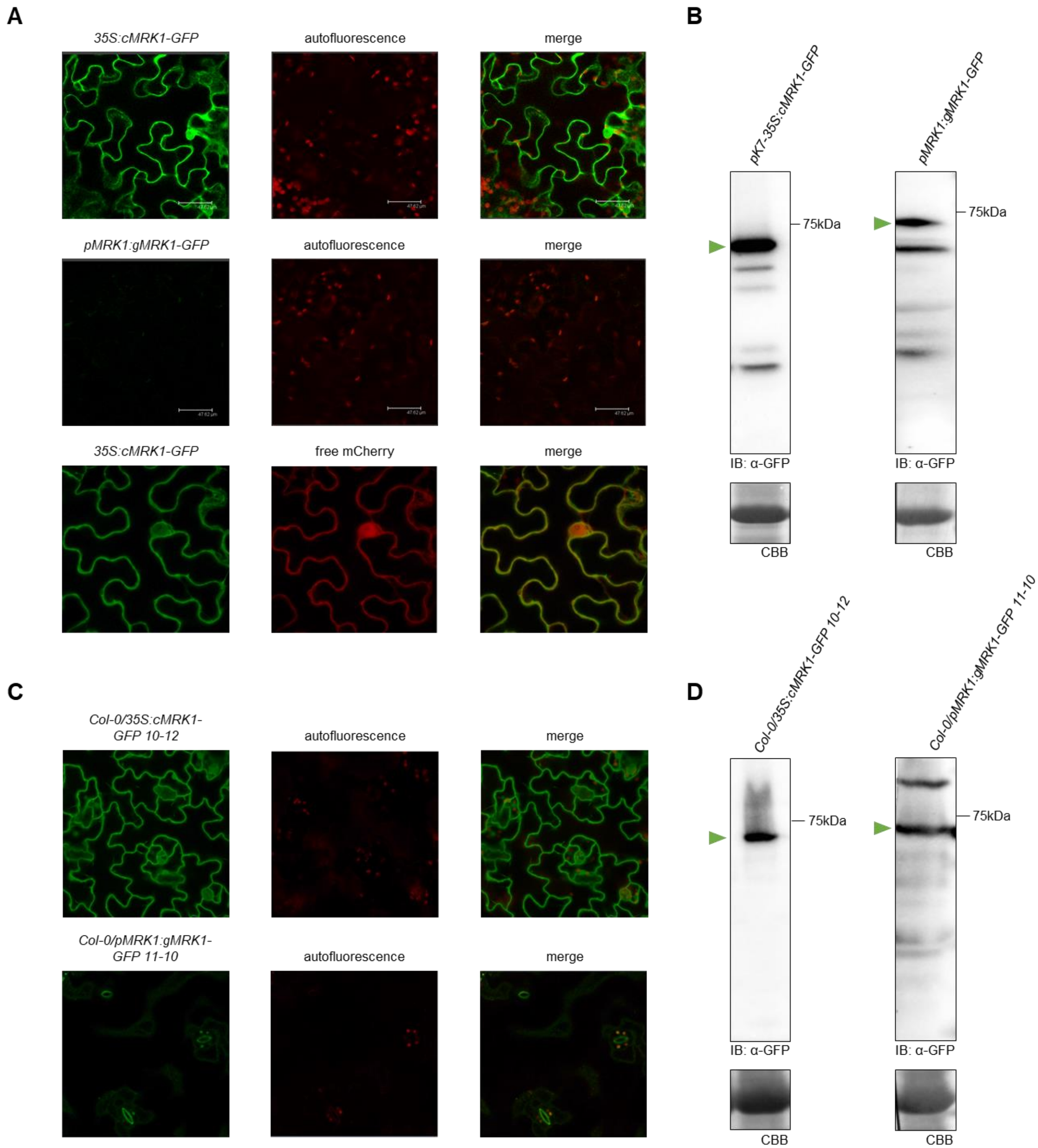

Figure 9. MRK1 localizes to the cytosol in *N. benthamiana* and Arabidopsis. (A) Confocal imaging was performed at 3 dpi using *N. benthamiana* tissue that was infiltrated with either *35S:cMRK1-GFP*, *pMRK1:gMRK1-GFP*, or co-infiltrated with *35S:cMRK1-GFP* and the

cytosolic marker free mCherry. While *35S:cMRK1-GFP* localized to the cytosol, no signal could be detected in *pMRK1:gMRK1-GFP* tissue. Similar results were observed in four independent replicates. Scale bars = 47.62 µM. (B, D) Tissue used in confocal imaging from either *N. benthamiana* (B) or Arabidopsis (D) was flash-frozen in liquid N_2, total protein was extracted, and accumulation of MRK1-GFP was confirmed by immunoblotting. CBB was included as a protein loading control. (C) Confocal imaging was performed using stable, homozygous T_3 *Col-0/35S:cMRK1-GFP 10-12* and *Col-0/pMRK1:gMRK1-GFP 11-10* lines. Localization to the cytosol was detected in *Col-0/35S:cMRK1-GFP 10-12* tissue. As *MRK1-GFP* had weak expression, only autofluorescence of lignified stomatal pores was observed in *Col-0/pMRK1:gMRK1-GFP 11-10* tissue. Similar results were obtained in three independent replicates. The middle panel displays either chlorophyll autofluorescence, or fluorescence from the cytosolic marker free mCherry.

4. DISCUSSION

As unnecessary activation can lead to developmental defects (van Wersch et al., 2016), the plant innate immune response is tightly controlled downstream of pattern recognition. While few negative regulators of immunity have been identified, this attenuation is achieved through several parallel mechanisms, such as modulating the activity or accumulation of key signalling components. Recently, a negative regulatory module acting downstream of multiple PRRs was elucidated (Monaghan et al., 2014; Wang et al., 2018b). Upon PAMP perception, the RLCK BIK1 promotes apoplastic ROS production through the phosphorylation and activation of RBOHD (Kadota et al., 2014; Li et al., 2014). This response is regulated by CPK28 and two ubiquitin E3 ligases, PUB25 and PUB26, which negatively affectBIK1 accumulation (Wang et al., 2018b). Through CPK28-mediated activation of PUB25 and PUB26, these E3 ligases can polyubiquitinate inactive pools of BIK1 and target it for degradation by the 26S proteasome (Wang et al., 2018b). As increasing levels of BIK1 cause enhanced immune output (Li et al., 2014; Monaghan et al., 2014), the CPK28-PUB25/26 module limits unnecessary immune activation by facilitating BIK1 turnover (Wang et al., 2018b). Critically, BIK1 and its negative regulatory module function downstream of many RLKs, including BAK1, FLS2, EFR, and PEPR1/2 (Lehti-Shiu et al., 2009; Lu et al., 2010; Zhang et al., 2010; Liu et al., 2013). To identify novel positive and negative regulators of innate immunity, our lab previously conducted an investigation of putative CPK28-associated proteins using a comprehensive reverse genetics screen. Briefly, CPK28 and its interacting proteins were affinity purified from *cpk28-1/CPK28-YFP* and kinase-dead *cpk28-1/CPK28^{D188A}-YFP* lines both before and after treatment with the bacterial elicitor elf18, and putative CPK28-associated proteins were identified through LC/MS-MS (Bender et al., 2017). A plasma membrane control was similarly processed to ensure that potential interactors were specifically associated with CPK28. As validation of our initial approach, the reverse genetics screen identified multiple established regulators of immunity, including the LRR-RLK SUPPRESSOR OF BAK1-INTERACTING RECEPTOR-LIKE KINASE 1-1which regulates NLP-mediated immunity (Albert et al., 2015), and the scaffold protein FERONIA which mediates PRR complex formation (Stegmann et al., 2017). We also identified members of the BIK1 regulatory module in this dataset, such as RBOHD and BIK1-related proteins (Kadota et al., 2014), which further validates this approach and corroborates existing CPK28 interactions. In addition, our lab preliminarily observed association between CPK28 and SUPPRESSOR OF BAK1-INTERACTING RECEPTOR-LIKE KINASE 1-1using coIP assays in *N. benthamiana* (Siegel and Monaghan, 2017), suggesting that this screen can successfully uncover novel CPK28 interactors. From the list of putative CPK28-associated proteins, I selected MRK1 for further analysis as it is relatively uncharacterized and has some evidence for its involvement in immunity. MRK1 is a putative Raf-like MAPKKK belonging to Subgroup C7 and has four family members: Raf26, Raf39, Raf33, and Raf38 (MAPK Group, 2002). While it was originally isolated from cDNA over 20 years ago (Ichimura et al., 1997), the function of MRK1 has not yet been elucidated. However, MRK1 is upregulated following treatment with OGs and its protein abundance is reduced by 50% in plasma membrane fractions after flg22 treatment (Moscatiello et al., 2006; Benschop et al., 2007), which may provide some support for a role in immune signalling. Other Subgroup C7 members, Raf33 and Raf38, were recently established as positive regulators of blue-light and CO_2-induced stomatal opening (Hiyama et al., 2017). Based on this information and its identification in the CPK28 IP-MS screen (Figure 1A), I assessed whether MRK1 and related Raf-like MAPKKK Subgroup C7 members may be acting as novel regulators of innate immunity.

4.1. MRK1-CPK28 association could not be confirmed using two distinct approaches

As confirmation of the initial reverse genetics screen, I first tested association between MRK1 and CPK28 with two complementary techniques *in vivo*. Using coIP in *N. benthamiana*, MRK1 was found to associate non-specifically with both CPK28 and the negative bead control (Figure 2A). As increasing the number of column wash steps can reduce non-specific binding in coIPs (Free et al., 2009), I attempted this assay using five wash steps instead of three (see Section 2.5 for the standard protocol). Unfortunately, MRK1 was still identified in immunoprecipitates for CPK28 and the negative bead control after additional washing (data not shown). For protein-protein association assays, fusion of large epitope tags and protein overexpression can increase the rate of false positives and non-specific binding (Fukao, 2012; Xing et al., 2016). In this assay, both MRK1 and CPK28 were translationally fused to 32 kDa and 26 kDa C-terminal epitope tags, respectively. As the molecular weight of MRK1 is 42.5 kDa, these tags are proportionally quite large. Additional replicates could be performed using smaller FLAG or hemagglutinin epitope tags fused at the N-terminus of each protein of interest, as this may reduce binding with the negative control caused by tag orientation or size. For these assays, MRK1 and CPK28 constructs were also driven by the constitutive CaMV 35S promoter, which may force association due to excess protein production (Xing et al., 2016). A native *MRK1* promoter-driven construct with a GFP epitope tag was generated in this work (Appendix Table 1), and subsequent coIP assays could benefit from its relatively weak expression. Finally, truncations using only the N-terminal domain, kinase domain, or C-terminal domain of a MAPKKK have been used to identify specific protein-protein associations, namely for MAPKKK5 and PBL27 in yeast 2-hybrid(Yamada et al., 2016). As MRK1 contains three distinct domains based on sequence analysis (Figure 1B), we may be able to generate N-terminal, kinase domain, or C-terminal truncations to determine if this non-specific binding is derived from a particular domain. However, should specific association with CPK28 be observed using a truncated variant of MRK1, this result should be cautiously interpreted as truncations do not necessarily retain their normal protein function.

The association of CPK28-MRK1 and BIK1-MRK1 was subsequently tested using a second approach, BiFC in *N. benthamiana*. Similarly, strong reconstitution of YFP was observed when MRK1 was co-expressed with either CPK28, BIK1, a negative protein control, or an empty vector control (Figure 2B). As epitope tag size may be playing a role in this promiscuous association (Fukao, 2012), I performed BiFC assays using MRK1 tagged with either nYFP or cYFP, which are 17.6 kDa and 9.7 kDa respectively. In both cases, association was observed between the empty vector control and either MRK1-nYFP (data not shown) or MRK1-cYFP (Figure 2B), suggesting that this non-specific binding occurs irrespective of tag size. A greater limitation of BiFC, the spontaneous reassembly of split-YFP fragments, has been covered extensively (Horstman et al., 2014). Even in the absence of associating proteins, split-YFP halves may undergo "self-assembly" and generate background signal, leading to a high rate of false positive interactions (Horstman et al., 2014). Using other fluorescent proteins with a specific split position, such as mVenus split at residue 210 (Gookin and Assmann, 2014), can reduce background fluorescence due to self-assembly and may serve as an alternative to traditional split-YFP methods. Unequal dosage of nYFP- and cYFP-tagged proteins may also result in aberrant YFP reconstitution, as *Agrobacterium*-mediated co-transfection of both constructs can cause high variability in expression (Xing et al., 2016). Should MRK1 exhibit non-specific binding due to gene dosage effects, this may be corrected using a "2in1" plasmid which allows transient expression of both fusion proteins from a single vector (Hecker et al., 2015). Ultimately, I was unable to confirm association between CPK28 and MRK1 using coIP or BiFC assays. Additional work may be needed to address the non-specific binding of MRK1 in negative controls, either through native promoter-driven coIP assays, applying a different split fluorescent protein system for BiFC, simultaneous transfection of two association partners using a “2in1” vector, and/or another protein-protein association technique such as split-luciferase complementation assays.

4.2. Raf-like MAPKKK Subgroup C7-1 members may negatively regulate immune-induced oxidative burst in a partially redundant manner

To determine whether Raf-like MAPKKK Subgroup C7 members may play a role in immunity, I analyzed their expression profiles following pathogen or elicitor treatment using the Bio-Analytic Resource for Plant Biology (Toufighi et al., 2005). Interestingly, Raf26 was strongly upregulated upon infection with virulent and avirulent strains of the biotrophic bacterial pathogen *P. syringae* pv. *maculicola*, the hemi-biotrophic oomycete *H. arabidopsidis*, the necrotrophic fungus *B. cinerea*, and the biotrophic fungus *E. orontii* (Figure 3C). This may support the involvement of Raf26 in innate immune responses to both avirulent and virulent pathogens with diverse infection strategies, and future studies may wish to examine possible Raf26-mediated responses in greater detail. However, transcript expression does not necessarily correlate with protein expression or biological function. For example, the Subgroup C5 member Raf43 is highly upregulated following infection with *P. syringae* pv. *tomato* DC3000, though both *raf43-1* or *RAF43-OE* lines exhibit wild-type resistance upon infection with *P. syringae* pv. *tomato* DC3000, suggesting that Raf43 is not involved in mediating this response or higher-order mutants may be required to observe a phenotype (Virk et al., 2015). While *MRK1* expression was not strongly induced after pathogen or elicitor treatment (Figure 3C), it may be modified at the protein or phosphoprotein level following immune activation to elicit a response.

Using single and double null lines, I characterized the role of Raf-like MAPKKK Subgroup C7 members in early pattern-triggered responses. Following PAMP treatment, the apoplastic ROS burst of *mrk1 raf39* and *mrk1 raf26* double null lines was enhanced relative to wild-type in 8 of 12 replicates (Figure 4B). As oxidative burst did not differ from wild-type in single null lines (Figure 4A), this suggests that Subgroup C7-1 members may negatively regulate immune-induced oxidative burst downstream of pattern recognition and exhibit some functional redundancy. Coupled with the MEKK-like MAPKKK7 which attenuates ROS burst downstream of FLS2 (Mithoe et al., 2016), this is the second MAPKKK module that was shown to impair immune-induced ROS production in Arabidopsis. However, as this phenotype was not observed consistently in all replicates, measures should be taken to reduce variability in subsequent experiments. First, plants should be sampled in good health and at the same developmental stage between replicates, as healthy plants were sampled between 5-6 weeks and the consistency of immune-induced oxidative burst can vary with age (Bredow et al., 2019). Similarly, all plants should be grown under identical environmental conditions to increase reproducibility, including humidity, temperature, light intensity, and photoperiod (Bredow et al., 2019). Prior to overnight recovery, leaf discs may also be cut in half to increase the surface area exposed to elicitor solution upon treatment, as this could reduce variation between replicates (Smith and Heese, 2014; Bredow et al., 2019). Interestingly, the *raf26 raf39* double null line did not display aberrant ROS production following elicitation (Figure 4B), suggesting that the presence of MRK1 may be sufficient to produce a wild-type response. This complex pattern of redundancy is reminiscent of a MEKK-like MAPKKK family which includes ANP1, ANP2, and ANP3

(MAPK Group, 2002). Double null *anp2 anp3* lines have disrupted cell division and are severely stunted in growth, while *anp1 anp3* lines present floral organ defects and *anp1 anp2* lines are phenotypically normal (Krysan et al., 2002). As the triple *anp1 anp2 anp3* null line is embryo lethal (Krysan et al., 2002), it was hypothesized that members of this MAPKKK family regulate cytokinesis in a partially redundant manner. Similarly, the Raf-like MAPKKK Subgroup C7-1 members may regulate immune-induced oxidative burst through incomplete functional redundancy. Characterizing a *raf26 raf39 mrk1* triple null mutant will represent a critical step in unraveling the partially overlapping role of these protein kinases in the negative regulation of innate immunity.

While the Raf-like MAPKKK Subgroup B members EDR1 and CTR1 function upstream of MAPK activation (Yoo et al., 2008; Zhao et al., 2014), no Subgroup C members have been similarly placed in a cascade. I examined the immune-induced activation of MPK3/4/6/11 in Subgroup C7-1 null lines to determine if they may also regulate this early immune output. Following PAMP treatment, double *mrk1 raf39* and *mrk1 raf26* lines displayed wild-type levels of MAPK activation (Figure 6C), suggesting that Subgroup C7-1 members may not play a role in this response. Whether Subgroup C7-1 members function upstream of MPK3/4/6/11 or other MAPKs independently of pattern recognition remains to be seen, though this line of study has the potential to reshape our current understanding of Subgroup C members as non-canonical MAPKKKs (Tang and Innes, 2002). As ROS production and MAPK activation are independent early immune signalling events (Xu et al., 2014), Subgroup C7-1 members appear to regulate immunity downstream of PRR activation and upstream of RBOHD-mediated ROS production, with no confirmed function in MAPK activation.

To limit pathogen entry, stomatal pores on the plant epidermis are actively closed upon pattern recognition (Melotto et al., 2006). While several signal transduction pathways underlie this response, internalization of apoplastic ROS through transmembrane water channels, known as aquaporins, can facilitate PAMP-induced stomatal closure (Rodrigues et al., 2017). As double *mrk1 raf39* and *mrk1 raf26* lines have increased apoplastic ROS production following PAMP perception, I assessed immune-induced stomatal closure in Subgroup C7 null lines to determine whether this response may also be affected. In double null lines representing both Subgroup C7-1 and Subgroup C7-2 clades, normal stomatal closure was observed upon immune elicitation (Figure 6D). Prior to PAMP treatment, double *raf33 raf38* lines also had smaller stomatal aperture relative to wild-type (Figure 6D), in agreement with published data (Hiyama et al., 2017). Due to their enhanced oxidative burst, it may be expected that *mrk1 raf39* and *mrk1 raf26* lines would exhibit smaller stomatal aperture relative to wild-type following pattern detection. However, this assay is constrained by both high variability and low sensitivity, therefore it may be difficult to distinguish stomata that are significantly more closed after elicitation. Accordingly, immune-induced stomatal aperture is primarily used to identify positive regulators of immunity, such as BIK1 and RBOHD, which display insensitivity to flg22-mediated stomatal closure (Mersmann et al., 2010; Li et al., 2014). Further work may be required to validate these initial results using more sensitive assays or an indirect measure of stomatal defense, such as stomatal conductance or *P. syringae* proliferation, respectively.

Though phosphorylation of protein kinases does not always result in their activation (Li et al., 2016b), several CDPKs and MAPKs are phosphorylated and activated following PRR complex formation (Couto and Zipfel, 2016). As *MRK1* expression did not change after pathogen or elicitor treatment (Figure 3C), it may function downstream of receptor complex activation through modification of its protein abundance or phosphorylation status upon immune induction. In agreement with this hypothesis, the abundance of two phosphopeptides corresponding to MRK1, containing phosphorylated threonine residues at either position 41 or 121 (Figure 1C), were reported to have reduced abundance in plasma membrane fractions following PAMP treatment (Benschop et al., 2007; Nühse et al., 2007). Ideally, changes in the immune-induced phosphorylation status of MRK1 could be investigated through treatment of stable *mrk1-1/MRK1-GFP* complementation lines with or without an elicitor, affinity purification of MRK1, and analysis of total MRK1 phosphorylation using a phosphoprotein detection system. In one preliminary experiment, I attempted this workflow using a pIMAGO phosphoprotein detection kit and observed reduced total phosphorylation of MRK1 following elf18 treatment (Appendix Figure 4). However, this assay was only performed once, had substantial background noise, and may be confounded by excessive or unequal protein loading. In subsequent replicates, this procedure may be improved by testing protein loading using a dilution series to optimize assay sensitivity, performing a phosphatase treatment on affinity purified MRK1 to confirm that observed bands are a result of phosphorylation, and/or resolving phosphorylated proteins using another detection method with less background signal, such as Phos-Tag gels.

Taken together, MRK1 and related Raf-like MAPKKK Subgroup C7-1 members were tentatively placed as signal transducers downstream of PRR complex activation and upstream of RBOHD-mediated ROS burst. Future work will be required to contextualize these negative regulators of immunity in a signalling cascade, through identification of MAPKK or non-MAPKK substrates.

4.3. MRK1 may play a role in normal rosette development

To further investigate the role of MRK1 in the innate immune response, I generated four independent *MRK1-OE* lines. While three of these lines had somewhat increased expression of *MRK1* relative to wild-type, the *MRK1-OE 10-12* line had markedly increased *MRK1* accumulation (Figure 8B). Interestingly, *MRK1-OE 10-12* plants also had white, spiked leaves emerging at the center of the rosette and abnormal leaf shape (Figure 8A), suggesting that MRK1 may function in normal rosette development. As this was only observed in one of four *MRK1-OE* lines, this phenotype could be attributed to positional effects from insertion of the *MRK1-GFP* transgene. Isolating additional *MRK1-OE* lines with similar *MRK1* expression will be critical to validating this preliminary phenotype. Should MRK1 play a role in development, detailed analysis could place this protein kinase in a developmental pathway. This could be achieved through epistatic analysis with regulators of hormone biosynthesis and signalling or by assessing the *MRK1-OE* transcriptome relative to wild-type using RNA sequencing. Although *mrk1 raf39* and *mrk1 raf26* lines display an enhanced oxidative burst following immune elicitation, all *MRK1-OE* lines have a wild-type output (Figure 8C). These phenotypic differences are reminiscent of the Subgroup C5 member Raf43, as *raf43-1* mutants have reduced tolerance to abiotic stress while *RAF43-OE* are similar to Col-0 (Virk et al., 2015). In some cases, constitutive activation of a MAPK cascade component is required to observe a phenotype in overexpression lines. For example, phosphomimetic mutations in the MAPKK activation motif are necessary to detect enhanced disease resistance in *MKK3-OE* (Dóczi et al., 2007). As MRK1 may require activation by upstream signalling, overexpression of the inactive protein kinase would not result in lower immune-induced oxidative burst, as would be expected for a negative regulator of immunity. Unlike MAPKs and MAPKKs, generating constitutively active variants of MAPKKKs can be challenging, as no distinct activation motif has been identified (Suarez-Rodriguez et al., 2010). In select cases, constitutively active MAPKKKs have been produced by deleting portions of the N-terminal domain (Asai et al., 2002; Sopeña-Torres et al., 2018). Further analysis will be required to examine a putative dual role of MRK1 in rosette development and immunity, and whether its activation is required for function.

4.4. MRK1 localizes to the cytosol

The subcellular localization of a protein can serve as a predictive tool when assessing its function. Under the CaMV 35S promoter, MRK1 localized to the cytosol in both *N. benthamiana* and Arabidopsis (Figure 9A and B), which supports a role in intracellular signal transduction downstream of immune receptor complexes. No signal was observed using native promoter-driven constructs (Figure 9A and B), suggesting that this fluorescence may be beyond the detection limit of our confocal microscope. Interestingly, MRK1 has been identified in plasma membrane fractions in multiple proteomic and phosphoproteomic datasets (Benschop et al., 2007; Marmagne et al., 2007; Nühse et al., 2007). As it can be difficult to discern between plasma membrane and cytosolic localization at the cell surface (Serna, 2004), additional work may be required to determine if MRK1 also localizes to the plasma membrane upon plasmolysis.

4.5. PP2A-B subunits are putative CPK28-associated proteins that may not regulate early immune outputs

Several protein phosphatases attenuate immune activation by dephosphorylating positive regulators of immunity (Suarez-Rodriguez et al., 2010; Macho and Zipfel, 2014). A trimeric PP2A, composed of the catalytic subunit C4, the scaffolding subunit A1, and the regulatory subunits B'η or B'ζ, can dephosphorylate BAK1 both in the presence or absence of pathogen perception to dampen signalling (Segonzac et al., 2014). Two PP2A regulatory subunits, PP2A-

Bα and PP2A-Bβ, were identified as putative CPK28-associated proteins in the initial IP-MS screen and were evaluated for their potential role in regulating early immune responses. Loss-of-function *pp2a-bα-1* and *pp2a-bβ-1* did not display an aberrant immune-induced oxidative burst (Appendix Figure 6B), suggesting that they are not involved in the RBOHD-mediated branch of immunity. It remains to be seen whether these PP2A-B subunits play a role in RBOHD-independent immune signalling, such as in the immune-induced activation of MAPK cascades (Xu et al., 2014). Both PP2A-B subunits were previously identified as regulators of flowering time in Arabidopsis and the double *pp2a-bα pp2a-bβ* null mutant is embryo lethal (Heidari et al., 2013). Interestingly, loss-of-function *cpk28-1* plants display stunted stem elongation, anthocyanin accumulation, and abnormal vascular patterning following reproductive transition (Matschi et al., 2013), supporting a dual function of CPK28 in regulating immunity and development. It is tempting to speculate that the PP2A-B subunits may function in a CPK28-mediated developmental module due to their established role in flowering time (Heidari et al., 2013). Future work will be required to determine whether CPK28 and the PP2A-B subunits act in the same developmental pathway using epistatic analysis and protein-protein association assays.

4.6. Future directions

In the Arabidopsis genome, approximately 4% of all genes encode for protein kinases (Zulawski et al., 2014). Members of this expansive superfamily can target diverse substrates and regulate many cellular processes through post-translational modifications (Wang et al., 2007). The functional characterization of the 48-member Raf-like MAPKKK family, a subset of protein kinases, is currently ongoing (MAPK Group, 2002; Suarez-Rodriguez et al., 2010). While members of this family have been implicated in ethylene resistance, basal defense, CO_2-induced stomatal closure, seed dormancy, and salt tolerance (Kieber et al., 1993; Frye and Innes, 1998; Gao and Xiang, 2008; Lee et al., 2015b; Tian et al., 2015), almost no direct substrates of Raf-like MAPKKKs have been identified. In one case, the Raf-like MAPKKK Subgroup B member CTR1 was found to phosphorylate the C-terminal domain of ETHYLENE INSENSITIVE 2, a positive regulator of ethylene signalling (Ju et al., 2012). Few other Raf-like MAPKKK-mediated phosphorylation events have been shown, though associations between Raf-like MAPKKKs and other proteins were observed, such as the Subgroup C1 INTEGRIN-LINKED KINASE 1 with the K^+ transporter HIGH AFFINITY K^+ TRANSPORTER 5 (Brauer et al., 2016). An outstanding question of this thesis work and in broader MAPK signalling research is whether the Raf-like MAPKKK family should be classified as a group of canonical MAPKKKs or as MLKs. As plant Raf-like MAPKKKs are divergent from both animal Raf-like kinases and animal MLKs, they must be classified based on direct phosphorylation of a MAPKK (Tang and Innes, 2002). In this work, the Raf-like MAPKKK Subgroup C7-1 members were identified as negative regulators of immune-induced oxidative burst. While double null *mrk1 raf39* and *mrk1 raf26* lines displayed an enhanced ROS burst following elicitation (Figure 6B), no change in immune-induced MPK3/4/6/11 activation was identified (Figure 6C). This suggests that Subgroup C7-1 members may not be acting upstream of MPK3/4/6/11 in a MAPK cascade following immune elicitation, and could act on other downstream substrates independent from these cascades. I also tested association of MRK1 with CPK28 to validate our initial screen and identify a possible MRK1 interactor. Unfortunately, these assays were inconclusive due to unspecific binding of MRK1 (Figure 2), therefore it may be challenging to identify putative MRK1 substrates and association partners *in planta*. Further analysis will be required to reduce non-specific binding of MRK1 in protein-protein association assays, and better classify MRK1 as a canonical or non-canonical MAPKKK through identification of a MAPKK or non-MAPKK substrate. A second outstanding question of this thesis work is whether MRK1 may be playing a role in both immunity and developmental pathways. While the oxidative burst phenotype of *mrk1 raf39* and *mrk1 raf26* was observed in 8 of 12 replicates (Appendix Table 7), a triple *raf26 raf39 mrk1* mutant may present a more consistent phenotype due to the partially overlapping functions of Subgroup C7-1 members. Functional characterization of this triple mutant will be necessary to discern additional immune phenotypes of Subgroup C7-1 members, if any, and confirm that they exhibit partial redundancy. Similarly, more *MRK1-OE* lines must be isolated to confirm that any developmental phenotypes observed in this work were not a result of positional effects (Figure 8A). Ultimately, further work will be required to validate the preliminary immune and developmental phenotypes identified in Raf-like MAPKKK Subgroup C7-1 mutants. Should later analyses identify an association partner or substrate of MRK1, this may provide more detailed information about the function and classification of the diverse Raf-like MAPKKK members relative to their mammalian counterparts.

4.7. Concluding remarks

Though few negative regulators of immunity have been characterized, this work provides preliminary evidence for the attenuation of the immune-induced oxidative burst by a MAPKKK subclade. To uncover novel regulators of immune signalling, putative interactors of CPK28 were identified through IP-MS. This screen detected a Raf-like MAPKKK Subgroup C7 member, MRK1, as a potential CPK28-associated protein. I was unable to confirm association of MRK1 and CPK28 using coIP or BiFC in *N. benthamiana*, as MRK1 interacted promiscuously with negative controls. Using double null lines, I found that MRK1 and two closely related Raf-like MAPKKKs, Raf26 and Raf39, may negatively regulate the immune-induced oxidative burst in a partially redundant manner. I also identified a preliminary developmental phenotype for one *MRK1-OE* line, as these mutants displayed small, spiked leaves at the center of the rosette and abnormal leaf shape. Using confocal microscopy, I determined that MRK1 appears to localize to the cytosol in both *N. benthamiana* and Arabidopsis. Two PP2A regulatory subunits, PP2A-Bα and PP2A-Bβ, were also identified as putative CPK28-associated proteins and analyzed for their role in innate immunity. However, null lines for both regulatory subunits exhibited normal immune-induced oxidative burst. Taken together, this work suggests that MRK1, Raf26, and Raf39 may function as novel negative regulators of plant innate immunity. In addition, MRK1 may be playing a role in normal rosette development. Outstanding lines of inquiry from this work include confirming the immune and developmental phenotypes presented in null and overexpression lines for MAPKKK Subgroup C7-1 members, determining whether MRK1 functions as a canonical MAPKKK by phosphorylating a MAPKK, and assessing how MRK1 and related Rafs might exhibit partial redundancy to regulate the immune-induced oxidative burst.

The plant innate immune response must be tightly regulated to limit the developmental trade-offs associated with unnecessary immune activation (van Wersch et al., 2016). By identifying novel positive and negative regulators of plant immunity, we may be able to engineer crops with increased resistance to pathogens that can largely maintain normal growth and development. This thesis work provides foundational knowledge for assessing the role of three novel negative immune regulators, and may have far-reaching implications in the development of pathogen-resistant crop varieties.

5. SUMMARY

1) A reverse genetics screen for novel regulators of immunity was previously conducted through affinity purification of CPK28 and its interacting partners. The Raf-like MAPKKK MRK1 was identified as a putative CPK28-associated protein. Association of MRK1 and CPK28 could not be confirmed using coIP or BiFC assays, as MRK1 exhibited non-specific binding with negative controls.

2) Through functional characterization of null lines for MRK1 and related family members, MRK1, Raf26, and Raf39 were shown to negatively regulate immune-induced oxidative burst in a partially redundant manner. These lines did not display aberrant immune-induced MAPK activation or stomatal defense.

3) MRK1 may function in normal rosette development, as a highly expressing *MRK1-OE* line had white, spiked leaves emerging at the center of the rosette and abnormal leaf shape. Since this could be caused by positional effects of the MRK1 insertion, additional *MRK1-OE* lines must be generated to confirm this phenotype.

4) Through confocal imaging, MRK1 was found to localize to the cytosol in both *N. benthamiana* and Arabidopsis.

5) Two regulatory protein phosphatase subunits, PP2A-Bα and PP2A-Bβ, were also identified as putative CPK28-associated proteins. Immune-induced oxidative burst did not differ from wild-type in null *pp2a-bα* and *pp2a-bβ* lines, suggesting that they do not play a role in this early immune response.

6. LITERATURE CITED

Abramovitch RB, Anderson JC, Martin GB (2006) Bacterial elicitation and evasion of plant innate immunity. Nat Rev Mol Cell Biol **7**: 601–611

Albert I, Böhm H, Albert M, Feiler CE, Imkampe J, Wallmeroth N, Brancato C, Raaymakers TM, Oome S, Zhang H, et al (2015) An RLP23–SOBIR1–BAK1 complex mediates NLP-triggered immunity. Nat Plants **1**: 15140

Alonso JM, Stepanova AN, Leisse TJ, Kim CJ, Chen H, Shinn P, Stevenson DK, Zimmerman J, Barajas P, Cheuk R, et al (2003) Genome-wide insertional mutagenesis of *Arabidopsis thaliana*. Science **301**: 653–657

Asai T, Tena G, Plotnikova J, Willmann MR, Chiu W-L, Gomez-Gomez L, Boller T, Ausubel FM, Sheen J (2002) MAP kinase signalling cascade in *Arabidopsis* innate immunity. Nature **415**: 977–983

Athman R, Philpott D (2004) Innate immunity via Toll-like receptors and Nod proteins. Curr Opin Microbiol **7**: 25–32

Bartels S, Anderson JC, González Besteiro MA, Carreri A, Hirt H, Buchala A, Métraux J-P, Peck SC, Ulm R (2009) MAP KINASE PHOSPHATASE1 and PROTEIN TYROSINE PHOSPHATASE1 are repressors of salicylic acid synthesis and SNC1-mediated Responses in *Arabidopsis*. Plant Cell **21**: 2884–2897

Bender KW, Blackburn RK, Monaghan J, Derbyshire P, Menke FL, Zipfel C, Goshe MB, Zielinski RE, Huber SC (2017) Autophosphorylation-based calcium (Ca^{2+}) sensitivity priming and Ca^{2+}/Calmodulin inhibition of *Arabidopsis thaliana* Ca^{2+}-dependent protein kinase 28 (CPK28). J Biol Chem **292**: 3988–4002

Béné C, Barange M, Subasinghe R, Pinstrup-Andersen P, Merino G, Hemre G-I, Williams M (2015) Feeding 9 billion by 2050 – Putting fish back on the menu. Food Secur **7**: 261–274

Benschop JJ, Mohammed S, O'Flaherty M, Heck AJR, Slijper M, Menke FLH (2007) Quantitative phosphoproteomics of early elicitor signaling in *Arabidopsis*. Mol Cell Proteomics **6**: 1198–1214

Bi G, Zhou Z, Wang W, Li L, Rao S, Wu Y, Zhang X, Menke FLH, Chen S, Zhou J-M (2018) Receptor-like cytoplasmic kinases directly link diverse pattern recognition receptors to the activation of mitogen-activated protein kinase cascades in *Arabidopsis*. Plant Cell **30**: 1543–1561

van der Biezen EA, Freddie CT, Kahn K, Parker JE, Jones JDG (2002) *Arabidopsis* RPP4 is a member of the RPP5 multigene family of TIR-NB-LRR genes and confers downy mildew resistance through multiple signalling components. Plant J **29**: 439–451

Bigeard J, Colcombet J, Hirt H (2015) Signaling mechanisms in pattern-triggered immunity (PTI). Mol Plant **8**: 521–539

Böhm H, Albert I, Fan L, Reinhard A, Nürnberger T (2014) Immune receptor complexes at the plant cell surface. Curr Opin Plant Biol **20**: 47–54

Brauer EK, Ahsan N, Dale R, Kato N, Coluccio AE, Piñeros MA, Kochian LV, Thelen JJ, Popescu SC (2016) The Raf-like kinase ILK1 and the high affinity K^+ transporter HAK5 are required for innate immunity and abiotic stress response. Plant Physiol **171**: 1470–1484

Bredow M, Sementchoukova I, Siegel K, Monaghan J (2019) Pattern-triggered oxidative burst and seedling growth inhibition assays in *Arabidopsis thaliana*. J Vis Exp e59437

Büttner D, He SY (2009) Type III protein secretion in plant pathogenic bacteria. Plant Physiol

150: 1656–1664

Chinchilla D, Zipfel C, Robatzek S, Kemmerling B, Nürnberger T, Jones JDG, Felix G, Boller T, Zipfel C, Niwa Y, et al (2007) A flagellin-induced complex of the receptor FLS2 and BAK1 initiates plant defence. Nature **448**: 497–500

Choi HW, Klessig DF (2016) DAMPs, MAMPs, and NAMPs in plant innate immunity. BMC Plant Biol **16**: 232

Clark KL, Larsen PB, Wang X, Chang C (1998) Association of the *Arabidopsis* CTR1 Raf-like kinase with the ETR1 and ERS ethylene receptors. Proc Natl Acad Sci **95**: 5401–5406

Clough SJ, Bent AF (1998) Floral dip: a simplified method for *Agrobacterium*-mediated transformation of *Arabidopsis thaliana*. Plant J **16**: 735–743

Colcombet J, Hirt H (2008) *Arabidopsis* MAPKs: a complex signalling network involved in multiple biological processes. Biochem J **413**: 217–226

Conlan B, Stoll T, Gorman JJ, Saur I, Rathjen JP (2018) Development of a rapid *in planta* BioID system as a probe for plasma membrane-associated immunity proteins. Front Plant Sci **9**: 1882

Couto D, Niebergall R, Liang X, Bücherl CA, Sklenar J, Macho AP, Ntoukakis V, Derbyshire P, Altenbach D, Maclean D, et al (2016) The *Arabidopsis* protein phosphatase PP2C38 negatively regulates the central immune kinase BIK1. PLOS Pathog **12**: e1005811

Couto D, Zipfel C (2016) Regulation of pattern recognition receptor signalling in plants. Nat Rev Immunol **16**: 537–552

Cui H, Tsuda K, Parker JE (2015) Effector-triggered immunity: From pathogen perception to robust defense. Annu Rev Plant Biol **66**: 487–511

Cutler SR, Ehrhardt DW, Griffitts JS, Somerville CR (2000) Random GFP::cDNA fusions enable visualization of subcellular structures in cells of *Arabidopsis* at a high frequency. Proc Natl Acad Sci **97**: 3718–3723

Dangl JL, Horvath DM, Staskawicz BJ (2013) Pivoting the plant immune system from dissection to deployment. Science **341**: 746–751

Davidsson P, Broberg M, Kariola T, Sipari N, Pirhonen M, Palva ET (2017) Short oligogalacturonides induce pathogen resistance-associated gene expression in *Arabidopsis thaliana*. BMC Plant Biol **17**: 19

Dóczi R, Brader G, Pettkó-Szandtner A, Rajh I, Djamei A, Pitzschke A, Teige M, Hirt H (2007) The *Arabidopsis* mitogen-activated protein kinase kinase MKK3 is upstream of group C mitogen-activated protein kinases and participates in pathogen signaling. Plant Cell **19**: 3266–3279

Durian G, Rahikainen M, Alegre S, Brosché M, Kangasjärvi S (2016) Protein phosphatase 2A in the regulatory network underlying biotic stress resistance in plants. Front Plant Sci **7**: 812

Eschen-Lippold L, Bethke G, Palm-Forster MAT, Pecher P, Bauer N, Glazebrook J, Scheel D, Lee J (2012) MPK11-a fourth elicitor-responsive mitogen-activated protein kinase in *Arabidopsis thaliana*. Plant Signal Behav **7**: 1203–1205

Felix G, Duran JD, Volko S, Boller T (1999) Plants have a sensitive perception system for the most conserved domain of bacterial flagellin. Plant J **18**: 265–276

Feng F, Yang F, Rong W, Wu X, Zhang J, Chen S, He C, Zhou J-M (2012) A *Xanthomonas* uridine 5′-monophosphate transferase inhibits plant immune kinases. Nature **485**: 114–118

Ferrari S, Savatin D V, Sicilia F, Gramegna G, Cervone F, Lorenzo G De (2013) Oligogalacturonides: plant damage-associated molecular patterns and regulators of growth

and development. Front Plant Sci **4**: 49
Free RB, Hazelwood LA, Sibley DR (2009) Identifying novel protein-protein interactions using co-immunoprecipitation and mass spectroscopy. Curr Protoc Neurosci **Chapter 5**: Unit 5.28
Frye CA, Innes RW (1998) An *Arabidopsis* mutant with enhanced resistance to powdery mildew. Plant Cell **10**: 947–956
Fukao Y (2012) Protein-protein interactions in plants. Plant Cell Physiol **53**: 617–625
Gao L, Xiang C-B (2008) The genetic locus At1g73660 encodes a putative MAPKKK and negatively regulates salt tolerance in *Arabidopsis*. Plant Mol Biol **67**: 125–134
Gao M, Liu J, Bi D, Zhang Z, Cheng F, Chen S, Zhang Y (2008) MEKK1, MKK1/MKK2 and MPK4 function together in a mitogen-activated protein kinase cascade to regulate innate immunity in plants. Cell Res **18**: 1190–1198
Gibson DG, Young L, Chuang R-Y, Venter JC, Hutchison CA, Smith HO (2009) Enzymatic assembly of DNA molecules up to several hundred kilobases. Nat Methods **6**: 343–345
Gómez-Gómez L, Boller T (2000) FLS2: an LRR receptor-like kinase involved in the perception of the bacterial elicitor flagellin in *Arabidopsis*. Mol Cell **5**: 1003–1011
Gómez-Gómez L, Felix G, Boller T (1999) A single locus determines sensitivity to bacterial flagellin in *Arabidopsis thaliana*. Plant J **18**: 277–284
Gookin TE, Assmann SM (2014) Significant reduction of BiFC non-specific assembly facilitates *in planta* assessment of heterotrimeric G-protein interactors. Plant J **80**: 553–567
Grefen C, Donald N, Hashimoto K, Kudla J, Schumacher K, Blatt MR (2010) A ubiquitin-10 promoter-based vector set for fluorescent protein tagging facilitates temporal stability and native protein distribution in transient and stable expression studies. Plant J **64**: 355–365
Gust AA, Felix G (2014) Receptor like proteins associate with SOBIR1-type of adaptors to form bimolecular receptor kinases. Curr Opin Plant Biol **21**: 104–111
Halter T, Imkampe J, Mazzotta S, Wierzba M, Postel S, Bücherl C, Kiefer C, Stahl M, Chinchilla D, Wang X, et al (2014) The leucine-rich repeat receptor kinase BIR2 is a negative regulator of BAK1 in plant immunity. Curr Biol **24**: 134–143
Hashimoto M, Negi J, Young J, Israelsson M, Schroeder JI, Iba K (2006) *Arabidopsis* HT1 kinase controls stomatal movements in response to CO_2. Nat Cell Biol **8**: 391–397
Hayashi F, Smith KD, Ozinsky A, Hawn TR, Yi EC, Goodlett DR, Eng JK, Akira S, Underhill DM, Aderem A (2001) The innate immune response to bacterial flagellin is mediated by Toll-like receptor 5. Nature **410**: 1099–1103
Hayashi M, Inoue S, Ueno Y, Kinoshita T (2017) A Raf-like protein kinase BHP mediates blue light-dependent stomatal opening. Sci Rep **7**: 45586
Hecker A, Wallmeroth N, Peter S, Blatt MR, Harter K, Grefen C (2015) Binary 2in1 vectors improve *in Planta* (co)localization and dynamic protein interaction studies. Plant Physiol **168**: 776–787
Heidari B, Matre P, Nemie-Feyissa D, Meyer C, Rognli OA, Moller SG, Lillo C (2011) Protein phosphatase 2A B55 and A regulatory subunits interact with nitrate reductase and are essential for nitrate reductase activation. Plant Physiol **156**: 165–172
Heidari B, Nemie-Feyissa D, Kangasjärvi S, Lillo C (2013) Antagonistic regulation of flowering time through distinct regulatory subunits of protein phosphatase 2A. PLoS One **8**: e67987
Hendrickson EL, Guevera P, Peñaloza-Vàzquez A, Shao J, Bender C, Ausubel FM (2000) Virulence of the phytopathogen *Pseudomonas syringae* pv. *maculicola* is rpoN dependent. J

Bacteriol **182**: 3498–3507
Hiyama A, Takemiya A, Munemasa S, Okuma E, Sugiyama N, Tada Y, Murata Y, Shimazaki K (2017) Blue light and CO_2 signals converge to regulate light-induced stomatal opening. Nat Commun **8**: 1284
Horstman A, Tonaco IAN, Boutilier K, Immink RGH (2014) A cautionary note on the use of split-YFP/BiFC in plant protein-protein interaction studies. Int J Mol Sci **15**: 9628–9643
Huang Y, Li H, Gupta R, Morris PC, Luan S, Kieber JJ (2000) ATMPK4, an *Arabidopsis* homolog of mitogen-activated protein kinase, is activated *in vitro* by AtMEK1 through threonine phosphorylation. Plant Physiol **122**: 1301–1310
Huffaker A, Pearce G, Ryan CA (2006) An endogenous peptide signal in *Arabidopsis* activates components of the innate immune response. Proc Natl Acad Sci **103**: 10098–10103
Ichimura K, Mizoguchi T, Shinozaki K (1997) ATMRK1, an *Arabidopsis* protein kinase related to mammal mixed-lineage kinases and Raf protein kinases. Plant Sci **130**: 171–179
Ingle RA, Carstens M, Denby KJ (2006) PAMP recognition and the plant–pathogen arms race. BioEssays **28**: 880–889
Jagodzik P, Tajdel-Zielinska M, Ciesla A, Marczak M, Ludwikow A (2018) Mitogen-activated protein kinase cascades in plant hormone signaling. Front Plant Sci **9**: 1387
Jonak C, Okrész L, Bögre L, Hirt H (2002) Complexity, cross talk and integration of plant MAP kinase signalling. Curr Opin Plant Biol **5**: 415–424
Ju C, Yoon GM, Shemansky JM, Lin DY, Ying ZI, Chang J, Garrett WM, Kessenbrock M, Groth G, Tucker ML, et al (2012) CTR1 phosphorylates the central regulator EIN2 to control ethylene hormone signaling from the ER membrane to the nucleus in *Arabidopsis*. Proc Natl Acad Sci **109**: 19486–19491
Kadota Y, Sklenar J, Derbyshire P, Stransfeld L, Asai S, Ntoukakis V, Jones JD, Shirasu K, Menke F, Jones A, et al (2014) Direct regulation of the NADPH oxidase RBOHD by the PRR-associated kinase BIK1 during plant immunity. Mol Cell **54**: 43–55
Kieber JJ, Rothenberg M, Roman G, Feldmann KA, Ecker JR (1993) CTR1, a negative regulator of the ethylene response pathway in *Arabidopsis*, encodes a member of the Raf family of protein kinases. Cell **72**: 427–441
Kinoshita T, Doi M, Suetsugu N, Kagawa T, Wada M, Shimazaki K (2001) Phot1 and phot2 mediate blue light regulation of stomatal opening. Nature **414**: 656–660
Krysan PJ, Jester PJ, Gottwald JR, Sussman MR (2002) An *Arabidopsis* mitogen-activated protein kinase kinase kinase gene family encodes essential positive regulators of cytokinesis. Plant Cell **14**: 1109–1120
Kunze G, Zipfel C, Robatzek S, Niehaus K, Boller T, Felix G (2004) The N terminus of bacterial elongation factor Tu elicits innate immunity in *Arabidopsis* plants. Plant Cell **16**: 3496–3507
L'Haridon F, Besson-Bard A, Binda M, Serrano M, Abou-Mansour E, Balet F, Schoonbeek H-J, Hess S, Mir R, Léon J, et al (2011) A permeable cuticle is associated with the release of reactive oxygen species and induction of innate immunity. PLoS Pathog **7**: e1002148
Lakatos L, Szittya G, Silhavy D, Burgyán J (2004) Molecular mechanism of RNA silencing suppression mediated by p19 protein of tombusviruses. EMBO J **23**: 876–884
Lamberti G, Gügel IL, Meurer J, Soll J, Schwenkert S (2011) The cytosolic kinases STY8, STY17, and STY46 are involved in chloroplast differentiation in *Arabidopsis*. Plant Physiol **157**: 70–85
Lampard GR, MacAlister CA, Bergmann DC (2008) *Arabidopsis* stomatal initiation is

controlled by MAPK-mediated regulation of the bHLH SPEECHLESS. Science **322**: 1113–1116

Lee J, Eschen-Lippold L, Lassowskat I, Böttcher C, Scheel D (2015a) Cellular reprogramming through mitogen-activated protein kinases. Front Plant Sci **6**: 940

Lee S, Lee MH, Kim J-I, Kim SY (2015b) *Arabidopsis* putative MAP kinase kinase kinases Raf10 and Raf11 are positive regulators of seed dormancy and ABA response. Plant Cell Physiol **56**: 84–97

Lehti-Shiu MD, Zou C, Hanada K, Shiu S-H (2009) Evolutionary history and stress regulation of plant receptor-like kinase/pelle genes. Plant Physiol **150**: 12–26

Li B, Meng X, Shan L, He P (2016a) Transcriptional regulation of pattern-triggered immunity in plants. Cell Host Microbe **19**: 641–650

Li G, Meng X, Wang R, Mao G, Han L, Liu Y, Zhang S (2012) Dual-level regulation of ACC synthase activity by MPK3/MPK6 cascade and its downstream WRKY transcription actor during ethylene induction in *Arabidopsis*. PLoS Genet **8**: e1002767

Li L, Li M, Yu L, Zhou Z, Liang X, Liu Z, Cai G, Gao L, Zhang X, Wang Y, et al (2014) The FLS2-associated kinase BIK1 directly phosphorylates the NADPH oxidase RBOHD to control plant immunity. Cell Host Microbe **15**: 329–338

Li L, Yu Y, Zhou Z, Zhou J-M (2016b) Plant pattern-recognition receptors controlling innate immunity. Sci China Life Sci **59**: 878–888

Liebrand TWH, van den Burg HA, Joosten MHAJ (2014) Two for all: receptor-associated kinases SOBIR1 and BAK1. Trends Plant Sci **19**: 123–132

Liu Y, Zhang S (2004) Phosphorylation of 1-aminocyclopropane-1-carboxylic acid synthase by MPK6, a stress-responsive mitogen-activated protein kinase, induces ethylene biosynthesis in *Arabidopsis*. Plant Cell **16**: 3386–3399

Liu Z, Wu Y, Yang F, Zhang Y, Chen S, Xie Q, Tian X, Zhou J-M (2013) BIK1 interacts with PEPRs to mediate ethylene-induced immunity. Proc Natl Acad Sci**110**: 6205–6210

Lu D, Wu S, Gao X, Zhang Y, Shan L, He P (2010) A receptor-like cytoplasmic kinase, BIK1, associates with a flagellin receptor complex to initiate plant innate immunity. Proc Natl Acad Sci **107**: 496–501

Luo L (2012) Plant cytokine or phytocytokine. Plant Signal Behav **7**: 1513

Macho AP, Zipfel C (2014) Plant PRRs and the activation of innate immune signaling. Mol Cell **54**: 263–272

Malinovsky FG, Fangel JU, Willats WGT (2014) The role of the cell wall in plant immunity. Front Plant Sci **5**: 178

Mang H, Feng B, Hu Z, Boisson-Dernier A, Franck CM, Meng X, Huang Y, Zhou J, Xu G, Wang T, et al (2017) Differential regulation of two-tiered plant immunity and sexual reproduction by ANXUR receptor-like kinases. Plant Cell **29**: 3140–3156

MAPK Group (2002) Mitogen-activated protein kinase cascades in plants: a new nomenclature. Trends Plant Sci **7**: 301–308

Marmagne A, Ferro M, Meinnel T, Bruley C, Kuhn L, Garin J, Barbier-Brygoo H, Ephritikhine G (2007) A high content in lipid-modified peripheral proteins and integral receptor kinases features in the *Arabidopsis* Plasma Membrane Proteome. Mol Cell Proteomics **6**: 1980–1996

Marten H, Hedrich R, Roelfsema MRG (2007) Blue light inhibits guard cell plasma membrane anion channels in a phototropin-dependent manner. Plant J **50**: 29–39

Martin T, Sharma R, Sippel C, Waegemann K, Soll J, Vothknecht UC (2006) A protein kinase family in *Arabidopsis* phosphorylates chloroplast precursor proteins. J Biol Chem **281**: 40216–40223

Matschi S, Werner S, Schulze WX, Legen J, Hilger HH, Romeis T (2013) Function of calcium-dependent protein kinase CPK28 of *Arabidopsis thaliana* in plant stem elongation and vascular development. Plant J **73**: 883–896

Melotto M, Underwood W, He SY (2008) Role of stomata in plant innate immunity and foliar bacterial diseases. Annu Rev Phytopathol **46**: 101–122

Melotto M, Underwood W, Koczan J, Nomura K, He SY (2006) Plant stomata function in innate immunity against bacterial invasion. Cell **126**: 969–980

Meng X, Zhang S (2013) MAPK cascades in plant disease resistance signaling. Annu Rev Phytopathol **51**: 245–266

Mersmann S, Bourdais G, Rietz S, Robatzek S (2010) Ethylene signaling regulates accumulation of the FLS2 receptor and is required for the oxidative burst contributing to plant immunity. Plant Physiol **154**: 391–400

Mészáros T, Helfer A, Hatzimasoura E, Magyar Z, Serazetdinova L, Rios G, Bardóczy V, Teige M, Koncz C, Peck S, et al (2006) The *Arabidopsis* MAP kinase kinase MKK1 participates in defence responses to the bacterial elicitor flagellin. Plant J **48**: 485–498

Micali C, Göllner K, Humphry M, Consonni C, Panstruga R (2008) The powdery mildew disease of *Arabidopsis*: A paradigm for the interaction between plants and biotrophic fungi. Arabidopsis B **6**: e0115

Mithoe SC, Ludwig C, Pel MJ, Cucinotta M, Casartelli A, Mbengue M, Sklenar J, Derbyshire P, Robatzek S, Pieterse CM, et al (2016) Attenuation of pattern recognition receptor signaling is mediated by a MAP kinase kinase kinase. EMBO Rep **17**: 441–454

Monaghan J, Matschi S, Shorinola O, Rovenich H, Matei A, Segonzac C, Malinovsky FG, Rathjen JP, MacLean D, Romeis T, et al (2014) The calcium-dependent protein kinase CPK28 buffers plant immunity and regulates BIK1 turnover. Cell Host Microbe **16**: 605–615

Monaghan J, Zipfel C (2012) Plant pattern recognition receptor complexes at the plasma membrane. Curr Opin Plant Biol **15**: 349–357

Morita-Yamamuro C, Tsutsui T, Sato M, Yoshioka H, Tamaoki M, Ogawa D, Matsuura H, Yoshihara T, Ikeda A, Uyeda I, et al (2005) The *Arabidopsis* gene CAD1 controls programmed cell death in the plant immune system and encodes a protein containing a MACPF domain. Plant Cell Physiol **46**: 902–912

Moscatiello R, Mariani P, Sanders D, Maathuis FJM (2006) Transcriptional analysis of calcium-dependent and calcium-independent signalling pathways induced by oligogalacturonides. J Exp Bot **57**: 2847–2865

Nelson BK, Cai X, Nebenführ A (2007) A multicolored set of *in vivo* organelle markers for co-localization studies in *Arabidopsis* and other plants. Plant J **51**: 1126–1136

Nemoto K, Seto T, Takahashi H, Nozawa A, Seki M, Shinozaki K, Endo Y, Sawasaki T (2011) Autophosphorylation profiling of *Arabidopsis* protein kinases using the cell-free system. Phytochemistry **72**: 1136–1144

Nühse TS, Bottrill AR, Jones AME, Peck SC (2007) Quantitative phosphoproteomic analysis of plasma membrane proteins reveals regulatory mechanisms of plant innate immune responses. Plant J **51**: 931–940

O'Brien JA, Daudi A, Butt VS, Paul Bolwell G (2012) Reactive oxygen species and their role in plant defence and cell wall metabolism. Planta **236**: 765–779

O'Malley RC, Barragan CC, Ecker JR (2015) A user's guide to the *Arabidopsis* T-DNA insertion mutant collections. Methods Mol Biol **1284**: 323–342

Petersen M, Brodersen P, Naested H, Andreasson E, Lindhart U, Johansen B, Nielsen HB, Lacy M, Austin MJ, Parker JE, et al (2000) *Arabidopsis* MAP kinase 4 negatively regulates systemic acquired resistance. Cell **103**: 1111–1120

Philpott DJ, Girardin SE (2004) The role of Toll-like receptors and Nod proteins in bacterial infection. Mol Immunol **41**: 1099–1108

Ploetz RC (1994) Panama disease: Return of the first banana menace. Int J Pest Manag **40**: 326–336

Prelich G (2012) Gene overexpression: Uses, mechanisms, and interpretation. Genetics **190**: 841–854

Pringle H (1998) The slow birth of agriculture. Science **282**: 1446

Qiu J-L, Zhou L, Yun B-W, Nielsen HB, Fiil BK, Petersen K, MacKinlay J, Loake GJ, Mundy J, Morris PC (2008) *Arabidopsis* mitogen-activated protein kinase kinases MKK1 and MKK2 have overlapping functions in defense signaling mediated by MEKK1, MPK4, and MKS1. Plant Physiol **148**: 212–222

Ramachandiran I, Vijayakumar A, Ramya V, Rajasekharan R (2018) *Arabidopsis* serine/threonine/tyrosine protein kinase phosphorylates oil body proteins that regulate oil content in the seeds. Sci Rep **8**: 1154

Rao S, Zhou Z, Miao P, Bi G, Hu M, Wu Y, Feng F, Zhang X, Zhou J-M (2018) Roles of receptor-like cytoplasmic kinase VII members in pattern-triggered immune signaling. Plant Physiol **177**: 1679–1690

Rhee SY, Beavis W, Berardini TZ, Chen G, Dixon D, Doyle A, Garcia-Hernandez M, Huala E, Lander G, Montoya M, et al (2003) The *Arabidopsis* Information Resource (TAIR): a model organism database providing a centralized, curated gateway to *Arabidopsis* biology, research materials and community. Nucleic Acids Res **31**: 224–228

Rodrigues O, Reshetnyak G, Grondin A, Saijo Y, Leonhardt N, Maurel C, Verdoucq L (2017) Aquaporins facilitate hydrogen peroxide entry into guard cells to mediate ABA- and pathogen-triggered stomatal closure. Proc Natl Acad Sci **114**: 9200–9205

Schulze B, Mentzel T, Jehle AK, Mueller K, Beeler S, Boller T, Felix G, Chinchilla D (2010) Rapid heteromerization and phosphorylation of ligand-activated plant transmembrane receptors and their associated kinase BAK1. J Biol Chem **285**: 9444–9451

Schweighofer A, Kazanaviciute V, Scheikl E, Teige M, Doczi R, Hirt H, Schwanninger M, Kant M, Schuurink R, Mauch F, et al (2007) The PP2C-Type phosphatase AP2C1, which negatively regulates MPK4 and MPK6, modulates innate immunity, jasmonic acid, and ethylene levels in *Arabidopsis*. Plant Cell **19**: 2213–2224

Schwessinger B, Ronald PC (2012) Plant innate immunity: Perception of conserved microbial signatures. Annu Rev Plant Biol **63**: 451–482

Segonzac C, Macho AP, Sanmartin M, Ntoukakis V, Sanchez-Serrano JJ, Zipfel C (2014) Negative control of BAK1 by protein phosphatase 2A during plant innate immunity. EMBO J **33**: 2069–2079

Segonzac C, Monaghan J (2019) Modulation of plant innate immune signaling by small peptides. Curr Opin Plant Biol **51**: 22–28

Serna L (2004) A simple method for discriminating between cell membrane and cytosolic proteins. New Phytol **165**: 947–952

Shi H, Shen Q, Qi Y, Yan H, Nie H, Chen Y, Zhao T, Katagiri F, Tang D (2013) BR-

SIGNALING KINASE1 physically associates with FLAGELLIN SENSING2 and regulates plant innate immunity in *Arabidopsis*. Plant Cell **25**: 1143–1157
Shiu S-H, Bleecker AB (2001) Receptor-like kinases from *Arabidopsis* form a monophyletic gene family related to animal receptor kinases. Proc Natl Acad Sci **98**: 10763–10768
Shtein I, Shelef Y, Marom Z, Zelinger E, Schwartz A, Popper ZA, Bar-On B, Harpaz-Saad S (2017) Stomatal cell wall composition: distinctive structural patterns associated with different phylogenetic groups. Ann Bot **119**: 1021–1033
Shubchynskyy V, Boniecka J, Schweighofer A, Simulis J, Kvederaviciute K, Stumpe M, Mauch F, Balazadeh S, Mueller-Roeber B, Boutrot F, et al (2017) Protein phosphatase AP2C1 negatively regulates basal resistance and defense responses to *Pseudomonas syringae*. J Exp Bot **68**: 1169–1183
Siegel K, Monaghan J (2017) Analysis of CALCIUM-DEPENDENT PROTEIN KINASE 28-associated proteins of the model plant *Arabidopsis thaliana* in plant immune homeostasis. Honour's thesis. Queen’s University, Kingston, ON.
Singh RP, Hodson DP, Huerta-Espino J, Jin Y, Bhavani S, Njau P, Herrera-Foessel S, Singh PK, Singh S, Govindan V (2011) The emergence of Ug99 races of the stem rust fungus is a threat to world wheat production. Annu Rev Phytopathol **49**: 465–481
Smith JM, Heese A (2014) Rapid bioassay to measure early reactive oxygen species production in *Arabidopsis* leaf tissue in response to living *Pseudomonas syringae*. Plant Methods **10**: 6
Sopeña-Torres S, Jordá L, Sánchez-Rodríguez C, Miedes E, Escudero V, Swami S, López G, Piślewska-Bednarek M, Lassowskat I, Lee J, et al (2018) YODA MAP3K kinase regulates plant immune responses conferring broad-spectrum disease resistance. New Phytol **218**: 661–680
Stegmann M, Monaghan J, Smakowska-Luzan E, Rovenich H, Lehner A, Holton N, Belkhadir Y, Zipfel C (2017) The receptor kinase FER is a RALF-regulated scaffold controlling plant immune signaling. Science **355**: 287–289
Suarez-Rodriguez MC, Adams-Phillips L, Liu Y, Wang H, Su S-H, Jester PJ, Zhang S, Bent AF, Krysan PJ (2007) MEKK1 is required for flg22-induced MPK4 activation in *Arabidopsis* plants. Plant Physiol **143**: 661–669
Suarez-Rodriguez MC, Petersen M, Mundy J (2010) Mitogen-activated protein kinase signaling in plants. Annu Rev Plant Biol **61**: 621–649
Sun T, Nitta Y, Zhang Q, Wu D, Tian H, Lee JS, Zhang Y (2018) Antagonistic interactions between two MAP kinase cascades in plant development and immune signaling. EMBO Rep **19**: e45324
Sun Y, Li L, Macho AP, Han Z, Hu Z, Zipfel C, Zhou J-M, Chai J (2013) Structural basis for flg22-induced activation of the *Arabidopsis* FLS2-BAK1 immune complex. Science **342**: 624–628
Taj G, Agarwal P, Grant M, Kumar A (2010) MAPK machinery in plants: recognition and response to different stresses through multiple signal transduction pathways. Plant Signal Behav **5**: 1370–1378
Takagi M, Hamano K, Takagi H, Morimoto T, Akimitsu K, Terauchi R, Shirasu K, Ichimura K (2019) Disruption of the MAMP-induced MEKK1-MKK1/MKK2-MPK4 pathway activates the TNL immune receptor SMN1/RPS6. Plant Cell Physiol **60**: 778–787
Tang D, Innes RW (2002) Overexpression of a kinase-deficient form of the EDR1 gene enhances powdery mildew resistance and ethylene-induced senescence in *Arabidopsis*. Plant J **32**: 975–983

Tanimoto M, Roberts K, Dolan L (1995) Ethylene is a positive regulator of root hair development in *Arabidopsis thaliana*. Plant J **8**: 943–948

Thulasi Devendrakumar K, Li X, Zhang Y (2018) MAP kinase signalling: interplays between plant PAMP- and effector-triggered immunity. Cell Mol Life Sci **75**: 2981–2989

Tian W, Hou C, Ren Z, Pan Y, Jia J, Zhang H, Bai F, Zhang P, Zhu H, He Y, et al (2015) A molecular pathway for CO_2 response in *Arabidopsis* guard cells. Nat Commun **6**: 6057

Toruño TY, Stergiopoulos I, Coaker G (2016) Plant-pathogen effectors: Cellular probes interfering with plant defenses in spatial and temporal manners. Annu Rev Phytopathol **54**: 419–441

Toufighi K, Brady SM, Austin R, Ly E, Provart NJ (2005) The Botany Array Resource: e-Northerns, expression angling, and promoter analyses. Plant J **43**: 153–163

Virk N, Li D, Tian L, Huang L, Hong Y, Li X, Zhang Y, Liu B, Zhang H, Song F (2015) *Arabidopsis* Raf-Like mitogen-activated protein kinase kinase kinase gene Raf43 is required for tolerance to multiple abiotic stresses. PLoS One **10**: e0133975

Waadt R, Jawurek E, Hashimoto K, Li Y, Scholz M, Krebs M, Czap G, Hong-Hermesdorf A, Hippler M, Grill E, et al (2019) Modulation of ABA responses by the protein kinase WNK8. FEBS Lett **593**: 339–351

Wang B, Liu G, Zhang J, Li Y, Yang H, Ren D (2018a) The Raf-like mitogen-activated protein kinase kinase kinases Raf22 and Raf28 are required for the regulation of embryogenesis in *Arabidopsis*. Plant J **96**: 734–747

Wang H, Chevalier D, Larue C, Ki Cho S, Walker JC (2007) The protein phosphatases and protein kinases of *Arabidopsis thaliana*. Arabidopsis B **5**: e0106

Wang J, Grubb LE, Wang J, Liang X, Li L, Gao C, Ma M, Feng F, Li M, Li L, et al (2018b) A regulatory module controlling homeostasis of a plant immune kinase. Mol Cell **69**: 493–504

Wang Y, Liu K, Liao H, Zhuang C, Ma H, Yan X (2008) The plant WNK gene family and regulation of flowering time in *Arabidopsis*. Plant Biol **10**: 548–562

Wawrzynska A, Christiansen KM, Lan Y, Rodibaugh NL, Innes RW (2008) Powdery mildew resistance conferred by loss of the ENHANCED DISEASE RESISTANCE1 protein kinase is suppressed by a missense mutation in KEEP ON GOING, a regulator of abscisic acid signaling. Plant Physiol **148**: 1510–1522

van Wersch R, Li X, Zhang Y (2016) Mighty dwarfs: *Arabidopsis* autoimmune mutants and their usages in genetic dissection of plant immunity. Front Plant Sci **7**: 1717

Wingenter K, Trentmann O, Winschuh I, Hörmiller II, Heyer AG, Reinders J, Schulz A, Geiger D, Hedrich R, Neuhaus HE (2011) A member of the mitogen-activated protein 3-kinase family is involved in the regulation of plant vacuolar glucose uptake. Plant J **68**: 890–900

Wu L, Chen H, Curtis C, Fu ZQ (2014) Go in for the kill: How plants deploy effector-triggered immunity to combat pathogens. [Corrected]. Virulence **5**: 710–721

Wu S, Zhao B (2017) Using clear nail polish to make *Arabidopsis* epidermal impressions for measuring the change of stomatal aperture size in immune response. Methods Mol. Biol. **1578:** 243–248

Xie M, Wu D, Duan G, Wang L, He R, Li X, Tang D, Zhao X, Liu X (2014) AtWNK9 is regulated by ABA and dehydration and is involved in drought tolerance in *Arabidopsis*. Plant Physiol Biochem **77**: 73–83

Xing S, Wallmeroth N, Berendzen KW, Grefen C (2016) Techniques for the analysis of

protein-protein interactions *in vivo*. Plant Physiol **171**: 727–758
Xu J, Xie J, Yan C, Zou X, Ren D, Zhang S (2014) A chemical genetic approach demonstrates that MPK3/MPK6 activation and NADPH oxidase-mediated oxidative burst are two independent signaling events in plant immunity. Plant J **77**: 222–234
Xue S, Hu H, Ries A, Merilo E, Kollist H, Schroeder JI (2011) Central functions of bicarbonate in S-type anion channel activation and OST1 protein kinase in CO_2 signal transduction in guard cell. EMBO J **30**: 1645–1658
Yamada K, Yamaguchi K, Shirakawa T, Nakagami H, Mine A, Ishikawa K, Fujiwara M, Narusaka M, Narusaka Y, Ichimura K, et al (2016) The *Arabidopsis* CERK1-associated kinase PBL27 connects chitin perception to MAPK activation. EMBO J **35**: 2468–2483
Yamada K, Yamaguchi K, Yoshimura S, Terauchi A, Kawasaki T (2017) Conservation of chitin-induced MAPK signaling pathways in rice and *Arabidopsis*. Plant Cell Physiol **58**: 993–1002
Yamaguchi Y, Huffaker A, Bryan AC, Tax FE, Ryan CA (2010) PEPR2 is a second receptor for the Pep1 and Pep2 peptides and contributes to defense responses in *Arabidopsis*. Plant Cell **22**: 508–522
Yamaguchi Y, Pearce G, Ryan CA (2006) The cell surface leucine-rich repeat receptor for AtPep1, an endogenous peptide elicitor in *Arabidopsis*, is functional in transgenic tobacco cells. Proc Natl Acad Sci **103**: 10104–10109
Yan H, Zhao Y, Shi H, Li J, Wang Y, Tang D (2018) BRASSINOSTEROID-SIGNALING KINASE1 phosphorylates MAPKKK5 to regulate immunity in *Arabidopsis*. Plant Physiol **176**: 2991–3002
Yoo S-D, Cho Y-H, Tena G, Xiong Y, Sheen J (2008) Dual control of nuclear EIN3 by bifurcate MAPK cascades in C_2H_4 signalling. Nature **451**: 789–795
Yoshida K, Schuenemann VJ, Cano LM, Pais M, Mishra B, Sharma R, Lanz C, Martin FN, Kamoun S, Krause J, et al (2013) The rise and fall of the *Phytophthora infestans* lineage that triggered the Irish potato famine. Elife **2**: e00731
Yu X, Feng B, He P, Shan L (2017) From chaos to harmony: Responses and signaling upon microbial pattern recognition. Annu Rev Phytopathol **55**: 109–137
Zadoks JC (2008) The potato murrain on the european continent and the revolutions of 1848. Potato Res **51**: 5–45
Zhang J, Li W, Xiang T, Liu Z, Laluk K, Ding X, Zou Y, Gao M, Zhang X, Chen S, et al (2010) Receptor-like cytoplasmic kinases integrate signaling from multiple plant immune receptors and are targeted by a *Pseudomonas syringae* effector. Cell Host Microbe **7**: 290–301
Zhang Z, Liu Y, Huang H, Gao M, Wu D, Kong Q, Zhang Y (2017) The NLR protein SUMM2 senses the disruption of an immune signaling MAP kinase cascade via CRCK3. EMBO Rep **18**: 292–302
Zhang Z, Wu Y, Gao M, Zhang J, Kong Q, Liu Y, Ba H, Zhou J, Zhang Y, Chen S, et al (2012) Disruption of PAMP-induced MAP kinase cascade by a *Pseudomonas syringae* effector activates plant immunity mediated by the NB-LRR protein SUMM2. Cell Host Microbe **11**: 253–263
Zhao C, Nie H, Shen Q, Zhang S, Lukowitz W, Tang D (2014) EDR1 physically interacts with MKK4/MKK5 and negatively regulates a MAP kinase cascade to modulate plant innate immunity. PLoS Genet **10**: e1004389
Zipfel C (2014) Plant pattern-recognition receptors. Trends Immunol **35**: 345–351

Zipfel C, Kunze G, Chinchilla D, Caniard A, Jones JDG, Boller T, Felix G (2006) Perception of the bacterial PAMP EF-Tu by the receptor EFR restricts *Agrobacterium*-mediated transformation. Cell **125**: 749–760

Zulawski M, Schulze G, Braginets R, Hartmann S, Schulze WX (2014) The *Arabidopsis* kinome: Phylogeny and evolutionary insights into functional diversification. BMC Genomics **15**: 548

7. APPENDIX

Appendix Table 1. Clones generated or obtained for Gateway reactions and *in planta* expression.

Accession ID	Gene Name	Clone Name	Plasmid Stock	Glycerol Stock (in *E. coli*)	Antibiotic Resistance	Source	Reference
Gateway-Compatible Vectors							
AT3G63260	MRK1	pENTR-cMRK1 (no promoter, no stop codon)	JMp581	JMg589	Kanamycin	K. Siegel	N/A
AT3G63260	MRK1	pENTR223-cMRK1 (no promoter)	JMp551	JMg404	Spectinomycin	ABRC	(Rhee et al., 2003)
AT3G63260	MRK1	pENTR-gMRK1 (own promoter, no stop codon)	JMp582	JMg590	Kanamycin	K. Siegel	N/A
Plant Expression Vectors							
AT3G63260	MRK1	pGWB4-pMRK1: gMRK1-GFP	JMp614	JMg611	Kanamycin, Hygromycin	K. Siegel	N/A
AT3G63260	MRK1	pK7FWG2-35S: cMRK1-GFP	JMp610	JMg599	Spectinomycin	K. Siegel	N/A
AT3G63260	MRK1	pSY-35S: cMRK1-FLAG	JMp552	JMg415	Carbenicillin	ABRC	(Rhee et al., 2003)
AT3G63260	MRK1	LIC6-35S: cMRK1-Myc-His (DKLAT3G63260)	JMp465	JMg272	Spectinomycin	ABRC	(Rhee et al., 2003)
AT5G66210	CPK28	pXCSG-35S: CPK28-YFP	JMp15	JMg93	Kanamycin, Carbenicillin	S. Matschi	(Matschi et al., 2013)
Bimolecular Fluorescence Complementation Vectors							
AT3G63260	MRK1	pUBC-pUBQ10: cMRK1-nYFP	JMp728	JMg819	Spectinomycin	K. Siegel	N/A
AT3G63260	MRK1	pUBC-pUBQ10: cMRK1-cYFP	JMp611	JMg600	Spectinomycin	K. Siegel	N/A
AT5G66210	CPK28	pUBC-pUBQ10: cCPK28-nYFP	JMp573	JMg821	Spectinomycin	D. Holmes	N/A
AT5G66210	CPK28	pUBC-pUBQ10: cCPK28-cYFP	JMp729	JMg820	Spectinomycin	K. Siegel	N/A
AT2G39660	BIK1	pUBC-pUBQ10: cBIK1-nYFP	JMp612	JMg601	Spectinomycin	K. Siegel	N/A
AT2G39660	BIK1	pUBC-pUBQ10: cBIK1-cYFP	JMp574	JMg822	Spectinomycin	D. Holmes	N/A
AT1G29690	CAD1	pUBC-pUBQ10: gCAD1-nYFP	JMp609	JMg598	Spectinomycin	K. Siegel	N/A
AT1G29690	CAD1	pUBC-pUBQ10: gCAD1-cYFP	JMp571	JMg823	Spectinomycin	D. Holmes	N/A
N/A	N/A	pUBC-pUBQ10: nYFP (Empty Vector)	JMp561	JMg544	Spectinomycin	G. Wasteneys	(Grefen et al., 2010)
N/A	N/A	pUBC-pUBQ10: cYFP (Empty Vector)	JMp562	JMg545	Spectinomycin	G. Wasteneys	(Grefen et al., 2010)

Appendix Table 2. Primers used in Gibson assembly and Sanger sequencing.

Primer Name	Primer Sequence	Description
Gibson Assembly		
JMo548_pENTR_MRK1Gib_NP_LB	CCGCGGCCGCCCCCTTCACCATGGCC TCTGGCGGCGGAGA	Forward primer for amplification of cMRK1 (with no promoter)
JMo551_pENTR_MRK1Gib_OP_LB	CCGCGGCCGCCCCCTTCACCAGACCG GTACTGCAAGCAGA	Forward primer for amplification of gMRK1 (with native promoter)
JMo550_pENTR_MRK1Gib_NS_RB	GGGTCGGCGCGCCCACCCTTGGGGCC TCGAGGTTTGAAGAAAC	Reverse primer for amplification of MRK1 (with no stop codon)
JMo549_pENTR_MRK1Gib_OS_RB	GGGTCGGCGCGCCCACCCTTTCAGGG GCCTCGAGGTTTGAAG	Reverse primer for amplification of MRK1 (with stop codon)
Sanger Sequencing		
JMo577_cMRK1_Seq_F1	GGATGTCATTCAGCTCGCTT	Forward primers for sequencing MRK1 cDNA
JMo578_cMRK1_Seq_F2	TGATAGCTCCGGACCAGTT	
JMo579_cMRK1_Seq_R1	GGATGTGCACCGTTACCAC	Reverse primers for sequencing MRK1 cDNA
JMo580_cMRK1_Seq_R2	CAAGTGATTTATCCGCCTC	
JMo581_gMRK1_Seq_F1	GAATATGCTCTGGTGGATGC	Forward primers for sequencing MRK1 gDNA
JMo582_gMRK1_Seq_F2	ACCACCACCTTCGATCGAT	
JMo583_gMRK1_Seq_F3	TACTTACGGCACTGTCTACC	
JMo584_gMRK1_Seq_R1	CGGAATCTCTGGTCTCAGAT	Reverse primers for sequencing MRK1 gDNA
JMo585_gMRK1_Seq_R2	GTGACGCAATCTATCGA	
JMo586_gMRK1_Seq_R3	TGCTCAGTCAGACATCCT	
M13F (Invitrogen)	GTAAAACGACGGCCAG	Backbone-specific primers for pENTR
M13R (Invitrogen)	CAGGAAACAGCTATGAC	
JMo593_pUBCnYFP_seq_RB	AACTTCAGGGTCAGCTTG	Backbone-specific primers for pUBC, pGWB4, and pK7FWG2
JMo594_pUBCcYFP_seq_RB	GTGTTCTGCTGGTAGTGGT	

Appendix Table 3. Transgenic material generated by *Agrobacterium*-mediated floral dip.

Genotype	Isolated Line	Homozygosity	Antibiotic Resistance	Source
Col-0/pK7FWG2-35S:cMRK1-GFP	4-9	Homozygous	Kanamycin	K. Siegel
	4-10	Homozygous		
	10-11	Homozygous		
	10-12	Homozygous		
Col-0/pGWB4-pMRK1:gMRK1-GFP	1-9	Segregating in T_3 generation	Kanamycin	K. Siegel
	1-14	Segregating in T_3 generation		
	11-5	Segregating in T_3 generation		
	11-10	Homozygous		
mrk1-1/pK7FWG2-35S:cMRK1-GFP	1	Segregating in T_2 generation	Kanamycin	K. Siegel
	3	Segregating in T_2 generation		
mrk1-1/pGWB4-pMRK1:gMRK1-GFP	3	Segregating in T_2 generation	Kanamycin	K. Siegel
	7	Segregating in T_2 generation		

Appendix Table 4. T-DNA insertion lines obtained for Raf-like MAPKKK Subgroup C7 members or PP2A-B subunits.

Genotype	Line Name	Source	Reference
Single Null Lines (Subgroup C7)			
mrk1 (GK-252 E04)	*mrk1-1*	ABRC	(Alonso et al., 2003)
raf26 (SALK_029496C)	*raf26-1*		
raf26 (SALK_135277C)	*raf26-2*		
raf33 (SALK_011601)	*raf33-1*		
raf38 (SALK_005187)	*raf38-1*		
raf38 (SAIL_714_A07)	*raf38-2*		
raf39 (SALK_038064C)	*raf39-1*		
raf39 (WDL_413416L4)	*raf39-2*		
Double Null Lines (Subgroup C7)			
raf26 raf39 (SALK_029496C, SALK_038064C)	*raf26-1 raf39-1*	J. Monaghan and K. Siegel	N/A
raf26 raf39 (SALK_135277C, WDL_413416L4)	*raf26-2 raf39-2*		
raf33 raf38 (SALK_011601, SALK_005187)	*raf33-1 raf38-1*		
mrk1 raf39 (GK-252 E04, SALK_038064C)	*mrk1-1 raf39-1*		
mrk1 raf39 (GK-252 E04, WDL_413416L4)	*mrk1-1 raf39-2*		
mrk1 raf26 (GK-252 E04, SALK_029496C)	*mrk1-1 raf26-1*		
mrk1 raf26 (GK-252 E04, SALK_135277C)	*mrk1-1 raf26-2*		
Single Null Lines (PP2A-B Subunits)			
pp2a-bα (SALK_032080)	*pp2a-bα-1*	C. Lillo	(Heidari et al., 2013)
pp2a-bβ (SALK_062514)	*pp2a-bβ-1*		

Appendix Table 5. Primers used in PCR genotyping and qRT-PCR.

Accession ID	Template	Primer Name	Primer Sequence
Genotyping (Gene-Specific)			
AT3G63260	*mrk1-1* (GK-252 E04)	JMo599_GK-292E04_LB	ACTTACGGCACTGTCTACC
		JMo600_GK-292E04_RB	GGCATGTCACAGCAGTAT
AT4G14780	*raf26-1* (SALK_029496C)	JMo571_SALK_029496C_LB	AAGTTGTGTGATCTTCTTGTTTGC
		JMo572_SALK_029496C_RB	ATCGCACCTTCTGTTGTATGG
AT4G14780	*raf26-2* (SALK_135277C)	JMo573_SALK_135277C_LB	GGGAGATTGATTTGGCTAAGC
		JMo574_SALK_135277C_RB	TCAGGATAAGGCATATCGCAG
AT5G50000	*raf33-1* (SALK_011601)	JMo565_SALK_011601_LB	GACATGACAGGAGAGACTG
		JMo566_SALK_011601_RB	CCTGTCGAGTGTAGTTGGT
AT3G01490	*raf38-1* (SALK_005187)	JMo597_SALK_005187_LB	CCATGTGGTCACGTGTAA
		JMo598_SALK_005187_RB	CATCTTGACCATCGTAGA
AT3G01490	*raf38-2* (SAIL_714_A07)	JMo595_SAIL_714_A07_LB	GCTGTGTCGTGGTTGAGTA
		JMo596_SAIL_714_A07_RB	GAACGTAGTGCATGTGTGT
AT3G22750	*raf39-1* (SALK_038064C)	JMo567_SALK_038064C_LB	GACGACGAGTCGGTGTCTTAG
		JMo568_SALK_038064C_RB	AGTTCTCCGTCTCAGCTGATG
AT3G22750	*raf39-2* (WDL_413416L4)	JMo629_WDL413-316L4_LB	AAGTCGTGGTTCAACTCG
		JMo621_qPCR_WDL413-416L4_DS_R	AACAGCCAGGTCTCTGAT
AT1G51690	*pp2a-bα-1* (SALK_032080)	JMo591_SALK_032080_LB	GTGAAGTAGGAACTACAG
		JMo592_SALK_032080_RB	TGGTATCGGTTCTCTCGA
AT1G17720	*pp2a-bβ-1* (SALK_062514)	JMo587_SALK_062514_LB	TTCCATCTCAGGAAACAATGC
		JMo588_SALK_062514_RB	AGAAAGAAGCTCTCACCCTGG
Genotyping (T-DNA Insertion-Specific)			
N/A	N/A	JMo9_GKo8409LB	ATATTGACCATCATACTCATTGC
N/A	N/A	JMo10_SalkLBb1.3	ATTTTGCCGATTTCGGAAC
N/A	N/A	JMo247_WDL_LB	AACGTCCGCAATGTGTTATTAAGTTGTC
N/A	N/A	JMo541_SAIL_LB-1	TAGCATCTGAATTTCATAACCAATCTCG ATACAC
qRT-PCR			
AT3G63260	*mrk1-1* (GK-252 E04)	JMo622_qPCR_GK-252E04_DS_F	TAGAGGGCTTAGTTACCTCC
		JMo623_qPCR_GK-252E04_DS_R	GCCATGTATCCAAGTGTTCC
AT4G14780	*raf26-1* (SALK_029496C)	JMo624_qPCR_SALK_029496C_DS_F	CAGAGGGCTAAGCTATTTGCA
		JMo572_SALK_029496C_RB	ATCGCACCTTCTGTTGTATGG
AT4G14780	*raf26-2* (SALK_135277C)	JMo625_qPCR_SALK_135277C_DS_F	CCTGAGGTCATTGATGGTAAG
		JMo626_qPCR_SALK_135277C_DS_R	GACAGCATCTCGGTATCTC
AT5G50000	*raf33-1* (SALK_011601)	JMo627_qPCR_SALK_011601_DS_F	GATTCGTGTCCTTGCTTC
		JMo807_qPCR_SALK_011601_DS_R	GCAACCATTAGATCCCT
AT3G01490	*raf38-1* (SALK_005187)	JMo615_qPCR_SALK_005187_DS_F	TCACCAAGTTCATAGGAGCG
		JMo616_qPCR_SALK_005187_DS_R	TAACTCAACCCGCGAGCAA
AT3G01490	*raf38-2* (SAIL_714_A07)	JMo617_qPCR_SAIL_714_A07_DS_F	GATGTTGTCCAAGCTCGCT
		JMo618_qPCR_SAIL_714_A07_DS_R	CAGCCTTGTTGTTGGTCAG
AT3G22750	*raf39-1* (SALK_038064C)	JMo619_qPCR_SALK_038064C_DS_F	GGTCAAGATGTTGCTGTGAAAG
		JMo568_SALK_038064C_RB	AGTTCTCCGTCTCAGCTGATG
AT3G22750	*raf39-2* (WDL_413416L4)	JMo620_qPCR_WDL413-416L4_DS_F	CTGAGACCGGATATTCCAAG
		JMo621_qPCR_WDL413-416L4_DS_R	AACAGCCAGGTCTCTGAT

Appendix Table 6. Antibodies and titers used in western blots.

Antibody	Biological Source	Titer Used	Vendor	Catalogue Number
α-GFP	Mouse	1:5000	Roche Life Science	11 814 460 001
α-p44/42 MAPK (ERK1/2)	Rabbit	1:2000	Cell Signaling Technology	9102S
α-His	Mouse	1:5000	Cell Signaling Technology	2366S
α-Mouse-HRP	Rabbit	1:10000	Sigma-Aldrich	A9044
α-Rabbit-HRP	Goat	1:10000	Sigma-Aldrich	A9169

Appendix Table 7. Summary of individual replicates for immune-induced oxidative burst assays using *mrk1 raf39* and *mrk1 raf26*.

Biological Replicate	Technical Replicate	Elicitor Used	*mrk1-1 raf39-1*	*mrk1-1 raf39-2*	*mrk1-1 raf26-1*	*mrk1-1 raf26-2*
1	1	flg22	■	■	■	(not tested)
		elf18	■	■		
		AtPep1	■	■	■	
	2	flg22	■	■	■	(not tested)
		elf18	■	■	■	
		AtPep1	■	■	■	
	3	flg22				(not tested)
		elf18		■	■	
		AtPep1		■	■	
2	1	flg22	■	■	■	■
		elf18	■	■	■	■
		AtPep1		■		
	2	flg22	■	■	■	■
		elf18	■	■		■
		AtPep1				
	3	flg22		■	■	■
		elf18		■		■
		AtPep1	■	■	■	■
3	1	flg22				
		elf18	■	■	■	■
		AtPep1	■	■	■	■
	2	flg22				
		elf18		■	■	■
	3	flg22				
		elf18		■		■
4	1	flg22				■
		elf18		■		■
		AtPep1	■	■		■
	2	flg22	■			■
		elf18		■		■
		AtPep1				
	3	flg22	■	■	■	■
		elf18	■	■	■	■
		AtPep1	■		■	

■ = increased ROS relative to Col-0

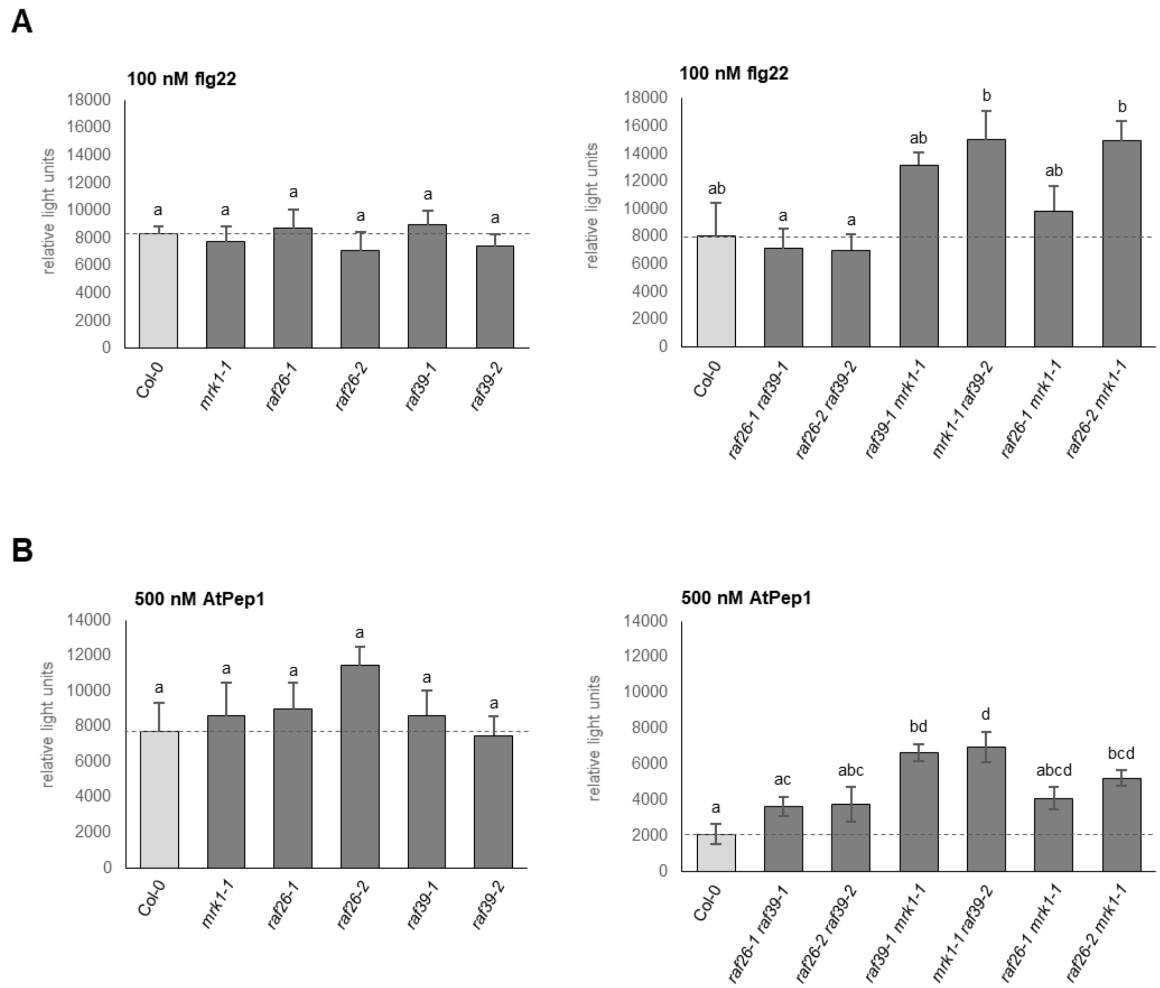

Appendix Figure 1. Raf-like MAPKKK Subgroup C7-1 members also function redundantly to regulate flg22- and AtPep1-induced oxidative burst. Oxidative burst was analyzed in single and double null lines for MRK1, Raf39, and Raf26 at 5 weeks post-germination following elicitation with 100 nM flg22 (A) or 500 nM AtPep1 (B). Average total photon counts over 40 minutes are shown in relative light units, and error bars represent standard error of the mean (n = 6 leaf discs from independent plants). Statistical differences were calculated by one-way ANOVA followed by a post-hoc Tukey's Honest Significant Difference test ($p<0.05$) and groupings are represented by lower-case letters. The dashed line indicates the average total photon count for the wild-type control (Col-0). Similar results were observed in 8 of 12 technical replicates from three independent biological replicates (Appendix Figure 7).

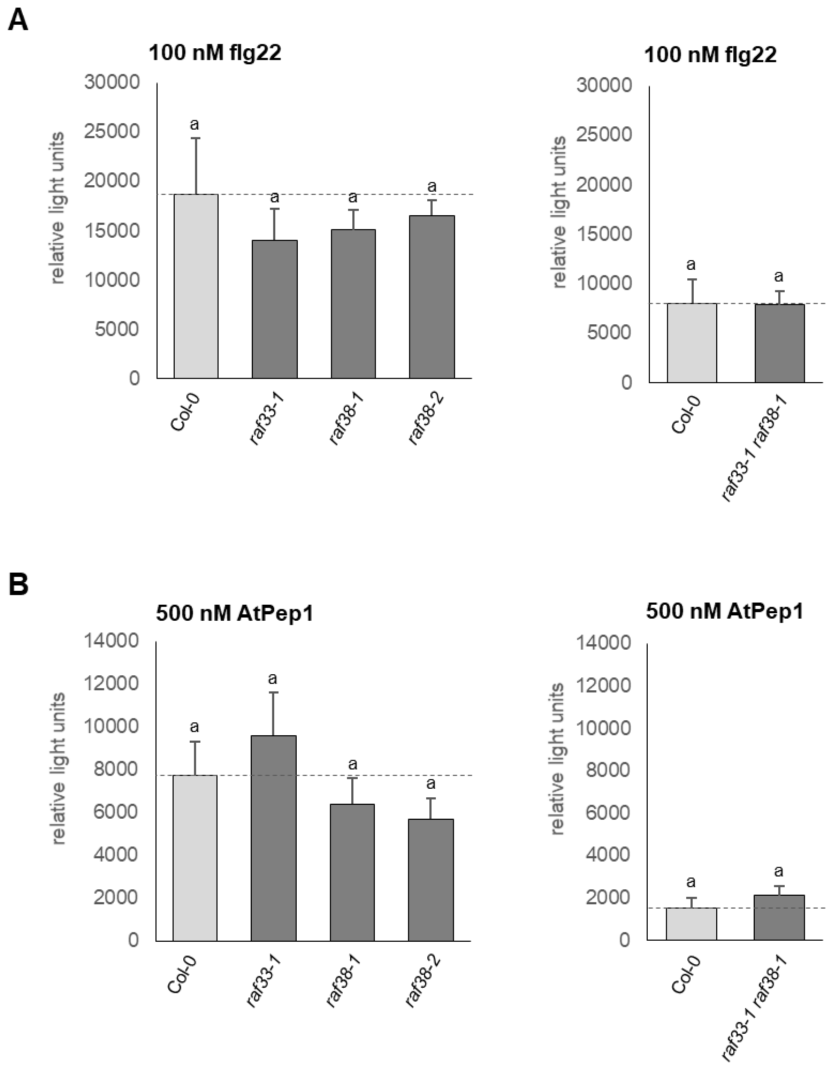

Appendix Figure 2. Raf-like MAPKKK Subgroup C7-2 members do not play a role in flg22- and AtPep1-induced oxidative burst. Oxidative burst was analyzed in single and double null lines for Raf33 and Raf38 at 5 weeks post-germination following elicitation with 100 nM flg22 (A) or 500 nM AtPep1 (B). Average total photon counts over 40 minutes are shown in relative light units, and error bars represent standard error of the mean (n = 6 leaf discs from independent plants). Statistical differences were calculated by one-way ANOVA followed by a post-hoc Tukey's Honest Significant Difference test ($p<0.05$) and groupings are represented by lower-case letters. The dashed line indicates the average total photon count for the wild-type control (Col-0). Similar results were observed in three independent replicates.

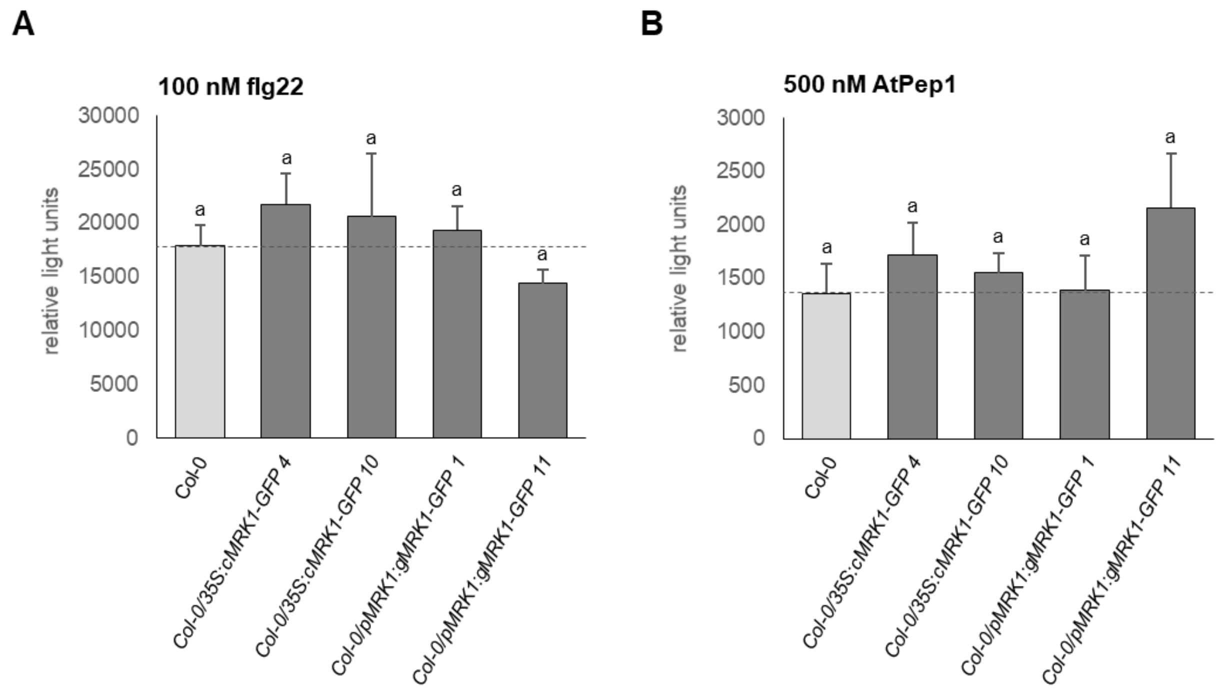

Appendix Figure 3. *MRK1-OE* lines have a wild-type oxidative burst following elicitation with flg22 or AtPep1. Oxidative burst was analyzed in antibiotic-selected T_2 or T_3 *MRK1-OE* lines at 5 weeks post-germination following elicitation with 100 nM flg22 (A) or 500 nM AtPep1 (B). Average total photon counts over 40 minutes are shown in relative light units, and error bars represent standard error of the mean (n = 6 leaf discs from independent plants). Statistical differences were calculated by one-way ANOVA followed by a post-hoc Tukey's Honest Significant Difference test (p<0.05) and groupings are represented by lower-case letters. The dashed line indicates the average total photon count for the wild-type control (Col-0). Similar results were observed in three independent replicates.

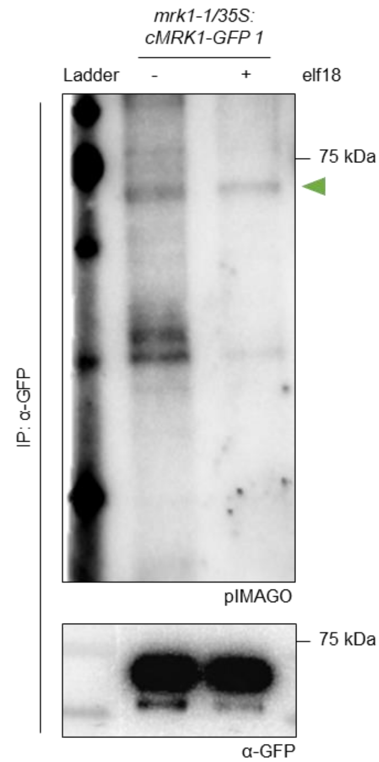

Appendix Figure 4. Preliminary work suggests that MRK1 may be less phosphorylated following immune treatment. Stable *mrk1-1/35S:cMRK1-GFP* lines were generated through *Agrobacterium*-mediated floral dip, and 12 leaves from antibiotic-selected T_2 plants were treated with or without 200 nM elf18 for 20 min. Total protein was extracted and *MRK1-GFP* was immunoprecipitated using μMACs α-GFP beads. Phosphorylated protein was detected using the pIMAGO™-biotin Phosphoprotein Detection Kit (Tymora Analytical Operations), and immunoblotting against MRK1-GFP was performed to serve as a loading control. As this assay was performed only once and protein loading is not even in this replicate, further work is needed to assess the phosphorylation status of MRK1 before and after immune treatment.

A

ACCESSION ID	IDENTIFIED PROTEIN	MOLECULAR WEIGHT (kDa)	PEPTIDE COUNTS				
			cpk28-1/ CPK28-YFP (-elf18)	*cpk28-1/ CPK28-YFP (+elf18)*	*cpk28-1/ CPK28^{D188A} -YFP (-elf18)*	*cpk28-1/ CPK28^{D188A} -YFP (+elf18)*	*PM-GFP (control)*
AT1G51690.3	PP2A-Bα (protein phosphatase 2A 55 kDa regulatory subunit b alpha isoform)	67	6	6	6	3	1
AT1G17720.2	PP2A-Bβ (protein phosphatase 2A 55 kDa regulatory subunit b beta isoform)	56	2	1	1	1	0

B

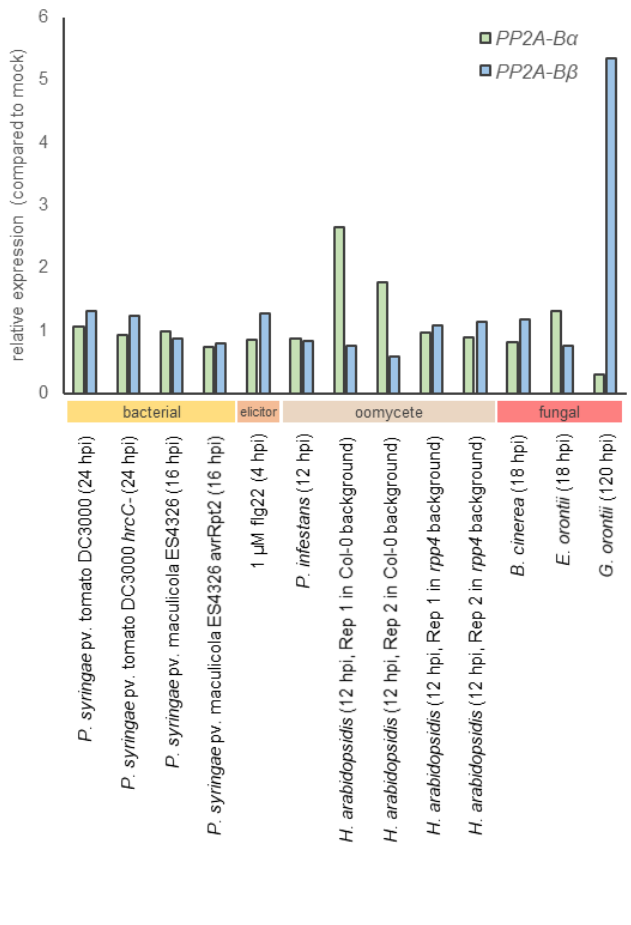

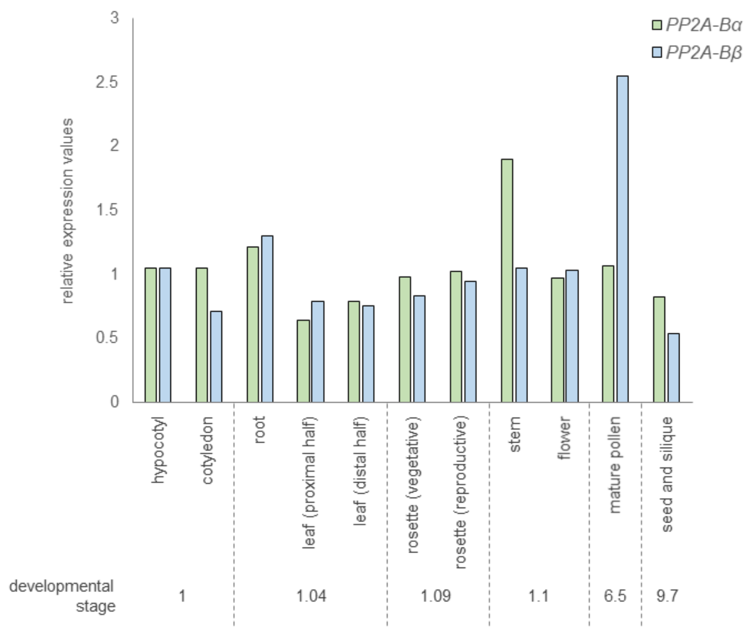

Appendix Figure 5. PP2A-B subunits were identified as putative CPK28-associated proteins in a reverse genetics screen. (A) Peptide counts for PP2A-Bα (AT1G51690) and PP2A-Bβ (AT1G17720) identified in CPK28-YFP or plasma-membrane control LOW TEMPERATURE-INDUCED PROTEIN 6B-GFP (‘PM-GFP’) immunoprecipitates through LC/MS-MS. Loss-of-function *cpk28-1* lines were stably transformed with wild-type or kinase-dead (CPK28^{D188A}) variants of CPK28-YFP (Matschi et al., 2013), treated with or without 200 nM elf18, and subjected to affinity purification and LC-MS/MS as previously described (Bender et al., 2017) alongside the *Col-0/PM-GFP* control. (B) Gene expression of PP2A-B subunits from Arabidopsis following immune elicitation or at various developmental stages. For immune-induced expression, expression values relative to a “mock” control were extracted using the Pathogen Series under the eNorthern Expression Browser tool from the Bio-Analytic Resource for Plant Biology. For tissue-specific expression, relative expression values were extracted using the Extended Tissue Series from the same tool. *PP2A-Bβ* was highly expressed following treatment with the fungal pathogen *Golovinomyces orontii*, and *PP2A-Bα* expression was relatively unchanged following immune elicitation. Both *PP2A-Bα* and *PP2A-Bβ* were evenly expressed across most tissue types, though *PP2A-Bβ* had higher expression in mature pollen.

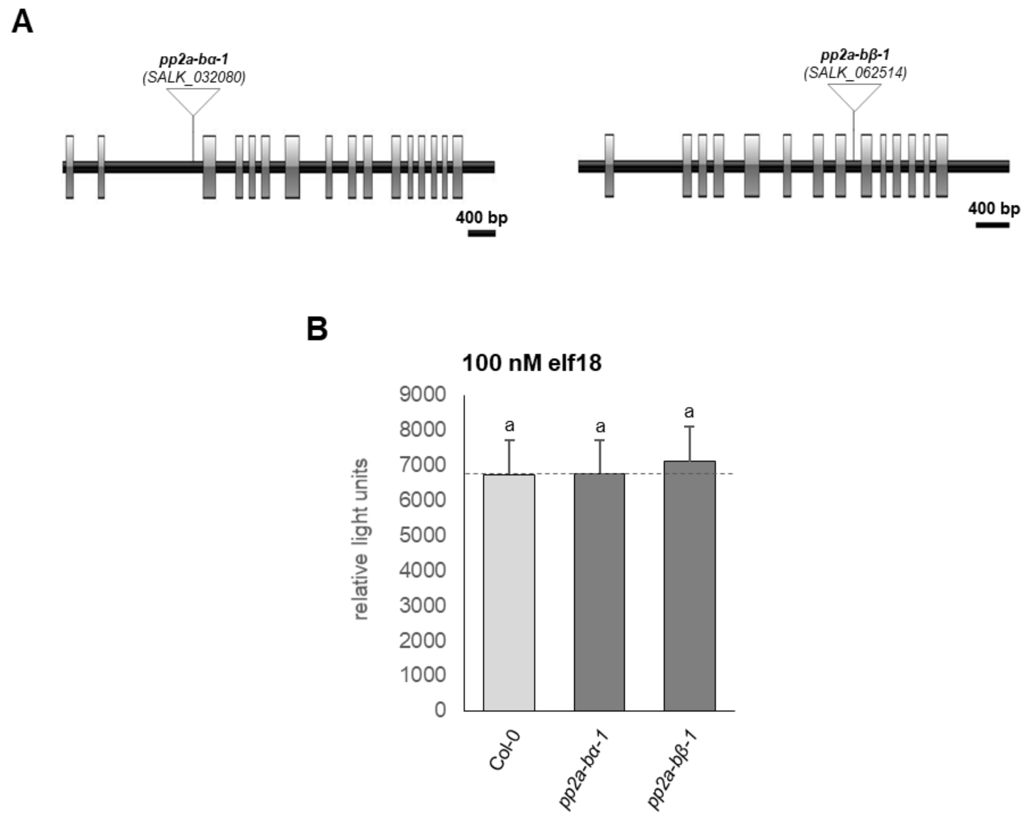

Appendix Figure 6. PP2A-B subunits do not play a role in immune-induced oxidative burst. (A) The gene structure of *PP2A-Bα* (AT1G51690) and *PP2A-Bβ* (AT1G17720) was visualized using the IBS: Illustrator for Biological Sequences version 1.0.3, and T-DNA insertions were annotated using information curated from TAIR. Introns and untranslated regions are represented by a black line, and exons are annotated using light gray boxes. (B) Oxidative burst was analyzed in single null lines for *PP2A-Bα* and *PP2A-Bβ* at 5 weeks post-germination following elicitation with 100 nM elf18. Average total photon counts over 40 minutes are shown in relative light units, and error bars represent standard error of the mean (n = 6 leaf discs from independent plants). Statistical differences were calculated by one-way ANOVA followed by a post-hoc Tukey's Honest Significant Difference test ($p<0.05$) and groupings are represented by lower-case letters. The dashed line indicates the average total photon count for the wild-type control (Col-0). Similar results were observed in two independent replicates.